

Breakdown and repair of the aging brain metabolic system

Polina Shichkova¹, Jay S. Coggan¹, Lida Kanari¹, Elvis Boci¹, Cyrille Favreau¹, Stefano Maximiliano Antonel¹, Daniel Keller¹ and Henry Markram^{1,2}

1 Blue Brain Project, École Polytechnique Fédérale de Lausanne, Geneva, Switzerland,

2 Laboratory of Neural Microcircuitry, Brain Mind Institute, École Polytechnique Fédérale de Lausanne, Lausanne, Switzerland

Corresponding Authors: polina.shichkova@alumni.epfl.ch, henry.markram@epfl.ch

Abstract

The study presented explores the complex relationship between the aging brain, energy metabolism, blood flow and neuronal activity by introducing a comprehensive, data-driven molecular model of the neuro-glial vascular system, including all key enzymes, transporters, metabolites, and blood flow vital for neuronal electrical activity with 16'800 interaction pathways. We find significant alterations in metabolite concentrations and differential effects on ATP supply in neurons and astrocytes and within subcellular compartments within aged brains, and identify reduced Na⁺/K⁺-ATPase as the leading cause of impaired neuronal action potentials. The model predicts that the metabolic pathways cluster more closely in the aged brain, suggesting a loss of robustness and adaptability. Additionally, the aged metabolic system displays reduced flexibility, undermining its capacity to efficiently respond to stimuli and recover from damage. Through transcription factor analysis, the estrogen-related receptor alpha (ESRRA) emerged as a central target connected to these aging-related changes. An unguided optimization search pinpointed potential interventions capable of restoring the brain's metabolic flexibility and restoring action potential generation. These strategies include increasing the NADH cytosol-mitochondria shuttle, NAD⁺ pool, ketone β-hydroxybutyrate, lactate and Na⁺/K⁺-ATPase and reducing blood glucose levels. The model is open-sourced to help guide further research in brain metabolism.

Main

Mechanisms of brain aging

The risk of numerous disorders, including neurodegenerative diseases, increases dramatically with age (Niccoli and Partridge, 2012; Hou et al., 2019). At the core of brain aging lies energy metabolism (López-Otín et al., 2013, 2023; Mattson and Arumugam, 2018). Neuronal activity is energetically demanding, requiring substantial amounts of ATP, as reflected in the brain's disproportionate oxygen and glucose consumption compared to the rest of the body (Kety, 1957; Mink et al., 1981; Sokoloff, 1996; Rolfe and Brown, 1997). Metabolic support and neuronal activity are closely linked (Mann et al., 2021), suggesting that age-related loss of metabolic support impacts the generation of electrical activity in the brain. But the vast number of biochemical reactions forming the metabolic system constitute a highly complex system that makes it exceedingly difficult to isolate how changes in the metabolic system impact neuronal activity.

Various dynamic models of brain metabolism have been developed over the decades. Early models (Aubert et al., 2001; Cloutier et al., 2009) focused on core components of the metabolic system and generalized many processes such as mitochondrial respiration. Recent models have incorporated more detailed descriptions for selected subsystems, such as the pentose phosphate pathway (Winter et al., 2018), mitochondrial metabolism (Berndt et al., 2015; Theurey et al., 2019) or neuronal electrophysiology (Jolivet et al., 2015). While well-validated and suited for the target questions possible with these models, a considerably more biologically detailed model is required to address more complex questions such as how age-related changes in metabolism impact action potential generation and responses to stimuli.

The model we developed brings the previous models together with greater detail and adds previously omitted subsystems such as glutathione metabolism and regulation of glycogenolysis. The model also extends previous models by coupling the metabolic system to the intricate cellular processes underlying action potential generation such as the Na^+/K^+ -ATPase pump, the glutamate-glutamine cycle, and ATP production by mitochondria and cytosol. The model allows, for the first time, a view on how electrical activity impacts the metabolic system and vice versa. Finally, the model also integrates blood flow and dynamic exchanges between the vasculature and the neurons and glia to yield a comprehensive view of the biochemical network operating across the Neuro-Glia-Vascular

(NGV) system. The model therefore also allows addressing questions related to nutrient supply to the brain.

Since there is a vast amount of data related to brain metabolism in the literature and databases, we adopted a strict data-driven strategy to constrain the construction of the biochemical network of the NGV system. This strategy allowed us to use data relevant to the young and aged brain's metabolic system and reconstruct and simulate their respective metabolic systems. The model integrates all key metabolites, transporters and enzymes with all key cellular and extracellular processes underlying neuronal firing and interactions with the blood (Fig. 1). Subcompartments such as mitochondrial matrix and intermembrane space, cytosol in neurons and astrocytes, blood flow bringing nutrients and oxygen in capillaries, endothelium, and the extracellular space (interstitium and basal lamina) are captured using their data-driven volumes (see the model at <https://bbp.epfl.ch/ngv-portal-dev/>), allowing modeling of their cross-compartment processes such as transport and exchange. The model does not capture metabolic waste management, such as lactate removal. Concentrations of molecules are specified in molar units (mM) and fluxes of reactions and transport processes are given in molar concentrations per second (mM/second).

We validated the model extensively against a corpus of data reported in the literature on how enzyme and transporter activities and metabolite concentrations change in response to stimulation that were not used to construct the model (Supplementary Fig. 1, Supplementary Table 1). For example, the model shows that Na⁺/K⁺ pump ATP use in the astrocyte is comparable with that of the neuron (Fig. 3g) consistent with recent evidence (Barros, 2022). In line with previous studies (Bélanger et al., 2011), mitochondrial ATP production as a share of total ATP production is higher in neurons than in astrocytes, at 84% versus 70% (Supplementary Fig. 2), closely matching experimental estimates of 75% in astrocytes (Bouzier-Sore et al., 2006; Barros, 2022). These data emerged when the model was simulated and their consistency with a range of reported experimental data suggests that the model accurately captures the most essential elements of the brain's metabolic system.

Alterations in enzyme expression have recently been shown to actively contribute to tissue aging and therefore potential drug targets to counter aging (Palla et al., 2021). To model aging of NGV metabolism, we therefore used RNA expression changes (RNA FCs) from a comprehensive study on mouse cell-type changes (Schaum et al., 2020; Zhang et al., 2021a) to scale enzyme and transporter concentrations. These concentrations determine the output from their corresponding reaction/transport rate equations. After applying the RNAseq data (Schaum et al., 2020; Zhang et al., 2021a) to their

respective metabolic pathways, we obtained a map of the decrease in expression of most enzymes with aging in both neurons and astrocytes. The map revealed, for example, that succinate dehydrogenase (SDH) is differentially affected by aging in neurons and astrocytes. SDH is a mitochondrial energy nexus and serves as complex II of the mitochondrial electron transport chain (ETC). SDH connects the tricarboxylic acid cycle (TCA) to the ETC. This result indicates that pre- and post-SDH enzymes of TCA (fumarase and succinate CoA ligase) display opposite changes in aged neurons and astrocytes. SDH itself decreases more in aged neurons than in aged astrocytes. In neurons, aging reduces both succinate CoA ligase and SDH, while increasing fumarase. Unlike in neurons, succinate CoA ligase levels rise in astrocytes during aging. SDH decreases slightly while fumarase levels decline more.

In addition to changes in enzyme and transporter expression, we used published values to adjust arterial glucose, lactate, β -hydroxybutyrate levels, the total NAD (reduced and oxidized) pool, as well as glutamate concentration changes caused by synaptic transmission (Dong and Brewer, 2019; Cox et al., 2022). The young brain's metabolic system is in an equilibrium at rest - i.e. when no stimulus is applied. To be able to compare the young and aged models we could ensure that the aged system was also at steady state by reducing the NADH shuttle capacity between the cytosol and mitochondria. All aging data applied to the model are summarized in Fig. 2, with further details available in the Methods section. When we simulated the dynamics of this complex system, driven by either synaptic input or current injection that generated action potentials, we observed numerous age-specific differences that are consistent with prior reports (Supplementary Table 1) further validating the model and providing a spectrum of new insights into how the NGV metabolic system may age.

Aging affects metabolite levels at rest and during stimuli

The simulated aging phenotype exhibits a distinct resting state profile of metabolite concentrations when compared to that of the young brain (Supplementary Fig. 3a), the change in concentrations in response to stimuli also differs (Fig. 3c, d, Supplementary Fig. 3b, 4, 5d, 6a), but the changes in responses to stimuli of varying amplitudes are not uniform across different metabolites (Supplementary Fig. 6, 7). We performed Uniform Manifold Approximation and Projection for Dimension Reduction (UMAP) dimensionality reduction on relative differences in concentration traces between the two ages, and observed numerous interdependencies between pathways. The pentose phosphate pathway (PPP) and TCA tend to form pathway-related clusters (Supplementary Fig. 8). Moreover, pairwise Kendall correlation between metabolic concentration temporal profiles is also affected by aging (Supplementary Fig. 9). This effect may be caused by widely described metabolic dysregulation in aging (Mattson and Arumugam, 2018). Reaction and transport fluxes are impacted as

well (Supplementary Fig. 10-12). Aging effects on metabolite concentrations at rest and in response to stimuli are therefore metabolite-specific and largely uncorrelated, indicative of a fragmentation of the metabolic network in aging.

Lactate transport directionality changes in the aging metabolic system

In the aged metabolic system, neuronal lactate import is lower, while astrocyte lactate export is slightly higher. This effect can be explained by mitochondrial hypometabolism, which results in increased pyruvate levels and correspondingly higher levels of lactate. To examine the dependence of lactate transport directionality upon glucose levels in aged and young metabolic systems (Supplementary Fig. 13), we simulated the effects of varying resting blood glucose levels in a range of 1.6 to 14.6 mM with increments of 1 mM.

In the young system, we observed the expected astrocyte-to-neuron lactate shuttle (ANLS) at all tested blood glucose levels; as blood glucose levels increase, lactate export from astrocytes rises while lactate import to neurons decreases. This directionality is consistent with higher glucose availability reducing the need for neurons to import lactate and more lactate is available in and exported from astrocytes. In the aged metabolic system, the lactate shuttle has the same directionality as in the young system for moderate blood glucose levels (6.45 to 10.6 mM), consistent with a recent publication (Acevedo et al., 2023), but both neurons and astrocytes export lactate when glucose levels are low-to-normal (1.6 to 5.6 mM) and both neurons and astrocytes import lactate when glucose levels are high (11.6 to 14.6 mM). A possible explanation for this dysregulation in the aged metabolic system could involve NAD^+/NADH and ATP/ADP ratios due to their regulatory role over the entire metabolic network, but this counterintuitive prediction requires experimental verification.

Aging-associated changes in metabolism alter electrophysiological characteristics

We show for the first time how the aging metabolic system leads to changes in the generation of action potential by both synaptic input (Fig. 3) and current injection (Supplementary Fig. 5). Age-related differences in neuronal firing characteristics evoked by current injection are particularly important because it excludes the metabolic demand caused by glutamate release. We found similar changes in metabolic profiles following synaptic input and current injection (Supplementary Fig. 14), suggesting that metabolic changes mostly impact the action potential generation ability of neurons. A more detailed molecular coupling between the metabolic system and the entire glutamate cycle would however need to be included in the model to strengthen this prediction.

We found that changes in action potential shape and size are caused by a reduction in Na^+/K^+ -ATPase expression in the aged brain, supporting a recent theory of non-canonical control of neuronal energy status (Baeza-Lehnert et al., 2019). To better understand whether other aspects of the metabolic system, such as reduced supply of ATP, also contribute to these changes, we increased the Na^+/K^+ -ATPase expression levels in the aged brain model to the same as in the young brain while leaving all other aspects of the aging metabolic system in their aged state. There were no significant differences in action potentials at low frequencies (4-8 Hz) and only slight changes at much high-frequencies (78-79 Hz) suggesting that the decreased expression of the Na^+/K^+ -ATPase pump is the main factor impairing the ability of neurons to generate action potentials. It is however still possible that other aspects of the NGV metabolic network become more important after sustained neuronal activity such as those during intense cognitive demand.

Lower supply and demand for energy in the aged brain

Energy deficiency is a prominent hypothesis in brain aging (Bonvento and Bolaños, 2021), but it is not clear if the supply is limiting and/or demand is reduced and whether astrocytes and neurons are impacted in the same way. Adenylate energy charge (AEC), a widely used proxy for cellular energy availability (Atkinson, 1968), is higher in the young compared to the old state (Fig. 3e). However, this value does not separate supply from demand. To separate the two factors, we first computed the total ATP cost of firing action potentials. We find that the young brain model consumes approximately 2 billion ATP molecules per second per NGV unit (where one unit is one neuron, one astrocyte and their associated extracellular matrix and capillaries) at 8 Hz firing, and the aged brain model consumes around 1.8 billions molecules per second, which aligns well with literature estimates (Howarth et al., 2012; Yi and Grill, 2019; Zhu et al., 2019). We find that ATP production is lower in aged cytosol of both neuron and astrocytes, and in aged neuronal mitochondria as shown in Supplementary Fig. 2, but if one considers the reduced ATP-consumption (Fig. 3f) because of the lower levels of Na^+/K^+ -ATPase (Niven, 2016; Meyer et al., 2022), then ATP supply is not limiting for the Na^+/K^+ -ATPase that is present. While reduced ATP supply does not seem to be limiting action potential generation in the acute state, it remains possible that a persistently lower supply of ATP may still be the cause of a loss of Na^+/K^+ -ATPase expression and hence impaired action potential generation over a longer period.

We also find that neurons and astrocytes are differentially impacted with age. Normally, astrocytic Na^+/K^+ -ATPases consume slightly less than $\frac{2}{3}$ of ATP of the neuronal Na^+/K^+ -ATPases (Fig. 3g). In astrocytes, the ATP supply is only reduced in the cytosol and not in the mitochondria and the catalytic subunit of the Na^+/K^+ -ATPases expression is unchanged with aging. While ATP consumption of the

Na^+/K^+ -ATPase pump in neurons decreases with aging (Fig. 3f), it slightly increases in astrocytes resulting in an increase in the ratio of astrocyte to neuron Na^+/K^+ -ATPases ATP consumption from around 0.69 in the young brain to around 0.72 with aging. Since astrocytes do not need to fire action potentials, this finding suggests that there is an increase in the demand placed on astrocytes to support the neurons to clear extracellular K^+ in order to help neurons generate their action potentials.

Aging brain metabolism is more fragile and susceptible to damage

Protein dysfunction is associated with several aging hallmarks, including loss of proteostasis, oxidative damage, and impaired DNA repair (Mattson and Arumugam, 2018; Schaum et al., 2020). Moreover, reduced fidelity of protein translation leads to a phenotype resembling an early stage of Alzheimer's disease (Brilkova et al., 2022). To mimic molecular damage and simulate the effect on enzyme and transporter functions, we introduced one perturbation at a time for each protein's kinetic parameter (Michaelis constant, inhibition and activation constants, catalytic rate constant, i.e. a parameter in the enzyme rate equation), adjusting its value by 20% (increasing or decreasing in separate simulations). We then calculated the changes in the response of all metabolites to obtain a measure of how sensitive their concentrations are to the individual perturbations. We ran 2,264 simulations with perturbed parameters to measure metabolite sensitivities at rest and during a stimulus for the young and aged systems (see formula in Fig. 4b). The difference between the resting and stimulated state's sensitivities, normalized by the resting state sensitivities, yielded a rest-normalized sensitivity. Since a larger value for a metabolite implies that a stimulus produces a larger change in its concentration as compared to rest when another parameter in the system is perturbed, we interpret such a change as the ability to adapt to damage of the system, and therefore call this metric, "metabolic adaptability" (Fig. 4d).

This metric allowed us to compare how the whole metabolic system of neurons and in astrocytes in the young and aged brain (Fig. 4d). Most of the metabolites in neurons decrease their adaptability with age, while adaptability of the astrocyte mostly increases. This observation is in line with the literature on astrocyte reactivity, which measures a set of phenotypic characteristics, including those of metabolism, inflammatory cytokines secretion and cytoskeleton rearrangements (Weber and Barros, 2015). However, in contrast to the "selfish" astrocyte hypothesis (Weber and Barros, 2015), we suggest that the increase in astrocytic adaptability is rather a "self-sacrifice" in an attempt to support the declining neurons.

We visualized the adaptability of the entire NGV metabolic network in the two age groups by

positioning the nodes of both metabolites and enzymes using the Fruchterman-Reingold force-directed algorithm (Hagberg et al., 2008). The length of each of the 16800 edges were weighted by the inverse of metabolic adaptability (Fig. 4e; see Supplementary Information) to more intuitively reflect “metabolic fragility”. These networks displayed clustering of nodes largely by function and also revealed more evenly distributed clusters in young than in old systems, indicative of a robust network. To quantify the network differences between young and aged systems, we calculated the centrality of nodes, which is the reciprocal of the sum of shortest path distances between each node and all other nodes. The aged network showed on average longer distances than the young network (Fig. 4f), suggesting that the aged brain’s metabolic system is more fragile than in the young brain.

To quantify metabolic fragility in the network of the aged metabolic system we progressively removed edges below a given percentile and calculated the number of connected components in young and old networks (Fig. 4g). This analysis revealed that the aged network is fragmented into clusters or “islands”. Both networks are fully connected at thresholds below 76% and fully disconnected at 100%, but between 76% and 93% thresholds, we observed a higher number of connected islands in the aged network. We computed directed simplices, a type of all-to-all connected clique, using algebraic topology (Reimann et al., 2017; Sizemore et al., 2018), to quantify the topological complexity of the network. This analysis revealed that the dimensions (number of nodes) of simplices and the number of simplices (see Methods) are higher in the young state (Fig. 4h-j), indicating that the young metabolic network is more topological complex, more distributed and more robust than in the aged system.

Potential drug targets to repair the aging metabolic system

The scale of the challenge of finding new drugs for therapeutic interventions is revealed by the more than 16800 possible enzyme/transporter-metabolite interaction pathways that we identified in the NGV's metabolic network, in addition to the complexity of the metabolic response when any one pathway is perturbed. The measure of metabolic adaptability can guide identification of targets in the context of this complex dynamical system. Here, interaction pathways with the highest differences in metabolic adaptability (Supplementary Fig. 16) are potential targets to repair the aged metabolic system (Fig. 5a) with high priority targets being those that improve adaptability for the highest number of pathways. The ideal drug to repair the metabolic system is one that acts like transcription factors (TFs), regulating multiple enzymes and transporters to modulate an even larger number of metabolic pathways. We therefore applied the ChEA3 optimization algorithm (Keenan et al., 2019), which isolates the TFs with the largest overlap between a prioritized set of genes for those enzymes and transporters that show the biggest improvement in metabolic adaptability for the largest number of interaction pathways (Fig. 5b). We identified ten highest priority potential targets.

The TF with the best score was ESRRA (estrogen-related receptor alpha). This TF regulates expression of multiple metabolism-related genes, including those of mitochondrial function, biogenesis and turnover, as well as lipid catabolism (Tripathi et al., 2020). It is also linked to autophagy and NF- κ B inflammatory response via Sirt1 signaling (Cantó et al., 2009; Yuk et al., 2015; Kim et al., 2018; Suresh et al., 2018). Mitochondrial dysfunction and autophagy impairments are consistently among the hallmarks of aging (López-Otín et al., 2013, 2023; Mattson and Arumugam, 2018; Amorim et al., 2022). Notably, ESRRA expression is downregulated in aging according to various studies (Schaum et al., 2020; Tripathi et al., 2020). Altogether, ESRRA acts as a regulatory hub of multiple aging-associated pathways as outlined in Supplementary Fig. 19. The other transcription factors that we identified are also validated by literature reports on TFs implicated in aging and neurodegeneration (see Supplementary Information).

To identify the major proteins associated with the top-scoring ESRRA (Fig. 5c), we searched the STRING database (Szklarczyk et al., 2019) and found Hif1a, Sirt1, Hdac8, Ppargc1a, Ppargc1b, Mef2c, Nrip1, Ncoa1, Tfam, Perm1 as the most prominent proteins involved. Numerous literature reports implicate these proteins in aging and neurodegeneration. The repair targets identified using our molecular model of the NGV system therefore largely aligns with experimental data in the literature on therapeutics for healthy aging (Campisi et al., 2019). We additionally suggest a role for less studied

TFs in aging brain energy metabolism and provide insights into the links between molecular mechanisms implicated in aging and neurodegeneration (see Supplementary Information).

Potential strategic interventions to repair the aging metabolic system

As an alternative to specifically targeting the enzymes and transporters, we investigated whether key features of the aged brain phenotype, such as energy deficiency and altered neuronal firing, could be repaired through strategic interventions. We conducted constrained optimizations (see Methods) for 1) the interaction pathway targets identified by the differences in metabolic adaptability (same as the input for transcription factor enrichment analysis above), 2) the interaction pathways potentially regulated by top transcription factor from the enrichment results mentioned earlier (ESRRA), 3) parameters corresponding to arterial blood glucose and ketone levels (mimicking dietary factors), 4) parameters corresponding to arterial blood lactate levels (mimicking exercise factors), and 5) total NAD-pool parameter in neuron and astrocyte (NAD-related supplementation). Surprisingly, optimization using a combination of diet (lower blood glucose and higher blood beta-hydroxybutyrate), exercise (higher blood lactate), and NAD-related supplementation and modulation of the cytosol-mitochondria NAD-associated reducing equivalents shuttle (hereafter referred to as DEN therapy), resulted in increase ATP levels in both neurons and astrocytes towards values of the young metabolic system comparable to that of the top-scoring drug targets (Fig. 5d, Supplementary Table 3). Interestingly, even though the parameter bounds for the optimisation were allowed to search for increasing or decreasing values, the DEN-therapy optimization converged unguided to a lower blood glucose, higher blood beta-hydroxybutyrate, higher blood lactate, and NAD-modulation, which are consistent with commonly accepted benefits of calorie restriction, exercise and NAD supplementation.

The DEN therapy restored the aged metabolic system, but not the action potential generation of neurons. As previously presented, restoring action potential amplitude and shape in our model can only be achieved by increasing the levels of the Na⁺/K⁺ pump back to youthful levels. We therefore additionally reversed the Na⁺/K⁺ pump's age-related downregulation for each intervention (top-scored and DEN-therapy). This approach indeed, restored neuronal firing characteristics similar to those of a young state for each intervention (Fig. 5e) as well as ATP levels of both neurons and astrocytes. Interestingly, insulin is a common factor that activates the Na⁺/K⁺-ATPase, increases its expression, and also lowers blood glucose, consistent with DEN-therapy. When we performed a sensitivity analysis and calculated adaptabilities for the DEN-therapy and top-scored therapy we found that not only could network fragility be repaired, but even improved more than the young state (Fig. 5f).

Discussion

This study presents a molecular model of the neuro-glial vascular system that brings together the key cellular and subcellular systems, molecules, metabolic pathways and processes required to couple neuronal electrical behavior with brain energy metabolism and blood flow. The data-driven strategy developed allows applying experimental data, in principle from any condition, to produce a model of that condition. We applied experimental data from the young and aged brain metabolic systems to produce a model for their respective metabolic systems. We identified 16'800 enzyme/transporter - metabolite interaction pathways in the brain's metabolic system. A sensitivity analysis for each pathway produced a comprehensive view of how each pathway impacts each other pathway to support action potential generation. We find that the impact of one pathway on all the others is remarkably evenly distributed, indicative of a highly robust system with multiple routes to respond to changing metabolic demands and a system that is resilient to damage of any one pathway. By normalizing to resting sensitivities of each pathway we could develop a systems measure for metabolic adaptability for each pathway to evaluate changes in a different condition such as in the aged brain. Our analysis suggests that the aged metabolic system breaks down into islands where enzyme/transporter-metabolite interaction pathways cluster more than in the young brain, leaving this complex molecular system less robust to damage and more restricted when responding to stimuli. We identified the transcription factor, ESRRA and several key proteins it regulates, as top potential drug targets and a prioritization of potential strategic interventions that can repair the aging metabolic system.

The data-driven model we developed captures how brain energy metabolism interacts with neuronal activity with a high degree of biological fidelity. Each enzyme and transporter is modeled using an experiment-derived rate equation featuring its concentration, key kinetic properties, and effects of inhibitors and activators (where applicable and relevant). This approach allows integration of proteomics and transcriptomics data for modeling various conditions and diseases in which molecular levels and properties are affected. Compared to the more generalized phenomenological metabolic models, the model features 183 processes, including 95 enzymatic reactions, 19 processes for the transport of molecules across the cell and mitochondrial membranes, and 69 other processes for ionic currents, blood flow dynamics and other related non-enzymatic processes. Changing molecular concentrations are simulated using 151 differential equations. Additionally, cytosolic ADP, creatine, NAD, NADP are computed from the conservation law and total pool of relevant molecules.

The strategy we followed to build such a complex model was to apply biologically reported parameters for the components of the model (see Methods) and avoid overriding biological values to fit reports on time series of metabolic responses found in the literature that are few and often contradictory. In order for the system of equations to have a solution, we optimized the parameters by only requiring steady state solutions at rest, rather than changing the parameters to fit the metabolic time series responses reported in the literature, which are limited and often contradictory. Alternative approaches that have been used by others include likelihood-based optimisation targeting the reference time series data. This approach was not suitable in our case because the data was not available for most metabolites for meaningful likelihood-based parameter estimation with recorded traces of metabolite levels in the neurons and astrocytes. Bayesian parameter estimation, also previously used, was computationally too costly for the scale and complexity of our model. To increase the biological dataset for parameterization, we merged data across *in vitro* and *in vivo* conditions and averaged across natural biological variability. In some cases, we had to optimize weakly constrained parameters or include only the most relevant components, pathways and processes (see Methods). The model, while containing an unprecedented level of detail, is also not yet at a whole genome level. Similarly, while the model captures the key cellular elements, compartments and sub-compartments it does not yet capture explicitly the details on all possible geometric constraints.

The model validated against numerous experimental datasets, but a key litmus test was simply whether computational convergence occurred for this complex system. Parameters were minimally optimized to allow convergence for a steady state at rest, but a self-constrained converged state emerged when the system was stimulated with current injection and synaptic input. On the other hand, when we introduced random modifications to enzyme and transporter concentrations and their kinetic parameters, some numeric solutions failed or diverged far from the steady state at rest. It is therefore even more remarkable that simulations converged without significant modifications introduced when we imported and applied the data from the aged brain. Furthermore, single parameter perturbations introduced instabilities in the simulations more often than when multiple RNA-seq derived changes were introduced, suggesting that the set of parameters are self-constraining.

Our results in both young and aged brain states align well with a wide range of published experimental reports. Aside from the time series profiles of specific metabolites, enzymatic activities and, aging-observations, it is particularly noteworthy that the estimates that emerged from the simulations for the ATP consumption (Howarth et al., 2012; Yi and Grill, 2019; Zhu et al., 2019) and how aging-associated changes in metabolism affect neuronal action potentials are consistent with

experimental reports (Power et al., 2002; Disterhoft and Oh, 2007; Kumar and Foster, 2007; Smithers et al., 2017; Vitale et al., 2021).

Calculating sensitivities is common when studying dynamical systems. In addition to sensitivity analysis, for the system undergoing transition between rest and stimulated states, we introduced adaptability and fragility as biologically interpretable measures. These measures capture the effects of perturbing an enzyme or transporter on all the metabolite levels in response to stimuli. These perturbations mimic the effects of conditions such as phosphorylation levels, transcription and translation errors, as well as molecular damage to enzyme and transporter kinetic properties. Perturbation analysis predicted diminished adaptability to changing energy demands with different changes in neurons and astrocytes in the aged brain. We could construct a network of enzyme-transporter - metabolite interaction pathways where each pathway can be evaluated in terms of metabolic adaptability allowing quantification of the changes. We find a structural breakdown and decreased topological complexity of the NGVmetabolic systems in the aged network as compared to young.

To identify potential targets where the youthful state can be restored, we identified the most fragile interaction pathways. We performed transcription factor enrichment analyses for the most sensitive enzymes and transporters. Functions of these targets largely overlap with known mechanisms of aging. Through constrained optimization, we identified a combination therapy that restores key features of the aging brain phenotype. This therapy involves maintaining specific levels of blood glucose, lactate, and β -hydroxybutyrate achievable through diet and exercise, coupled with redox state maintenance via NAD-supplementation, modulation of the cytosol-mitochondria reducing equivalent shuttle (related to NADH), and Na^+/K^+ -ATPase activation. For instance, reversing the aging phenotype can be achieved in part by regulating insulin signaling, which lowers blood glucose and activates Na^+/K^+ -ATPase.

Complex interventions that act on multiple enzymatic targets at the same time, including some of the top potential targets of DEN-therapy, also managed to restore ATP levels in cells. However, their development and implementation would require significantly more extensive research before they could be considered for practical application in treating aging-related conditions. The outcomes of these complex therapies appear to be comparable to those achieved with the simpler DEN-therapy.

The promising combination therapy identified in this study, which includes diet, exercise, NAD supplementation, NAD shuttle and Na^+/K^+ -ATPase modulation, agrees well with proposed anti-aging

interventions such as caloric restriction, the ketogenic diet, and exercise (López-Otín et al., 2023). Physical exercise shows beneficial anti-aging and brain-health effects mediated by the brain-derived neurotrophic factor (BDNF), insulin-like growth factor 1 (IGF-1) and lactate (Horowitz et al., 2020; Stillman et al., 2020; Xue et al., 2022). The ketogenic diet and caloric restriction, for example, impact the levels of β -hydroxybutyrate and glucose in the blood (Meidenbauer et al., 2014). Supplements such as urolithin (Singh et al., 2022), metformin (Kulkarni et al., 2020), and nicotinamide mononucleotide (Yoshino et al., 2018) affect mitochondrial health, energy supply and provide anti-inflammatory action, consistent with the important role of metabolism in aging.

The multiple validations and insights consistent with current findings suggest that the model can guide experiments on brain aging and diseases, including those on disease-associated genetic variants, enzymatic deficiencies, and the effects of different practical strategies. Energy-metabolism related transcriptomics, proteomics and metabolomics data can also be applied to the model to study their effects on metabolic dynamics and neuronal firing. Furthermore, the model can simulate a variety of stimuli to neurons to guide studies on the energy constraints of brain activity. To accelerate these research areas, the model is open sourced for public use (link provided after acceptance).

Data Availability

All the data used in this study are publicly available from referenced sources. The model is available on the web portal (<https://bbp.epfl.ch/ngv-portal-dev/>) [it will be available after peer-reviewed publication].

Funding

This study was supported by funding to the Blue Brain Project, a research center of the École Polytechnique Fédérale de Lausanne, from the Swiss government's ETH Board of the Swiss Federal Institutes of Technology.

Acknowledgements

The authors thank Judit Planas Carbonell, Claudia Savoia, and Jean-Denis Courcol for organizing web portal development and visualization, and Matthias Wolf for software support. We thank Karin Holm for writing assistance and Ayima Okeeva for the model notebook evaluation.

Author contributions.

PS: developed the model, performed analyses, developed the figures, contributed to conceptualization and interpretation of results, metabolic network metrics and writing. JSC: contributed to the conceptualization, interpretation of results and writing. LK: contributed the topological analysis and interpretation of network results, and related figures. EB: contributed to figures. CF: developed the movie on the portal. SA: developed the web portal. DK: contributed to conceptualization, interpretation of results, and writing. HM: contributed to conceptualization, interpretation of results, metabolic network metrics, and writing.

Declaration of interests.

The authors declare no competing interests.

Figures.

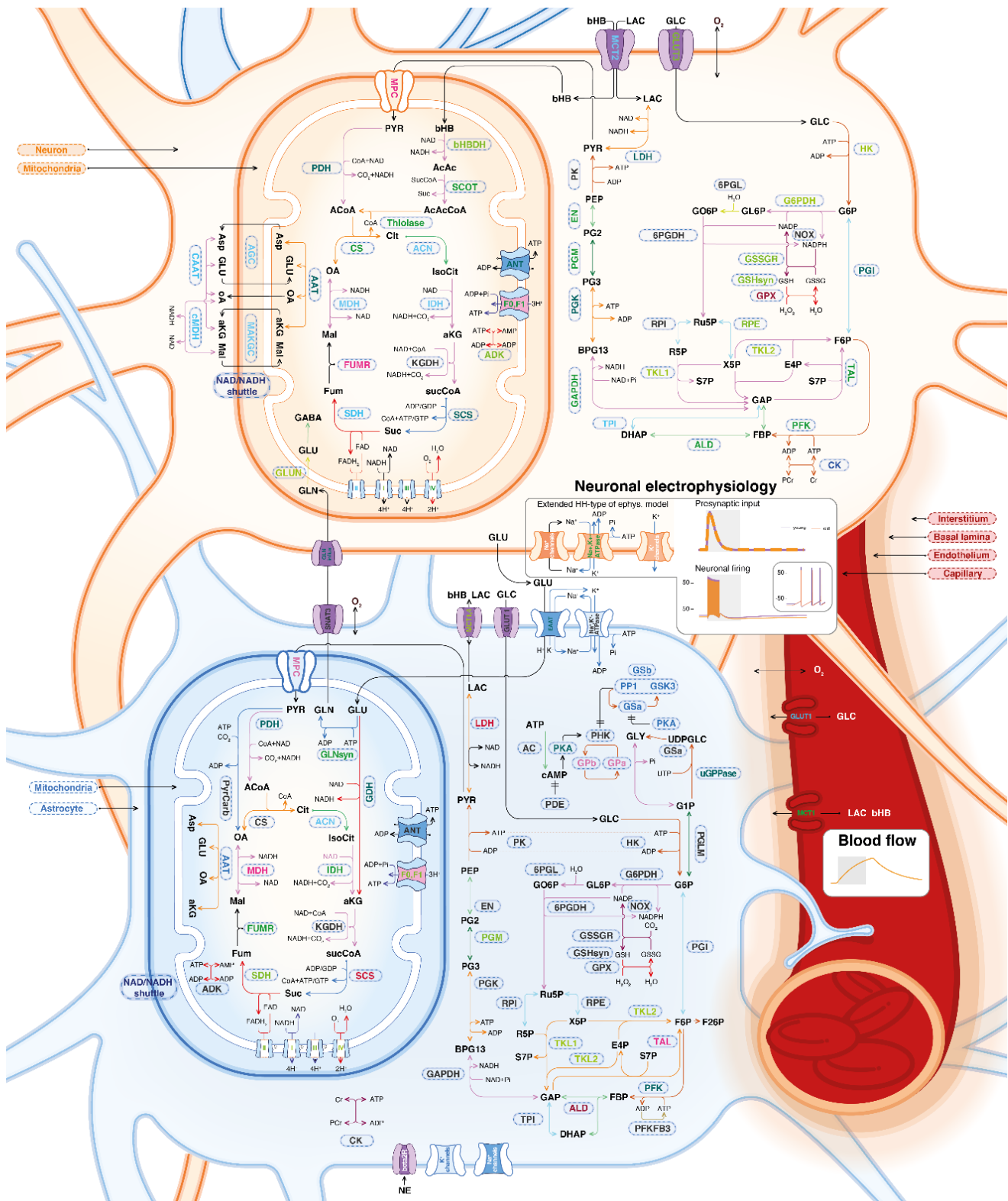
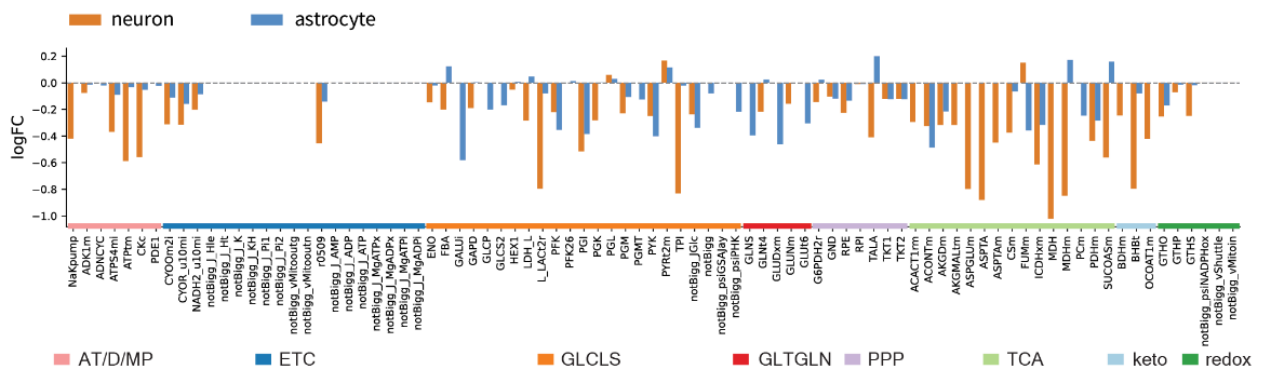


Fig. 1. Model overview. The model consists of three connected sub-systems: metabolism, neuronal electrophysiology and the blood flow. Compartments of the model include the neuronal and astrocytic cytosol, mitochondrial matrix and intermembrane space, interstitium, basal lamina, endothelium,

capillary, artery (only with fixed arterial concentrations of nutrients and oxygen), and endoplasmic reticulum (only with Ca^{2+} fixed pool). Enzymes and transporters shown in the figure correspond to the rate equations in the model which govern the dynamics of metabolite concentration changes. Neuronal electrophysiology is modeled in a slightly extended Hodgkin-Huxley type of model. Blood flow activation is described by a simple function dependent on the stimulus onset and duration according to the literature models.

a Aging model input

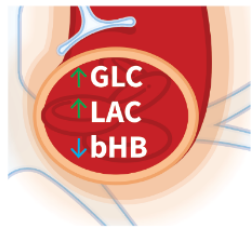
Changes of the enzymes and transporters RNA expression in aging



Additional changes in aging

↑ up ↓ down

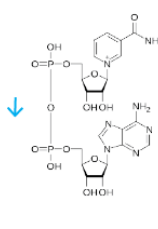
Blood nutrients availability



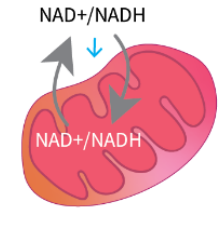
Synaptic glutamate release



NAD⁺, NADH pool



NAD⁺/NADH cyto-mito shuttle rate



NGV dynamical model of metabolism, neuronal electrical activity, blood flow

b Overview of metabolism changes associated with aging

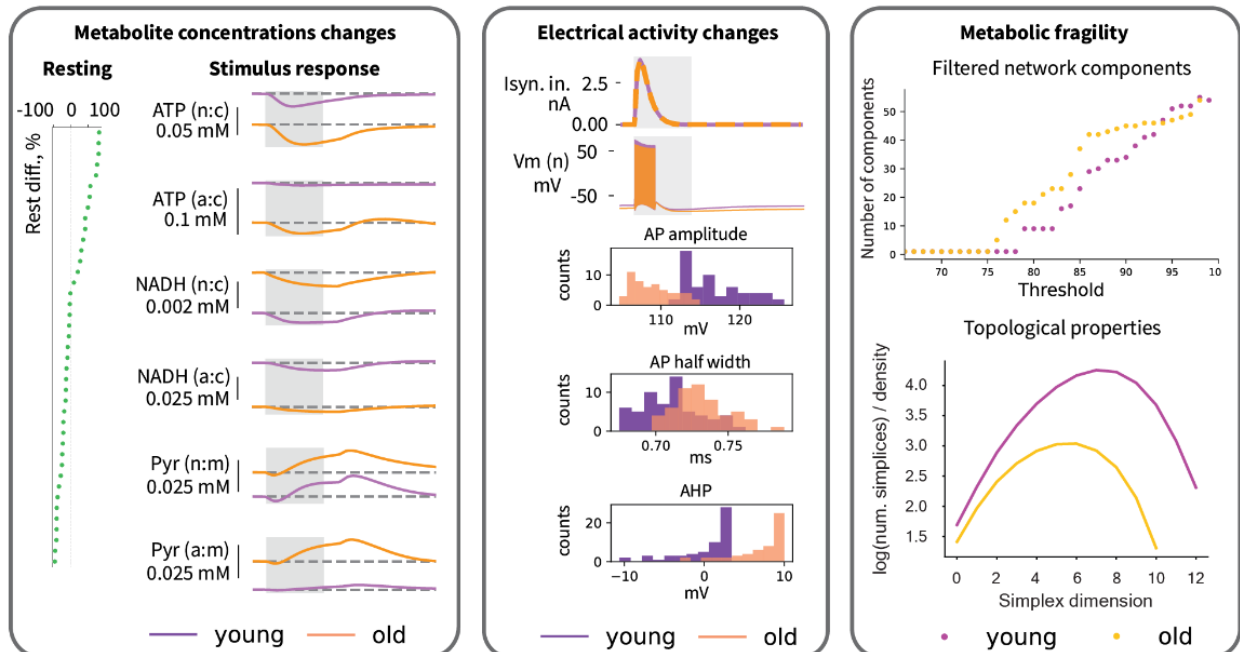


Fig. 2. Aging model input (a) and results overview (b). a, Aging input is modeled with RNA expression fold changes of enzymes and transporters, scaling of arterial glucose, lactate and b-hydroxybutyrate, as well as the total NAD (reduced and oxidized) pool, synaptic effects of glutamate

concentration changes upon release events, and the reducing equivalents (NADH-related) shuttle between cytosol and mitochondria. **b**, The key results include aging effects on metabolite levels, electrical activity of the neurons, and changes in adaptivity of the system in response to kinetic parameter perturbations (mimicking molecular damage and other conditions affecting enzyme and transporter functions).

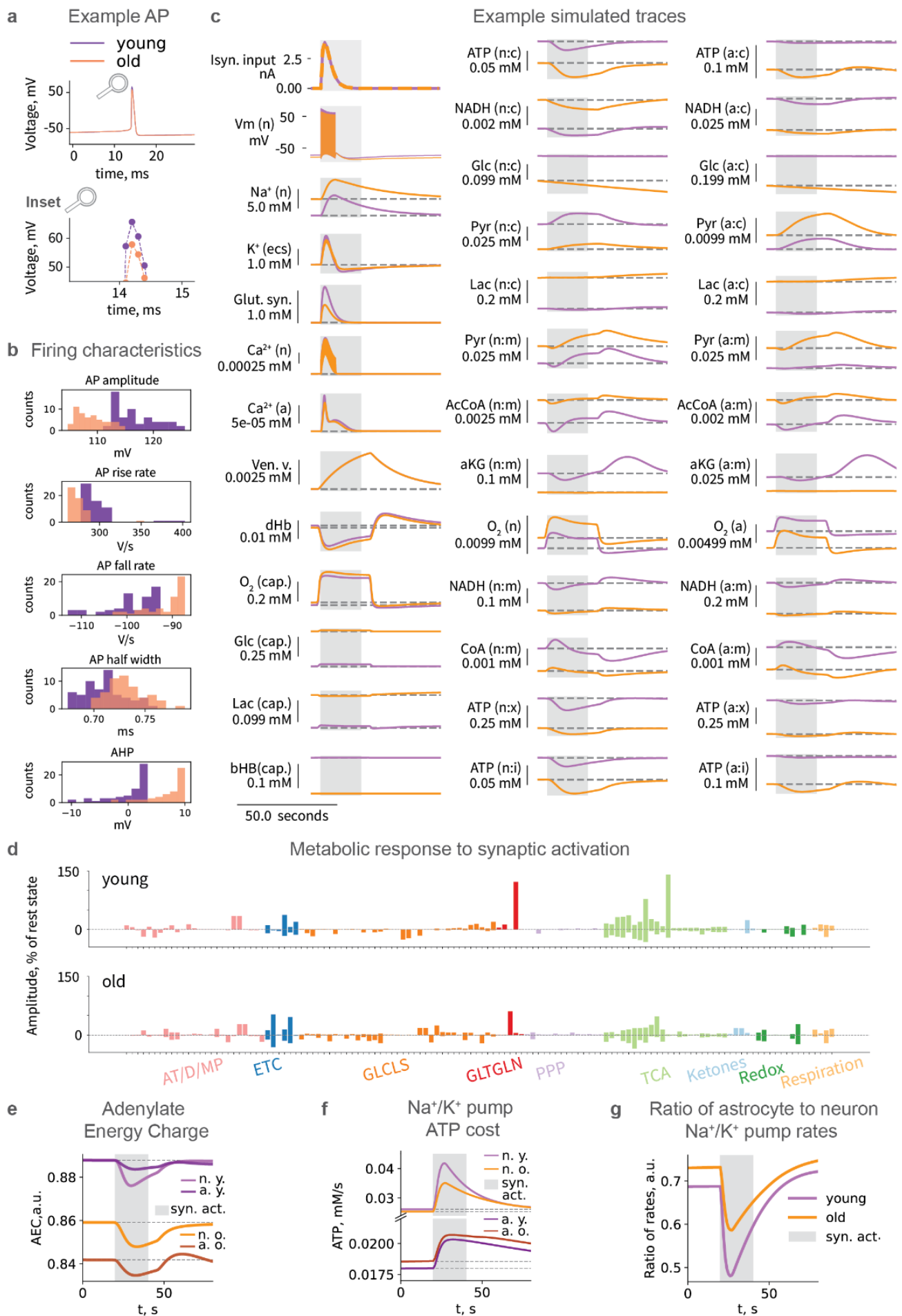


Fig. 3. Simulation results. a, Example AP in voltage traces in simulations of young and aged neurons with insets providing a closer view. **b**, Characteristics of neuronal firing in young and old ages upon synaptic activation. **c**, Dynamics of metabolism in response to synaptic activation at different ages (only a selection of the most important variables is shown). Compartment names abbreviations: n - neuron, a - astrocyte, c - cytosol, m - mitochondria, x - mitochondrial matrix, i - mitochondrial IMS, cap. - capillary. **d**, Amplitude of concentration changes in response to synaptic activation in young (top) and old (bottom), individual metabolites labels are available in **Supplementary Fig. 18**. **e**, AEC: Adenylate Energy Charge in young and old neurons and astrocytes ($AEC = (ATP + 0.5ADP)/(ATP + ADP + AMP)$). **f**, Main energy consumption: Na^+/K^+ -ATPase rate of ATP use. **g**, Ratio of astrocyte to neuron Na^+/K^+ pump rate.

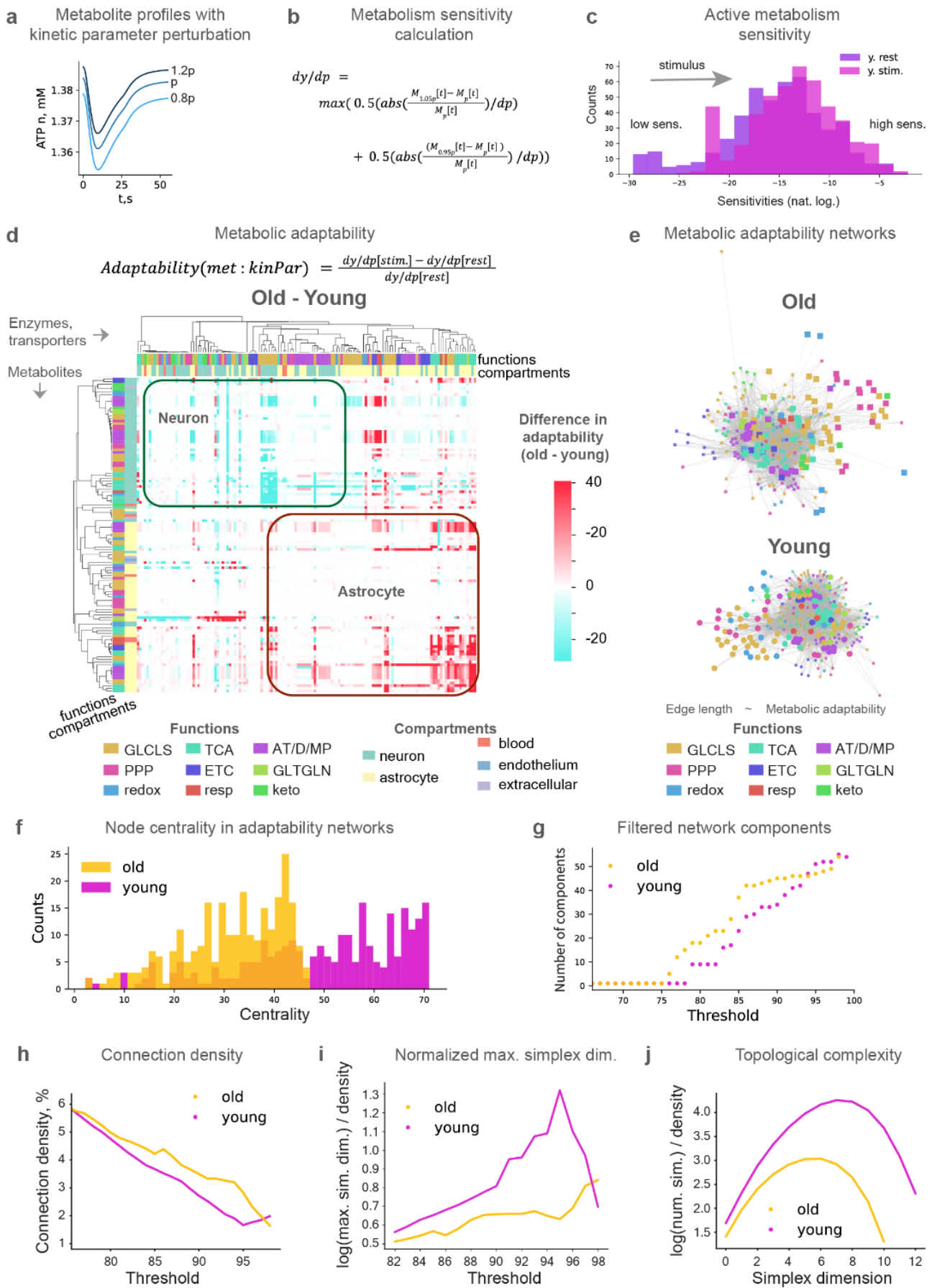


Fig. 4. Metabolic response to kinetic perturbations changes with age. **a**, Example metabolite level profiles in response to kinetic parameter perturbation. **b**, Calculation of metabolic sensitivity to kinetic parameter perturbations. **c**, Active metabolism sensitivity. **d**, Metabolic adaptability to kinetic parameter perturbations. **e**, Metabolic adaptability networks in young and aged (same function-color relation as in **d**). **f**, Centrality of the nodes in the networks of metabolic adaptability aggregated by enzymes. **g**, Number of connected components in filtered networks of metabolic adaptability aggregated by enzymes. Ions, membrane potential, gating variables, mitochondrial membrane potential, and metabolites with fixed concentrations are removed from the analysis for all figures in this panel. **h**, Connection density of filtered networks. **i**, Maximum simplex dimension (log-transformed) normalized by connection density. **j**, Number of simplices (log-transformed) normalized by connection density (at 88% filtering threshold).

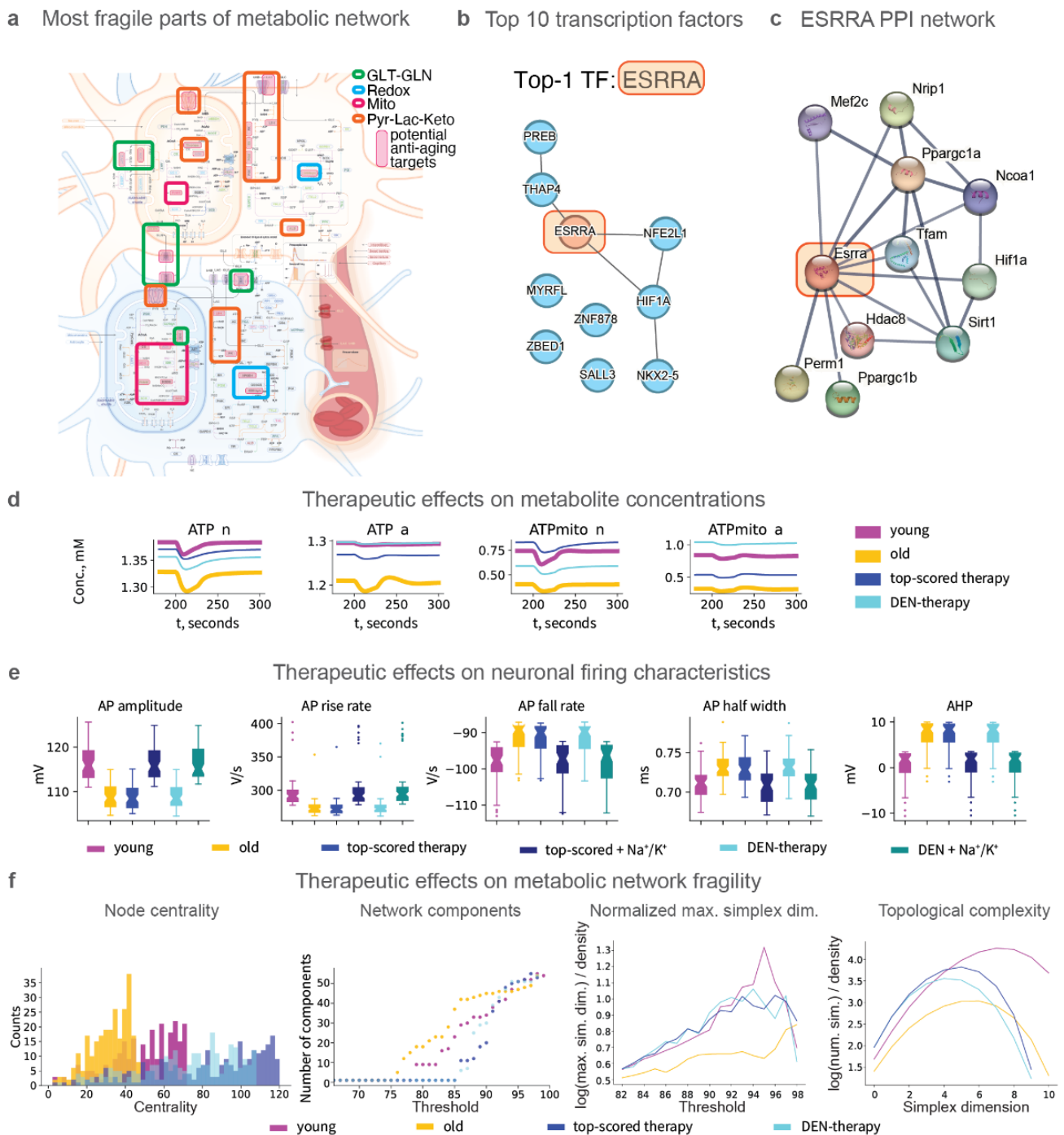


Fig. 5. Reversing aging via targeted metabolism interventions. **a**, Sensitivity analysis-based potential targets are outlined by pink boxes and grouped by function in thick line boxes in the modeled system. **b**, Transcription factor enrichment results obtained from ChEA3 analysis (the top 10 TFs are shown). **c**, Results of the STRING-database search for ESRRA (the top TF from ChEA3 analysis). **d**, Time series traces of selected variables in young, aged, and treated aged states. **e**, Characteristics of neuronal firing in young, aged, and treated aged with selected therapies. In addition to selected top-performing and top-translatable therapies, we restored Na^+/K^+ pump expression to the young state. Application of the Na^+/K^+ pump expression restoration and each of the treatments restored

characteristics of neuronal firing. Center line represents the median. **f**, Therapeutic effects on metabolic network fragility.

Methods

Baseline model building

We reconstructed and simulated a model of NGV metabolism coupled to a simple blood flow model and a Hodgkin-Huxley (HH) type of neuron model. The main concepts of electro-metabo-vascular coupling, as well as blood flow and neuronal electrophysiology model are based on the models available from the literature (Aubert et al., 2001; Jolivet et al., 2015; Calvetti et al., 2018; Winter et al., 2018). Our model specifically emphasizes the key brain energy metabolism pathways and processes involved in neuronal signal transduction. However, to gain a more comprehensive understanding of the various complementary molecular mechanisms and pathways involved in aging and disease, it is desirable to further expand the model to a whole-cell scale and incorporate more regulatory processes. At present, this task is hindered by data sparsity. As more data becomes available, the model can be iteratively refined and expanded.

Compared to the more generalized phenomenological metabolism models, our metabolism model features 183 processes (95 enzymatic reactions, 19 processes of transport of molecules across the cell and mitochondrial membranes, and 69 other processes related to ionic currents, blood flow dynamics and some miscellaneous non-enzymatic processes, e.g. Mg^{2+} binding to mitochondrial adenine nucleotides). Every reaction, transport or other process is represented by its rate equation, which is literature-derived. Changes of molecular concentrations are described by a system of 151 differential equations and additionally cytosolic ADP, creatine, NAD, NADP are calculated from the conservation law and total pool of relevant molecules.

The model is based on literature data for enzyme kinetics and molecular concentrations. We have meticulously collected all parameters and equations from literature sources, as referenced in Supplementary Table 2 and throughout the model code, and programmatically queried databases BRENDA (Chang et al., 2021), SabioRK (Wittig et al., 2018). However, observed discrepancies in the parameters reported by different sources define the need for an optimization procedure, to derive plausible biological middle-ground. The parameters with uncertainties observed in the literature were

constrained by their lower and upper bounds taking into account the type of the parameter (Michaelis constant of reaction, inhibition/activation constant, maximal rate of reaction, equilibrium constant, Hill coefficient) and optimized as described in the Optimization part of the Methods.

To have the most realistic biological average for the initial values of all variables (concentrations, membrane potential, mitochondria membrane potential, venous volume, gating variables) according to the literature, we considered not only measured and modeled literature data on the absolute values themselves, but also additional constraints, such as known ratios of NADH to NAD⁺ in the neuron (Neves, 2011; Dienel, 2012; Berndt et al., 2015; Mongeon et al., 2016) and astrocyte (Mongeon et al., 2016). One of the most important variables in the model, ATP concentration, was reported as being 2 mM in many experimental and modeling studies (Erecińska and Silver, 1989; Cloutier et al., 2009; Jolivet et al., 2015; Calvetti et al., 2018; Winter et al., 2018). However, some more recent data report it at 1 to 1.5 mM scale (Baeza-Lehnert et al., 2019; Köhler et al., 2020). Assuming that more recent measurement technologies can provide more precise data, we set cytosolic ATP in the neuron to approximately 1.4 mM according to Baeza-Lehnert et al. (Baeza-Lehnert et al., 2019) and to approximately 1.3 mM in the astrocyte according to Köhler et al. (Köhler et al., 2020) where it was reported in a range of 0.7 to 1.3 mM (acutely isolated cortical slices) and 1.5 mM (primary cultures of cortical astrocytes).

Mammalian ATP to ADP ratios are reported in a very wide range of values from 1 to more than 100 (Tantama et al., 2013). Ratio of ATP to AMP is around 100 (Erecińska and Silver, 1989). Furthermore, metabolite ratios from (Erecińska and Silver, 1989) were used to adjust initial concentrations of phosphocreatine and phosphate to the ATP levels. Lactate concentrations in different compartments, which is central to the ANLS debate, was set according to the recent Mächler et al. paper (Mächler et al., 2016). We also tested the model with all alternative literature concentrations for the metabolites mentioned above.

Glucose supply from blood is of key importance to brain energy metabolism (Benton et al., 1996). For this reason we approached it particularly meticulously. In our model, glucose concentrations are assigned to detailed compartments, such as arterial, capillary, endothelial, basal lamina, interstitium, neuronal cytosol and astrocytic cytosol (Barros et al., 2017). According to the literature, hexokinase flux is split approximately equally between neuron and astrocyte (Barros et al., 2007, 2017; Jolivet et al., 2010), so that we adjusted V_{max} of hexokinase so that its flux matched the literature data at rest.

Upon activation, the ratio of glucose influx to astrocyte versus neuron increases, consistently with the literature knowledge (Jolivet et al., 2010).

Implementation and simulation.

This metabolism model is implemented and simulated in Julia programming language (Bezanson et al., 2017). We used the DifferentialEquations.jl package (Rackauckas and Nie, 2017) to solve the differential equations system using order 2/3 L-stable Rosenbrock-W method (autodifferentiation disabled, both absolute and relative tolerances set to 1e-8). We chose to use the Julia language because of its high performance, its extensively developed mathematical methods ecosystem, and the readability of the code, which supports its future use. Most of the analysis and figures-making code is written in Python programming language.

The model is built in a modular way, so that every molecular process has a dedicated rate function, and combination of relevant rate functions defines the dynamics of variables. This supports convenient testing of various enzymatic mechanisms, parameters and initial values of concentrations, as well as easier model subsetting and expansion.

Once the manuscript is accepted for publication, we will provide the GitHub repository with the code for model simulation, optimization, validation and analysis. These scripts are aimed to facilitate the model's reuse in future studies.

Optimization.

Time series data on the dynamics of specific metabolites in neurons and astrocytes is very sparse and sometimes contradictory. To avoid favoring one data source over another, we only performed optimizations for the steady state (minimizing derivatives). We built and optimized the model bottom-up in multiple iterations, gradually expanding it with more details. We started with the model of neuronal electrophysiology (Pospischil et al., 2008; Øyehaug et al., 2012; Jolivet et al., 2015; Krishnan et al., 2015; Calvetti et al., 2018). We included detailed astrocytic ion management based on the existing literature model (Witthoft et al., 2013). Then for the metabolism model, we started with capillary dynamics, oxygen and glucose transport, and hexokinase, because they are very well studied and CMR of glucose is widely measured, which sets a strong constraint on hexokinase rate. Then we proceeded to add reaction by reaction and evaluate rates in simulations, each time adding a new reaction, first if needed roughly manually refining underconstrained parameters. Then after several

reactions were added, we ran optimization (with an objective to minimize derivatives) for a selected small set of parameters which are the least constraint by the literature. Then we modeled lactate transport and connected it to glycolysis. We separately optimized PPP for steady state (with an objective to minimize derivatives). For the mitochondria, we started from the electron transport chain, which is mitochondrial-membrane potential dependent and extremely sensitive to parameter variations. We mostly used the ETC model from Theurey and the colleagues (Theurey et al., 2019), and then we carefully selected a small number of parameters to optimize them (with an objective to minimize derivatives) to make the ETC model compatible with ATP and ADP concentrations from more recent experimental evidence. Then we added one-by-one TCA reactions to ETC, the same way as described above for other pathways. And we also added ketones metabolism, part of MAS, glutamate-glutamine cycle (after having both neuron and astrocyte together in the system).

The optimization procedure referenced above is single objective optimization performed using `BlackBoxOptim.jl` [<https://github.com/robertfeldt/BlackBoxOptim.jl> of Robert Feldt] with the default algorithm (adaptive differential evolution optimizer) iteratively selecting different sets of processes to reduce the parameter space.

To avoid non-physiological molecular concentrations (negative or too high values), we used Julia-callbacks and the “isoutofdomain” mechanism in solving the differential equations system during optimization. For these biological plausibility reasons, we utilized “isoutofdomain” to control the solution of the differential equations system to stay non-negative, so that the solver takes smaller time steps if the solution leaves the domain, unless the minimum step size is reached and integration is terminated. The same methods were applied for the anti-aging optimization, but the selection of neuronal firing related variables from the young state simulated time series data were used for the objective function.

Computational models are often optimized by fitting parameters to the data using a selected algorithm. Indeed, some time series data are available for various aspects of brain metabolism, including for concentrations of glucose, lactate, pyruvate, NADH and ATP, the BOLD signal, and cerebral metabolic rates of oxygen and glucose. However, to our knowledge these usually come from different experiments rather than simultaneous measurements of multiple metabolite concentrations and other characteristics. It has been demonstrated by numerous studies that one can fit system dynamics to selected data given a sufficient number of weakly constrained parameters and nonlinear rate equations (Dyson, 2004). An interesting case is when measurements with similar metadata from different studies

produce significantly different dynamics of metabolite concentrations, such as in the example of extracellular brain glucose from Kiyatkin and Lenoir (Kiyatkin and Lenoir, 2012) as compared to Fillenz and Lowry (Fillenz and Lowry, 1998), which was further used in one of the early integrative NGV models (Cloutier et al., 2009). We therefore aimed to avoid the global optimization of fitting parameters to selected time series. Instead we iteratively refined the bottom-up model by estimating parameters that would achieve the desired values of metabolite concentrations at steady state (in which the concentration derivatives with respect to time are minimized). More details are available in the next section (workflow and the key aspects) and the entire pipeline is shown in Supplementary Fig. 17. However, this approach has a downside: it does not guarantee exact matching of the experimentally recorded dynamics of any selected experiment. Good match with the time series observed experimentally and in other models can only be obtained if the underlying model has a sufficient level of detail, uses relevant kinetic data for initial parameterization and employs applicable constraints (e.g., physiological range of metabolite concentrations, typical range of values for kinetic parameters of a given type). While many time series produced by our model are close to the literature reports, glucose concentration traces and cerebral metabolic rate of glucose consumption have only modest stimulus responses as compared to the literature. This can be explained by our decision to follow the most detailed (to our knowledge) approach to glucose transport in the brain available in the literature (Barros et al., 2007; Simpson et al., 2007). This approach takes into account compartmentalisation into arterial, capillary, basal lamina, interstitial space, astrocytes and neurons, with glucose transfer between these compartments described by rates that consider intracellular/extracellular concentration-dependent trans-acceleration and asymmetry of transporters.

Workflow and the key aspects of the bottom-up model building and optimization

In order to build the model in a bottom-up data-driven way and avoid unreasonable preference for any particular data source, we developed a workflow, which resulted in the model performing surprisingly well for different setups. It produced quality simulation outcomes which are largely consistent with various literature. The only drawbacks are that the workflow is largely iterative, time-demanding, and requires manual intervention. Here are the steps and the key considerations.

Step 1. Collect as much reliable data as available. In our case of building a model which combines the metabolism, electrophysiology and the blood flow, the following data were needed: molar concentrations of molecules (metabolites, proteins, ions), enzymes and transporters kinetic parameters, electrophysiology and blood flow dynamics parameters, rate equations of all processes, mechanisms of

reactions and the data on their inhibitors and activators with corresponding mechanisms of action, existing models of pathways and their combinations. In most cases, reaction rate is modeled in the literature with at least a few different equations. This is due to the use of different formalisms. For example, the same reaction can be described in a precise mechanistic way considering multiple transition states of complexes formed by enzyme with substrates, products, regulators, or it can be described in a more simplified form of modular rate law or Michaelis-Menten kinetics, when assumptions about the reaction mechanism are met. It is important to keep collected models of reactions and how they are used in the existing models of pathways and systems, because for practical applications the scale of the model needs to be balanced with how many parameters are used for each equation in the model. For example, detailed mechanistic rate equations can be parameterized well for small models when there is enough consistent reliable data, but for cases with high uncertainty in the data, it is often hard to optimize and not overfit such models.

Step 2. Next, we model individual reactions. In some cases (most of which are relatively old biochemistry studies), time series data on individual enzymes are available. These can be used to optimize the parameters of enzymatic rate equations, especially if they are underconstrained, coming from different species or tissues. This step also allows us to evaluate how fast individual reactions are, how significant are the effects of inhibitors and activators and whether to include them in the model or not, and how problematic each particular reaction is in terms of the steady state and response to changing inputs.

Step 3. Once the data is collected, we bring together reactions one-at-a-time according to the reconstructed pathways networks. This process is highly iterative and needs to be repeated multiple times starting from different data. We need to try multiple combinations to see in which cases the optimization needed to bring the combination close to steady state is minimal. It is also important to combine those small subsets of reactions with pseudo-reactions of substrates source flux and products sink flux, to have an estimate of how this unit will perform once it is plugged into a bigger system. Iterating on this step, one can grow the system up to the models of pathways in individual cells, and existing models of those pathways are very helpful for initial choice of the most promising combinations of reaction rates and parameters. It is also useful to keep approximately the same level of detail for the equations of all reactions in the pathway. For the refinement of the parameters when connecting reactions in a pathway, instead of just following commonly used list of reactions of the pathway in order the metabolites enter it, it is useful to start from different steps of the pathway, especially with the reactions which are either known key regulators of the overall pathway flux

(bottlenecks) or close to connection points to other pathways, or those with the most complicated mechanisms. The key aspects to decide on the performance of selected parameters set in the model are the concentrations at the steady state (or pseudo-steady state if the formal one cannot be achieved in a reasonable time), their response to stimuli (at least qualitatively in which direction and approximately how fast do they change, when no data is available), reaction and transport fluxes. It is important to keep several best performing models for all subsystems/pathways, because once they are plugged into a bigger system, performance ranking can change.

Step 4. Once small units/pathways are built in at least a few variations, they can be connected into bigger systems. For the optimization of connecting reactions, it is important to start from different entry points, compare overall fluxes of the pathways, and consider volumetric scaling aspects. In some cases temporary use of pseudo-reactions for source and sink of some metabolites for the optimization significantly improves the performance.

Step 5. The large metabolic system can further be connected (using the same strategy as in Step 4) to the electrophysiology and blood flow models. Electrophysiology and blood flow models can be found in the literature in a number variations and need to be optimized separately if needed.

Step 6. The models of the neuron and the astrocyte can be connected in the same way as described above. Simulations and sensitivity analysis can further be used to select the parameters optimization of which has the highest effects and can efficiently improve the model according to available data. If no consistently reliable data is available, the objective function can be set to minimization of derivatives at rest state for the system to be at the steady state.

Validation.

First, we tested the response of the key metabolites (ATP, NADH, lactate, glucose) to the stimuli. All concentration related variables were ensured to stay in the range of biologically plausible values by the callbacks and the “isoutofdomain” parameter to a solver as described in the Optimization part of Methods. Next, we calculated the BOLD signal (Supplementary Figure 1d) and OGI (in range of 4.5-5 depending on stimulus, while literature data is in range of 4-5.5) using equations from Jolivet et al. 2015 to compare them with the literature (Jolivet et al., 2015; Winter et al., 2018; Jung et al., 2021). These two high-level phenomena are commonly used as benchmarks in NGV metabolism modeling papers (Jolivet et al., 2015; Calvetti et al., 2018; Winter et al., 2018). We also qualitatively compared dynamics of some key metabolites and reaction and transport fluxes to their expected response to

stimuli. Then we estimated energy use from the components of the Na^+/K^+ -ATPase rate equation (calculated from sum of neuron and astrocyte Na^+/K^+ pump ATP consumption flux in mM concentration per second with the volume of $17.8 \text{ } \mu\text{m}^3$ and the literature estimate of ionic gradients sharing 31% of total energy use) and compared it to the literature estimates (Howarth et al., 2012). We further validated aging-associated effects against the literature data shown in Supplementary Table 1.

Implementing aging effects in the model

Aging is a multifactor phenomenon which affects metabolism at different levels: transcriptome, proteome, metabolome, and potentially even kinetic properties of enzymes and transporters due to accumulated genetic damage, lower protein synthesis fidelity and higher chances of protein misfolding. To implement the aging effect in our model in a fully data driven way, the data on neuron and astrocyte specific proteomics, metabolomics and kinetics of enzymes are needed. However, most of such data is not yet publicly available.

We modeled the aging effects as following:

1. enzymes and transporters expression fold changes from TMS dataset (Schaum et al., 2020; Zhang et al., 2021a) applied as scaling factors to levels of corresponding enzymes and transporters
2. scaled initial concentrations of blood glucose, lactate, beta-hydroxybutyrate according to the literature data on difference in their levels in aging (approximation, because effect size depends on the literature source)
3. total NAD^+ and NADH concentration pool scaling, because it decreases in aging according to qualitative literature (approximation)
4. synaptic glutamate release pool (approximation, but synaptic input is set the same for comparability of the results)
5. scaling of reducing equivalents shuttles between cytosol and mitochondria: NADH shuttle is a generalized rate equation based on activity of multiple enzymes of malate-aspartate and glycerol-phosphate shuttles, for which we followed literature to model it (Jolivet et al., 2015).

For the above factors, which mention “approximative/approximation”, the direction of change is according to the literature, but the absolute number of scaling factors (not known/contradictory in the literature) is set with an objective for the model to be steady at rest.

We implemented the aging effects on enzyme and transporter levels in two parallel ways: 1) using cell-type specific transcriptomics data (Schaum et al., 2020; Zhang et al., 2021a) and 2) using integrated proteomics data from the metaanalysis we performed earlier (Shichkova et al., 2021). The first approach featured higher coverage depth for the astrocyte-specific data. So that, to reduce bias from inferring missing data in the second method, we decided to rely on RNA data for implementing aging effects into simulation, while we used the second data source as a part of validation.

RNA fold changes for modeling aging effects

An extensive single-cell transcriptomics mouse dataset has recently become available (Schaum et al., 2020; Zhang et al., 2021a), providing insights into the aging patterns of various cells including neurons and astrocytes. However, RNA needs to be translated into proteins. RNA data need to be used with caution when inferring age-dependent protein concentrations. Nonetheless, using RNA fold changes to scale enzyme and transporter levels results in metabolite concentration changes consistent with the literature (Supplementary Table 1).

We mapped reaction IDs to gene names using the gene-reaction-rules from a publicly available metabolism reconstruction Recon 3D (Brunk et al., 2018). Then for the cases of multiple genes per reaction (i.e. enzymes built of several protein subunits or different isoforms present at the same time) we calculated age-scaling in two ways: 1) by using geometric mean of all fold changes, and 2) taking fold changes which results in lowest levels of RNA in aging, i.e. using the assumption that each protein subunit or isoform can be rate limiting if its concentration is not sufficient to build fully-functional protein. We applied each of these methods twice: for all genes and only for those with significant changes (significance defined by the source data paper). Next, we manually went through the mapping of all genes to reactions and kept only those that are enzyme subunits/isoforms and not regulatory factors. We then refined it by subcellular location.

Protein levels for modeling aging effects

Several studies measured brain protein levels in different ages, but they provided mostly brain tissue/regions data, rather than single neuron and astrocyte age-specific protein levels. The other studies provided neuron and astrocyte specific protein levels, but they were either using cultured cells, or young/adult rodents. For these reasons even a combination of proteomics data sets remains sparse in terms of cell-type and age specific protein quantification. Even though using protein levels directly to scale V_{max} of the enzymes and transporters would allow consideration of posttranscriptional effects of

protein synthesis and degradation, to reduce potential bias, we decided to rely only on the RNAseq data for age-associated changes in enzyme and transporter levels.

Other necessary aging factors

Arterial glucose, lactate and b-hydroxybutyrate, as well as total NAD (reduced and oxidized) pool are fixed in the model, but multiple studies report that they change in aging. For this reason we scaled them according to the literature. The resulting model was far from steady state, which could be explained by some missing age-associated changes. We then scaled NADH exchange between mitochondria and cytosol, as it is also known to be affected by the aging process, and it resulted in a well-functioning model producing biologically meaningful observations. For a more realistic setup, we also scaled synaptic effects of glutamate concentration changes upon release events, but it had less effect and the age-associated changes in electric features extracted from simulations with only current injection are consistent with those driven synaptically.

Adaptability calculation and search for potential anti-aging strategies

As described in the main text, the adaptability calculation is a modification of sensitivity analysis with perturbation of one parameter at a time by 20% of its initial value and subsequent calculation of the difference between the resting and stimulated state's sensitivities, normalized by the resting state sensitivities (see formula in Fig. 4b). We then consider enzymes and transporters with the highest difference in adaptability between young and aged states as the most fragile and therefore potential anti-aging targets. Furthermore, to identify enriched transcription factors for these targets we applied the ChEA3 algorithm (Keenan et al., 2019). As described in the main text, we then performed constrained optimisation for 20 sets of parameters combining those of adaptability-based and the top transcription factor regulated enzymes and transporters, as well as parameters related to diet, exercise and NAD supplementation.

Topological analysis

For the topological analysis of the adaptability networks, we employed methodology from algebraic topology. The distribution of directed simplices, introduced in Reimann et al. 2017 (Reimann et al., 2017), has been essential for the study of brain networks and has revealed significant links between the maximum simplex dimension and the robustness of networks. The distribution of directed simplices was computed with the open software <https://github.com/JasonPSmith/flagser-count>. Due to varied connectivity density, defined as the number of edges over the total number of possible edges, for different sensitivity thresholds, we divided the logarithm of the number of simplices by the

connectivity density. This normalization allows us to compare networks of different connectivity densities and identify which parts of the networks are more susceptible to changes.

Supplementary Information

Supplementary Table 1. Observed aging effects and their comparison to the literature.

Decrease in aging is highlighted by blue background, increase in aging is highlighted by red; consistency with literature is highlighted by green background, inconsistency is highlighted by orange background; literature data from different sources providing contradictory evidence is highlighted by purple background.

Observation from simulation	Changes in aging	Literature data, reference, agrees or not
Energy budget characteristics		
Total energy use (neuron + astrocyte)	<p>At rest: approximately the same 1.5e9 molecules ATP/second in both young and old.</p> <p>During neuronal firing in response to synaptic activation: decrease from 2e9 molecules ATP/second (young) to 1.8e9 molecules ATP/second (old).</p> <p>Energy use for neuronal firing in response to synaptic input is more affected by aging than the baseline rest state metabolism.</p>	
Adenylate energy charge (AEC)	<p>AEC slightly decreases in aging in both neuron and astrocyte.</p> <p>Amplitude of AEC response to stimulation decreases very slightly in the aging neuron and astrocyte.</p> <p>Surprisingly, there is a small overshoot of AEC in the astrocyte right after the approx. 7 seconds interval of neuronal firing in response to synaptic activation in aging, but not in the young state.</p>	

Total Na ⁺ /K ⁺ -ATPase ATP consumption in response to synaptic activation	Na ⁺ /K ⁺ -ATPase ATP consumption in response to neuronal firing is slightly lower in aging. It is at least partially related to the lower mean firing frequency in aging.	“Activity decreases with aging” (Fraser and Arieff, 2001)
ATP cost of AP	Lower in aging. It may be the result of limited ATP availability, i.e. metabolic aging serves as a cause for aging-associated changes in neuronal firing characteristics.	
Astrocyte to neuron ratio of Na/K ATPase rate	Increases with aging.	
Neuronal firing characteristics		
Voltage base (the average voltage during the last 10% of time before the stimulus)	From approx. -72 mV in young to approx. -78.5 mV in aged.	“Aged Type I neurons exhibited a hyperpolarized resting membrane potential (RMP) of circa -80 mV compared to circa -70 mV in the Young” (Smithers et al., 2017)
Mean firing frequency	Lower in the aged than in young.	Different reports (increase, decrease, no change) in different cell types and species (Rizzo et al., 2015)
AP amplitude, height, and peak voltage	Lower in the aged than in young.	Different reports (increase, decrease, no change) in different cell types and species (Rizzo et al., 2015)
AP rise rate and maximum of rise rate of spike (AP peak upstroke)	Lower in the aged than in young.	
AP fall rate and minimum of fall rate from spike (AP peak downstroke)	Absolute values are lower in the aged than in young.	
Spike width	Wider spikes in the aged than in young.	Slightly increases from 1 month to 10 months [Fig. 4 in (Vitale et al., 2021)]
AHP depth	Higher amplitude. Mostly positive in	“Enhanced AHP in aging”

	the aged while mostly negative in young.	(Power et al., 2002) “Age-enhanced AHP” (Disterhoft and Oh, 2007) “The amplitude of the AHP increases during aging” [(Riddle, 2007), especially fig. 10.1] Increase or no change depending on cell type and species (Rizzo et al., 2015)
AHP depth from peak	Lower in the aged than in young.	
Difference of the amplitude of the first and the last peak	Lower in the aged than in young.	
Difference in amplitude of the first and the second peak, and difference in peak voltage of the second to first spike	Lower in the aged than in young.	
The decay time constant of the voltage right after the stimulus	Lower in the aged than in young.	
Irregularity index (Mean of the absolute difference of all ISIs, except the first one (see LibV1: ISI_values feature for more details.))	Higher in the aged than in young.	
Maximum difference of the height of two subsequent peaks	Lower in the aged than in young.	
Na ⁺	Up in both neuron and astrocyte	

Metabolism characteristics		
Mitochondrial membrane potential	From approx. 155 mV in young to approx. 145 mV in aged (observed from sim.)	<p>“Decreased mitochondrial membrane potential (DeltaPsi(M)) has been found in a variety of aging cell types from several mammalian species.” (Sugrue and Tatton, 2001)</p>
ATP	Down in all compartments (observed from sim.)	<p>“Decreased ATP concentration in the neuronal somata of aged flies” (Oka et al., 2021)</p> <p>“The neuronal metabolism of glucose declines steadily, resulting in a growing deficit of adenosine triphosphate (ATP) production - which, in turn, limits glucose access.” (Błaszczuk, 2020)</p> <p>“Decrease in mitochondrial energy transducing capacity” (Ivanisevic et al., 2016)</p> <p>Down in Fig 5. of (Ivanisevic et al., 2016)</p>
Mg ²⁺	Down in the mitochondrial matrix (observed from sim.)	<p>“Aging is very often associated with magnesium (Mg) deficit.” (Barbagallo et al., 2009)</p> <p>“Elevation of brain magnesium prevents synaptic loss and reverses cognitive deficits in Alzheimer’s disease mouse model” (Li et al., 2014)</p> <p>“Diminished Mg intake, impaired intestinal Mg absorption and renal Mg wasting” (Barbagallo et al., 2021)</p> <p>“The magnesium status of aging subjects is likely to be marginal, if not frankly deficient” (Seelig and Preuss, 1994)</p> <p>“The most common cause of Mg deficit in the elderly population is dietary Mg deficiency, although secondary Mg deficit in aging</p>

		may also results from many different mechanisms” (Barbagallo and Dominguez, 2010)
NAD pool (ox. + red.)	Down (implemented into the model)	“Its depletion has emerged as a fundamental feature of aging” (Fang et al., 2017) “A significant decline in intracellular NAD ⁺ levels and NAD:NADH ratio with ageing in the CNS” (Braidy et al., 2014) Down in Fig 5. of (Ivanisevic et al., 2016)
NAD ⁺ /NADH cytosol	Down in the cytosol of both the neuron and astrocyte (observed from simulations). Limitation: cytosol and mitochondria NAD pools are connected by poorly constrained NAD shuttles, which may influence this observation.	“A significant decline in intracellular NAD ⁺ levels and NAD:NADH ratio with ageing in the CNS” (Braidy et al., 2014) “An increased ratio of NAD ⁺ /NADH indicating an oxidative shift” (Dong and Brewer, 2019)
NAD ⁺ /NADH mitochondria	Up in mitochondria of both the neuron and astrocyte (observed from simulations). Observed increase in this ratio may be a compensatory mechanism for the decreased total NAD pool (ox. + red.) Limitation: cytosol and mitochondria NAD pools are connected by poorly constrained NAD shuttles, which may influence this observation.	“A significant decline in intracellular NAD ⁺ levels and NAD:NADH ratio with ageing in the CNS” (Braidy et al., 2014) “An increased ratio of NAD ⁺ /NADH indicating an oxidative shift” (Dong and Brewer, 2019)
Glucose in blood	Increases (implemented into the model)	“Circulating glucose concentrations generally increase during aging” (Mattson and Arumugam, 2018)
Glucose in neuron, astrocyte, basal lamina, interstitium	Decreases (observed from sim.)	“The neuronal metabolism of glucose declines steadily” (Błaszczuk, 2020) “Glucose metabolism is impaired in cells; reduced glucose utilization” (Mattson and Arumugam, 2018)

Lactate	Up in all compartments (in blood: implemented into the model, other compartments: observed from sim.)	“High brain lactate” (Ross et al., 2010) “Rise of lactate” (Datta and Chakrabarti, 2018)
Pyruvate in cytosol of neuron	Down	Down in aged (home cage and enriched environment) (Ge et al., 2021)
Pyruvate in cytosol of astrocyte	Up	
Pyruvate in mitochondria	Up in both neuron and astrocyte	
AcCoA in mitochondria	Up in both neuron and astrocyte	Up in aged (home cage and enriched environment) (Ge et al., 2021) Down in Fig 5. of (Ivanisevic et al., 2016)
CoA in mitochondria	Down in both neuron and astrocyte	
Fumarate in mitochondria	Down in both neuron and astrocyte	Down in aged (home cage and enriched environment) (Ge et al., 2021)
Malate in mitochondria	Down in both neuron and astrocyte	Not significant in (Ge et al., 2021)
Oxaloacetate in mitochondria	Down in both neuron and astrocyte	
aKG in mitochondria	Down in both neuron and astrocyte	Down in aged rats (Curtis et al., 2022) Not significant (Ge et al., 2021)
Succinate in mitochondria	Up in both neuron and astrocyte	Down in aged home cage, up in aged enriched environment (Ge et al., 2021)
Succinate-CoA	Down in both neuron and astrocyte	
Isocitrate	Down in both neuron and astrocyte	
Citrate	Down in both neuron and astrocyte	Down in aged rats (Curtis et al., 2022) Not significant (Ge et al., 2021)
Acetoacetate	Up in neuron	
AcAcCoA	Down in neuron	

bHB cells and extracellular	Down in neuron (observed from sim.), extracellular space	Up in aged enriched environment, comparable to young in home cage (Ge et al., 2021)
bHB blood	Down in blood (implemented into the model)	Down in blood (Eap et al., 2022)
QH2 in mitochondria	Down in astrocyte; almost no difference in neuron at rest, but lower response to stimulus	Down (Mantle et al., 2021; Hosseini et al., 2022)
Cytochrome C in mitochondria	Down in astrocyte; almost no difference in neuron at rest, but lower response to stimulus	Down (Jones and Brewer, 2009)
(Jones and Brewer, 2009)IP3 astrocyte	Lower amplitude of response to synaptic activation	
G1P astrocyte	Up	
F26BP astrocyte	Up	
G6P	Up in both neuron and astrocyte	Up in aged with enriched environment (Ge et al., 2021)
F6P	Up in both neuron and astrocyte	
FBP neuron	Up	Up in Fig 5. of (Ivanisevic et al., 2016)
FBP astrocyte	Down	
GAP neuron	Up	
GAP astrocyte	Down	
DHAP neuron	Up	Up in aged (home cage) (Ge et al., 2021)
DHAP astrocyte	Down	
BPG13	Down in both neuron and astrocyte	
PG3	Down in both neuron and astrocyte	Not significant in (Ge et al., 2021) Up in Fig 5. of (Ivanisevic et al., 2016)
PG2	Down in both neuron and astrocyte	

PEP	Down in both neuron and astrocyte	Not significant in (Ge et al., 2021) Up in Fig 5. of (Ivanisevic et al., 2016)
NADPH neuron	Down	“age-related declines in NAD(P)H” (Ghosh et al., 2014)
NADPH astrocyte	Up	
PPP except E4P	All metabolite concentrations increase in both neuron and astrocyte	R5P, R1P up in Fig 5. of (Ivanisevic et al., 2016)
E4P neuron	Up	
E4P astrocyte	Down in both neuron and astrocyte	
GSH	Down in both neuron and astrocyte	Comparable to young in human aging (Tong et al., 2016), but down in various neurodegenerative diseases (Iskusnykh et al., 2022) Up (Hupfeld et al., 2021)
PCr	Down in both neuron and astrocyte	“Aging is associated with lower levels of creatine and phosphocreatine” (Smith et al., 2014)
cAMP	Down in astrocyte (not implemented in the neuron model)	Down (Kelly, 2018)
Glutamate	Lower amplitude of glutamate concentration change in response to synaptic input in neuron (observed from sim.) and synaptic compartment (implemented into the model), down in astrocyte	Down (Kaiser et al., 2005; Hädel et al., 2013; Cox et al., 2022)
Glutamine neuron	Up in neuron	Up (Kaiser et al., 2005)
Glutamine astrocyte, ecs	Down in astrocyte and ecs	
Derived properties		
CMR glucose	Down	“The neuronal metabolism of glucose declines steadily” (Błaszczuk, 2020) “Glucose metabolism is impaired in cells; reduced glucose

		utilization” (Mattson and Arumugam, 2018)
--	--	---

Supplementary Table 2. Data sources.

Data	References
Electrophysiology model data	(Takahashi et al., 1981; Pospischil et al., 2008; Witthoft et al., 2013; Jolivet et al., 2015; Calvetti et al., 2018)
Blood flow dynamics	(Jolivet et al., 2015; Winter et al., 2018)
Glucose transport	(Simpson et al., 2007; DiNuzzo et al., 2010; Barros et al., 2017)
Lactate transport	(Simpson et al., 2007; Jolivet et al., 2015; Calvetti et al., 2018)
bHB transport	(Halestrap and Denton, 1974; Roeder et al., 1982; Neves et al., 2012; Pérez-Escuredo et al., 2016; Calvetti et al., 2018)
Oxygen transport	(Jolivet et al., 2015)
Hexokinase	(Barros et al., 2007, 2017; DiNuzzo et al., 2010; Jolivet et al., 2010, 2015)
PGLM (astrocyte only)	(Lambeth and Kushmerick, 2002)
Glycogen phosphorylase	(Lambeth and Kushmerick, 2002; DiNuzzo et al., 2010; Xu et al., 2011; Coggan et al., 2020)
Glycogen synthase	(Lambeth and Kushmerick, 2002; DiNuzzo et al., 2010; Xu et al., 2011; Coggan et al., 2020)
Glycogen metabolism regulation	(Lambeth and Kushmerick, 2002; Xu et al., 2011; Coggan et al., 2020)
PDE	(Rybalkin et al., 2013)
PGI	(Gaitonde et al., 1989; Mulukutla et al., 2014; Berndt et al., 2015; Bouzier-Sore and Bolaños, 2015)
PFK	(Mulukutla et al., 2014; Berndt et al., 2015; Bouzier-Sore and Bolaños, 2015; Jolivet et al., 2015)

PFKFB3 (astrocyte only)	(Mulukutla et al., 2014; Berndt et al., 2015)
Aldolase	(Mulukutla et al., 2014; Berndt et al., 2015)
TPI	(Mulukutla et al., 2014; Berndt et al., 2015)
GAPDH	(Mulukutla et al., 2014; Berndt et al., 2015)
PGK	(Sharma and Rothstein, 1984; Mulukutla et al., 2014; Berndt et al., 2015)
PGM	(Mulukutla et al., 2014; Berndt et al., 2015)
Enolase	(Mulukutla et al., 2014; Berndt et al., 2015)
Pyruvate kinase	(Mulukutla et al., 2014; Berndt et al., 2015)
LDH	(Jolivet et al., 2015)
PPP	(Winter et al., 2018)
Pyruvate transport to mitochondria	(Berndt et al., 2015)
PDH	(Berndt et al., 2015; Mulukutla et al., 2015; Zhang et al., 2018)
Pyruvate carboxylase (astrocyte only)	(Barden et al., 1972; Mahan et al., 1975; Schousboe et al., 2019)
Thiolase	(Gilbert et al., 1981; Huth and Menke, 1982; Yang et al., 1987; Antonenkov et al., 2000)
SCOT	(Hersh and Jencks, 1967; White and Jencks, 1976)
bHBDH	(Nielsen et al., 1973; Dombrowski et al., 1977)
Citrate synthase	(Berndt et al., 2015; Mulukutla et al., 2015)
Aconitase	(Berndt et al., 2015; Mulukutla et al., 2015)
IDH	(Wu et al., 2007; Berndt et al., 2012; Mulukutla et al., 2015)
aKGDH	(Smith et al., 1974; McCormack and Denton, 1979; Luder et al., 1990; Mogilevskaya et al., 2006; Berndt et al., 2012)
SCS	(Berndt et al., 2015)
SDH (Complex II ETC)	(Theurey et al., 2019)
Fumarase	(Berndt et al., 2015)
MDH	(Berndt et al., 2015)
MAS	(Wilcock et al., 1973; Huynh et al., 1980; Recasens et al., 1980; Berndt et al., 2015; Mulukutla et al., 2015; Borst, 2020)
GLT-GLN	(Pamiljans et al., 1962; Listrom et al., 1997; Chaudhry et al., 1999; Calvetti and Somersalo, 2011; Botman et al., 2014; Mulukutla et al., 2015; Flanagan et al., 2018)
Creatine kinase	(Jolivet et al., 2015)

NADH/NAD ⁺ shuttles	(Jolivet et al., 2015)
ETC	(Theurey et al., 2019)
C_H_mitomatr_n	(Theurey et al., 2019)
K_x_n	(Theurey et al., 2019)
Mg_x_n	(Theurey et al., 2019)
NADHmito_n	(Jolivet et al., 2015)
QH2mito_n	(Theurey et al., 2019)
CytCredmito_n	(Theurey et al., 2019)
O2_n	(Jolivet et al., 2015; Calvetti et al., 2018)
ATPmito_n	(Theurey et al., 2019)
ADPmito_n	(Theurey et al., 2019)
ATP_mx_n	(Theurey et al., 2019)
ADP_mx_n	(Theurey et al., 2019)
Pimito_n	(Theurey et al., 2019)
ATP_i_n	(Theurey et al., 2019)
ADP_i_n	(Theurey et al., 2019)
AMP_i_n	(Theurey et al., 2019)
ATP_mi_n	(Theurey et al., 2019)
ADP_mi_n	(Theurey et al., 2019)
Pi_i_n	(Theurey et al., 2019)
MitoMembrPotent_n	(Theurey et al., 2019)
Ctot_n	(Theurey et al., 2019)
Qtot_n	(Theurey et al., 2019)
C_H_ims_n	(Theurey et al., 2019)
ATP_n	(Baeza-Lehnert et al., 2019)
ADP_n	(Erecińska and Silver, 1989; Mironov, 2007; Tantama et al., 2013; Jolivet et al., 2015; Calvetti et al., 2018)
FUMmito_n	(Fink et al., 2018)
MALmito_n	(Garrett and Grisham, 2013; Fink et al., 2018)
OXAmito_n	(Williamson et al., 1967; Nazaret et al., 2009; Choi and Gruetter, 2012; Byrne et al., 2014; Fink et al., 2018)
SUCmito_n	(Byrne et al., 2014; Tretter et al., 2016; Fink et al.,

	2018)
SUCCOAmito_n	(Park et al., 2016)
CoAmito_n	(Rock et al., 2000; Mogilevskaya et al., 2006; Poliquin et al., 2013)
AKGmito_n	(Nazaret et al., 2009; Byrne et al., 2014; Park et al., 2016)
CaMito_n	(Brocard et al., 2001; Mogilevskaya et al., 2006)
ISOCITmito_n	(Frezza, 2017)
CITmito_n	(Ronowska et al., 2018)
AcCoAmito_n	(Cai et al., 2011; Lee et al., 2014; Park et al., 2016; Ronowska et al., 2018)
AcAc_n	(Nehlig, 2004)
AcAcCoA_n	(Menahan et al., 1981; Berndt et al., 2018)
PYRmito_n	(Nazaret et al., 2009; Arce-Molina et al., 2020)
bHB_n	(Chowdhury et al., 2014)
bHB_ecs	(Nehlig, 2004; Chowdhury et al., 2014; Achanta and Rae, 2017)
bHB_a	(Chowdhury et al., 2014)
bHB_b	(Nehlig, 2004; Chowdhury et al., 2014; Achanta and Rae, 2017)
ASPmito_n	(Maletic-Savatic et al., 2008)
ASP_n	(Maletic-Savatic et al., 2008)
GLUmito_n	(Roberg et al., 1999; Nazaret et al., 2009; Featherstone, 2010)
MAL_n	(Mueggler and Wolfe, 1978)
OXA_n	(Williamson et al., 1967; Choi and Gruetter, 2012)
AKG_n	(Pritchard, 1995)
GLU_n	(Shestov et al., 2007; Byrne et al., 2014)
NADH_n	(Neves et al., 2012; Jolivet et al., 2015; Park et al., 2016; Calvetti et al., 2018)
C_H_mitomatr_a	(Theurey et al., 2019)
K_x_a	(Theurey et al., 2019)
Mg_x_a	(Theurey et al., 2019)
NADHmito_a	(Jolivet et al., 2015)

QH2mito_a	(Theurey et al., 2019)
CytCredmito_a	(Theurey et al., 2019)
O2_a	(Jolivet et al., 2015; Calvetti et al., 2018)
ATPmito_a	(Theurey et al., 2019)
ADPmito_a	(Theurey et al., 2019)
ATP_mx_a	(Theurey et al., 2019)
ADP_mx_a	(Theurey et al., 2019)
Pimito_a	(Theurey et al., 2019)
ATP_i_a	(Theurey et al., 2019)
ADP_i_a	(Theurey et al., 2019)
AMP_i_a	(Theurey et al., 2019)
ATP_mi_a	(Theurey et al., 2019)
ADP_mi_a	(Theurey et al., 2019)
Pi_i_a	(Theurey et al., 2019)
MitoMembrPotent_a	(Theurey et al., 2019)
Ctot_a	(Theurey et al., 2019)
Qtot_a	(Theurey et al., 2019)
C_H_ims_a	(Theurey et al., 2019)
ATP_a	(Köhler et al., 2020)
ADP_a	(Erecińska and Silver, 1989; Tantama et al., 2013; Jolivet et al., 2015; Calvetti et al., 2018)
FUMmito_a	(Fink et al., 2018)
MALmito_a	(Garrett and Grisham, 2013; Fink et al., 2018)
OXAmito_a	(Byrne et al., 2014)
SUCmito_a	(Byrne et al., 2014)
SUCCOAmity_a	(Park et al., 2016)
CoAmity_a	(Rock et al., 2000; Poliquin et al., 2013)
AKGmito_a	(Byrne et al., 2014)
CaMity_a	(Brocard et al., 2001; Mogilevskaya et al., 2006)
ISOCITmito_a	(Frezza, 2017)
CITmito_a	(Ronowska et al., 2018)
AcCoAmity_a	(Cai et al., 2011; Lee et al., 2014; Park et al., 2016; Ronowska et al., 2018)

AcAc_a	(Nehlig, 2004)
AcAcCoA_a	(Menahan et al., 1981; Berndt et al., 2018)
PYRmito_a	(Arce-Molina et al., 2020)
GLN_n	(Shestov et al., 2007)
GLN_out	(Bröer and Brookes, 2001; Pochini et al., 2014)
GLN_a	(Hertz and Rothman, 2017)
GLUT_a	(Savtchenko et al., 2018; Verkhatsky and Nedergaard, 2018)
Va	(Breslin et al., 2018)
Na_a	(Witthoft et al., 2013)
K_a	(Witthoft et al., 2013; Flanagan et al., 2018)
K_out	(Takahashi et al., 1981)
GLUT_syn	(Robinson and Jackson, 2016; Hertz and Rothman, 2017; Verkhatsky and Nedergaard, 2018; Mahmoud et al., 2019)
VNeu	(Jolivet et al., 2015; Calvetti et al., 2018; Coggan et al., 2020)
Na_n	(Jolivet et al., 2015; Calvetti et al., 2018; Coggan et al., 2020)
h	(Jolivet et al., 2015)
n	(Jolivet et al., 2015)
Ca_n	(Jolivet et al., 2015)
pgate	(Pospischil et al., 2008)
nBK_a	(Witthoft et al., 2013)
mGluRboundRatio_a	(Witthoft et al., 2013)
IP3_a	(Witthoft et al., 2013)
hIP3Ca_a	(Witthoft et al., 2013)
Ca_a	(Witthoft et al., 2013; Verkhatsky and Nedergaard, 2018; Coggan et al., 2020)
Ca_r_a	(Bennett et al., 2008; Witthoft et al., 2013)
sTRP_a	(Witthoft et al., 2013)
vV	(Cloutier et al., 2009; Jolivet et al., 2015; Winter et al., 2018)
EET_a	(Witthoft et al., 2013)

ddHb	(Cloutier et al., 2009; Jolivet et al., 2015; Winter et al., 2018)
O2cap	(Jolivet et al., 2015; Calvetti et al., 2018)
Glc_b	(Jolivet et al., 2015)
Glc_t_t	(Barros et al., 2017)
Glc_ecsBA	(Pathak et al., 2015; Barros et al., 2017)
Glc_a	(Jolivet et al., 2015; Barros et al., 2017; Calvetti et al., 2018)
Glc_ecsAN	(Pathak et al., 2015; Barros et al., 2017)
Glc_n	(Jolivet et al., 2015; Barros et al., 2017; Calvetti et al., 2018)
G6P_n	(Kauffman et al., 1969; Anderson and Wright, 1980; Orosz et al., 2003; Cloutier et al., 2009; Park et al., 2016; Winter et al., 2018)
G6P_a	(Kauffman et al., 1969; Anderson and Wright, 1980; Orosz et al., 2003; Cloutier et al., 2009; Park et al., 2016; Winter et al., 2018)
F6P_n	(Kauffman et al., 1969; Cloutier et al., 2009; Winter et al., 2018)
F6P_a	(Kauffman et al., 1969; Cloutier et al., 2009; Winter et al., 2018)
FBP_n	(Byrne et al., 2014)
FBP_a	(Byrne et al., 2014)
f26bp_a	(Erecińska and Silver, 1994; Mulukutla et al., 2015)
GLY_a	(Cloutier et al., 2009; DiNuzzo et al., 2010; Waitt et al., 2017)
AMP_n	(Erecińska and Silver, 1989; Theurey et al., 2019)
AMP_a	(Erecińska and Silver, 1989; Theurey et al., 2019)
G1P_a	(Byrne et al., 2014)
GAP_n	(Tiveci et al., 2005; Cloutier et al., 2009; Jolivet et al., 2015)
GAP_a	(Tiveci et al., 2005; Cloutier et al., 2009; Jolivet et al., 2015)
DHAP_n	(Kauffman et al., 1969; Byrne et al., 2014)
DHAP_a	(Kauffman et al., 1969; Byrne et al., 2014)

BPG13_n	(Lambeth and Kushmerick, 2002; Shestov et al., 2007)
BPG13_a	(Lambeth and Kushmerick, 2002; Shestov et al., 2007)
NADH_a	(Jolivet et al., 2015; Park et al., 2016; Calvetti et al., 2018)
Pi_n	(Theurey et al., 2019)
Pi_a	(Theurey et al., 2019)
PG3_n	(Lambeth and Kushmerick, 2002; Berndt et al., 2015; Park et al., 2016)
PG3_a	(Lambeth and Kushmerick, 2002; Berndt et al., 2015; Park et al., 2016)
PG2_n	(Lambeth and Kushmerick, 2002; Berndt et al., 2015; Park et al., 2016)
PG2_a	(Lambeth and Kushmerick, 2002; Berndt et al., 2015; Park et al., 2016)
PEP_n	(Cloutier et al., 2009; Byrne et al., 2014; Jolivet et al., 2015)
PEP_a	(Cloutier et al., 2009; Byrne et al., 2014; Jolivet et al., 2015)
Pyr_n	(Lajtha and Reith, 2007; Byrne et al., 2014; Lerchundi et al., 2015; Calvetti et al., 2018; Muraleedharan et al., 2020)
Pyr_a	(Lajtha and Reith, 2007; Byrne et al., 2014; Lerchundi et al., 2015; Calvetti et al., 2018; Muraleedharan et al., 2020)
Lac_b	(Mächler et al., 2016; Calvetti et al., 2018)
Lac_ecs	(Mächler et al., 2016; Calvetti et al., 2018)
Lac_a	(Shestov et al., 2007; Calvetti et al., 2018)
Lac_n	(Shestov et al., 2007; Calvetti et al., 2018)
NADPH_n	(Winter et al., 2018; Bradshaw, 2019)
NADPH_a	(Winter et al., 2018; Bradshaw, 2019)
GL6P_n	(Winter et al., 2018)
GL6P_a	(Winter et al., 2018)
GO6P_n	(Gaitonde et al., 1989; Winter et al., 2018)
GO6P_a	(Winter et al., 2018)

RU5P_n	(Winter et al., 2018)
RU5P_a	(Winter et al., 2018)
R5P_n	(Winter et al., 2018)
R5P_a	(Winter et al., 2018)
X5P_n	(Winter et al., 2018)
X5P_a	(Winter et al., 2018)
S7P_n	(Winter et al., 2018)
S7P_a	(Winter et al., 2018)
E4P_n	(Winter et al., 2018)
E4P_a	(Winter et al., 2018)
GSH_n	(Vali et al., 2007; Koga et al., 2011; Duarte and Gruetter, 2013; Sedlak et al., 2019)
GSH_a	(Koga et al., 2011; McBean, 2017)
GSSG_n	(McBean, 2017)
GSSG_a	(McBean, 2017)
Cr_n	(Cloutier et al., 2009; Jolivet et al., 2015; Baeza-Lehnert et al., 2019)
PCr_n	(Cloutier et al., 2009; Jolivet et al., 2015; Baeza-Lehnert et al., 2019)
Cr_a	(Cloutier et al., 2009; Jolivet et al., 2015)
PCr_a	(Cloutier et al., 2009; Jolivet et al., 2015)
cAMP_a	(Coggan et al., 2018, 2020)
NE_neuromod	(Coggan et al., 2018, 2020)
UDPgluco_a	(Tsuboi et al., 1969; Park et al., 2016)
UTP_a	(Anderson and Wright, 1980; Park et al., 2016)
GS_a	(Xu et al., 2011; Coggan et al., 2020)
GPa_a	(Xu et al., 2011; Coggan et al., 2020)
GPb_a	(Xu et al., 2011; Coggan et al., 2020)

Supplementary Table 3. Anti-aging optimisation results.

Therapy (detailed list of parameters for each case is in antiage_opt/prep_opt.ipynb)	File ID	Fitness (lower is better)
--	---------	---------------------------

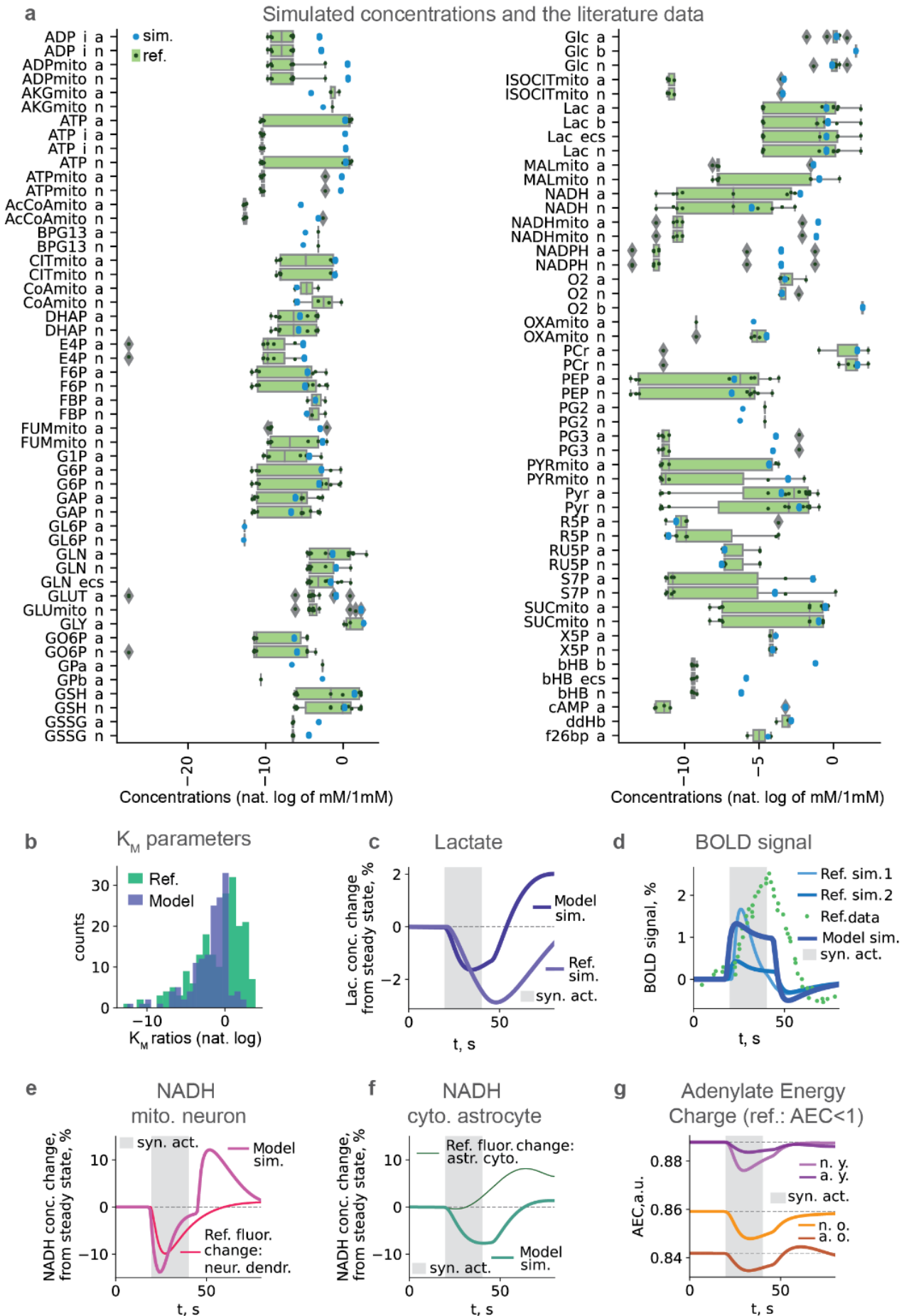
<p>01 DEN-therapy (diet represented by blood glucose and beta-hydroxybutyrate levels, exercise effects represented by blood lactate levels, NAD supplementation represented by total NAD, and NADH cytosol-mitochondria shuttle capacity modulation)</p>	<p>opt01_dietNadSuppShuttles_05 08_1716_FITNESS</p>	<p>324.6946224064965</p>
<p>02 Diet and exercise (diet represented by blood glucose and beta-hydroxybutyrate levels, exercise effects represented by blood lactate levels)</p>	<p>opt02_diet_0508_1736_FITNESS</p>	<p>330.8649909859092</p>
<p>03 Diet and exercise + targeted selection of enzymes and transporters (diet represented by blood glucose and beta-hydroxybutyrate levels, exercise effects represented by blood lactate levels, selection of top-vulnerable enzyme and transporter targets based on sensitivity analysis)</p>	<p>opt03_sel2diet_0508_1745_FITNESS</p>	<p>330.5296867114816</p>
<p>04 Diet and exercise + targeted selection of enzymes and transporters + top transcription factor regulated targets (as therapy-03 above, but with additional set of parameters representing ESRRA regulated targets)</p>	<p>opt04_sel2diettopTF_0508_1749_FITNESS</p>	<p>329.6195317070475</p>
<p>05 Diet and exercise + NAD supplementation + NADH cytosol-mitochondria shuttle capacity modulation + top transcription factor regulated targets (diet represented by blood glucose and beta-hydroxybutyrate levels, exercise effects represented by blood lactate levels, NAD supplementation represented by total NAD, NADH cytosol-mitochondria shuttle capacity modulation, ESRRA regulated targets)</p>	<p>opt05_dietNadSuppShuttlestopTF_0508_1754_FITNESS</p>	<p>321.4015401204615</p>
<p>06 Diet and exercise + NAD supplementation + top transcription factor regulated targets (as therapy-05, but without NADH</p>	<p>opt06_dietNadSupptopTF_0508_1800_FITNESS</p>	<p>326.52278564010174</p>

cytosol-mitochondria shuttle capacity modulation)		
07 Diet + exercise + NAD supplementation (as 01 DEN-therapy, but without NADH cytosol-mitochondria shuttle capacity modulation)	opt07_dietNadSupp_0508_1805_FITNESS	330.9287687071004
08 Diet and exercise + NAD supplementation + NADH cytosol-mitochondria shuttle capacity modulation + targeted selection of enzymes and transporters + top transcription factor regulated targets (as therapy-04, but additionally with NAD supplementation represented by total NAD, NADH cytosol-mitochondria shuttle capacity modulation)	opt08_sel3fulltopTF_0508_1809_FITNESS	322.00660105095636
09 Diet and exercise + NAD supplementation + NADH cytosol-mitochondria shuttle capacity modulation + targeted selection of enzymes and transporters (as therapy-08, but without ESRR regulated targets)	opt09_sel3full_0508_1814_FITNESS	321.46368653203
10 NAD supplementation + NADH cytosol-mitochondria shuttle capacity modulation + targeted selection of enzymes and transporters + top transcription factor regulated targets (as therapy-08, but without diet and exercise)	opt10_sel2nadfulltopTF_0508_1817_FITNESS	325.9331563280608
11 Targeted selection of enzymes and transporters + NAD supplementation + NADH cytosol-mitochondria shuttle capacity modulation	opt11_sel2nadfull_0508_1818_FITNESS	320.2230577011635
12 NADH cytosol-mitochondria shuttle capacity modulation	opt12_NADshuttles_cm_0508_1832_FITNESS	325.33028862691594
13 Diet and exercise + NAD supplementation + targeted selection of enzymes and transporters + top transcription factor regulated targets (as therapy-08, but without NADH	opt13_sel3topTF_0508_1835_FITNESS	332.51439560199486

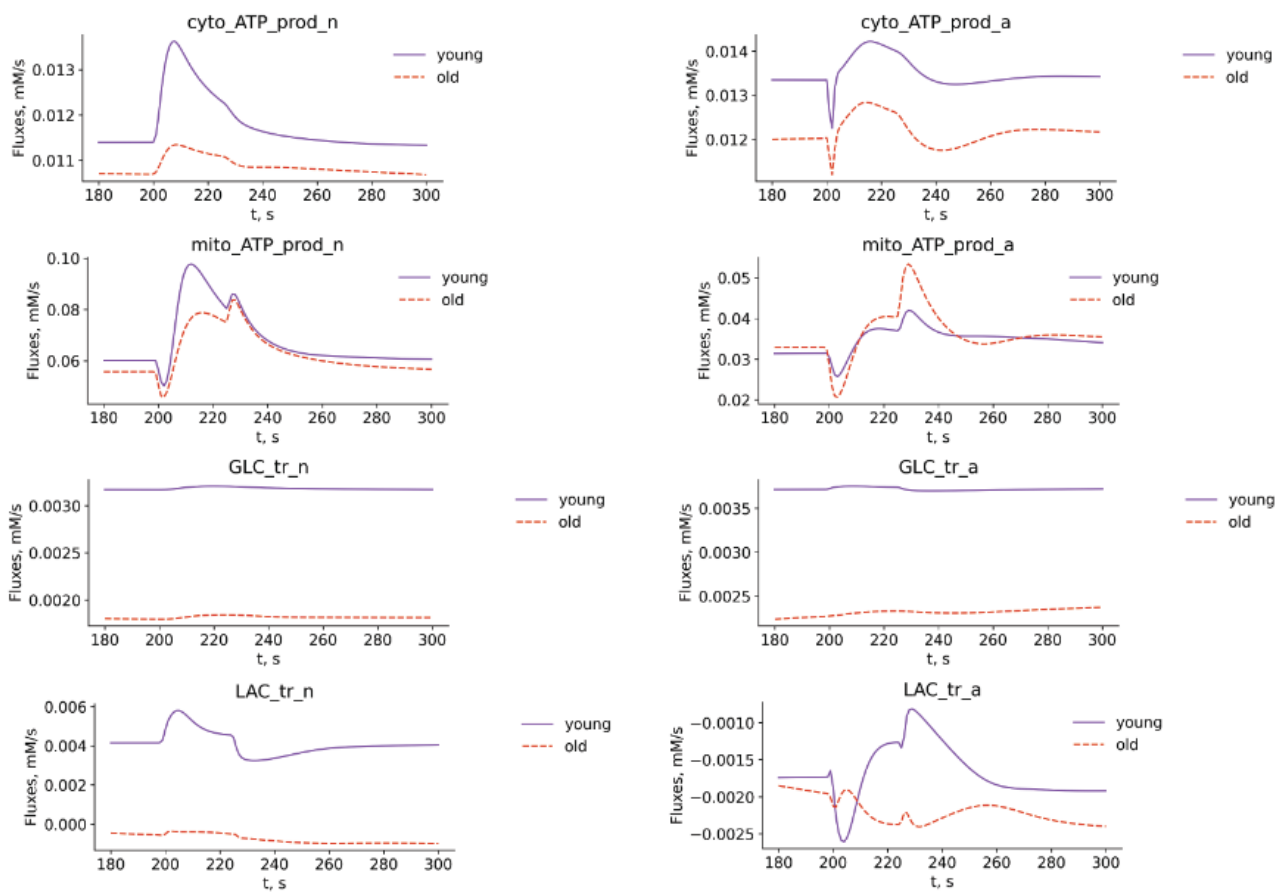
cytosol-mitochondria shuttle capacity modulation)		
14 Diet and exercise + NAD supplementation + targeted selection of enzymes and transporters (as therapy-13, but without top transcription factor regulated targets)	opt14_sel3_0508_1837_FITNESS	330.8959136554414
15 NAD supplementation + targeted selection of enzymes and transporters + top transcription factor regulated targets (as therapy-13, but without diet and exercise)	opt15_sel2nadtopTF_0508_1838_FITNESS	333.0797288342428
16 NAD supplementation + targeted selection of enzymes and transporters	opt16_sel2nad_0508_1840_FITNESS	323.72448628397404
17 NAD supplementation represented by total NAD	opt17_NADsupplements_0508_1841_FITNESS	325.9386339659428
18 Targeted selection of enzymes and transporters + top transcription factor (ESRRA) regulated targets	opt18_sel1topTF_0508_1844_FITNESS	329.8385866817131
19 Targeted selection of enzymes and transporters (based on sensitivity analysis)	opt19_sel1_0508_1847_FITNESS	330.32612175950476
20 Top transcription factor (ESRRA) regulated targets	opt20_sel_topTF_0508_1848_FITNESS	330.564190608832

Supplementary Figures.

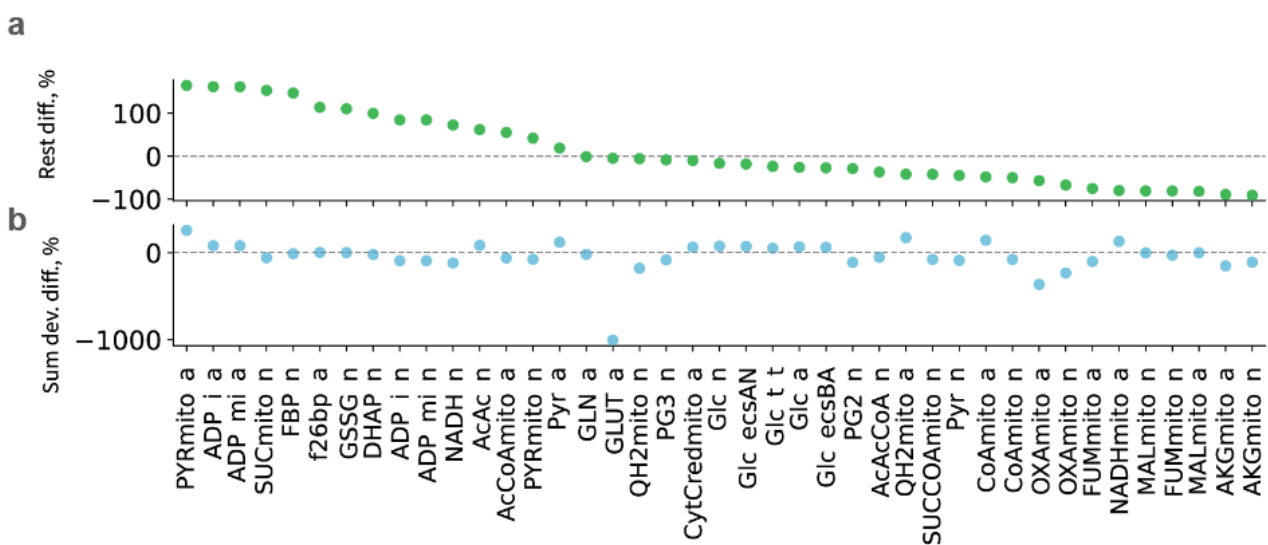
Supplementary Fig. 1. Validation, predicted energy budget. **a**, Simulated concentrations and the literature data. **b**, Comparison of ratios of model K_m to average mammalian data K_m for the same pairs enzyme-metabolite to min/mean and max/mean ratios of that mammalian data for the same pairs enzyme-metabolite, **c**, Lactate dynamics compared to simulation of the other model from the literature (Jolivet et al., 2015). **d**, BOLD dynamics (Jolivet et al., 2015; Winter et al., 2018; Jung et al., 2021). **e**, NADH dynamics in neuronal mitochondria compared to literature (Jolivet et al., 2015). **f**, NADH dynamics in astrocyte cytosol compared to literature (Jolivet et al., 2015). **g**, ATP consumption per AP in young and old ages.



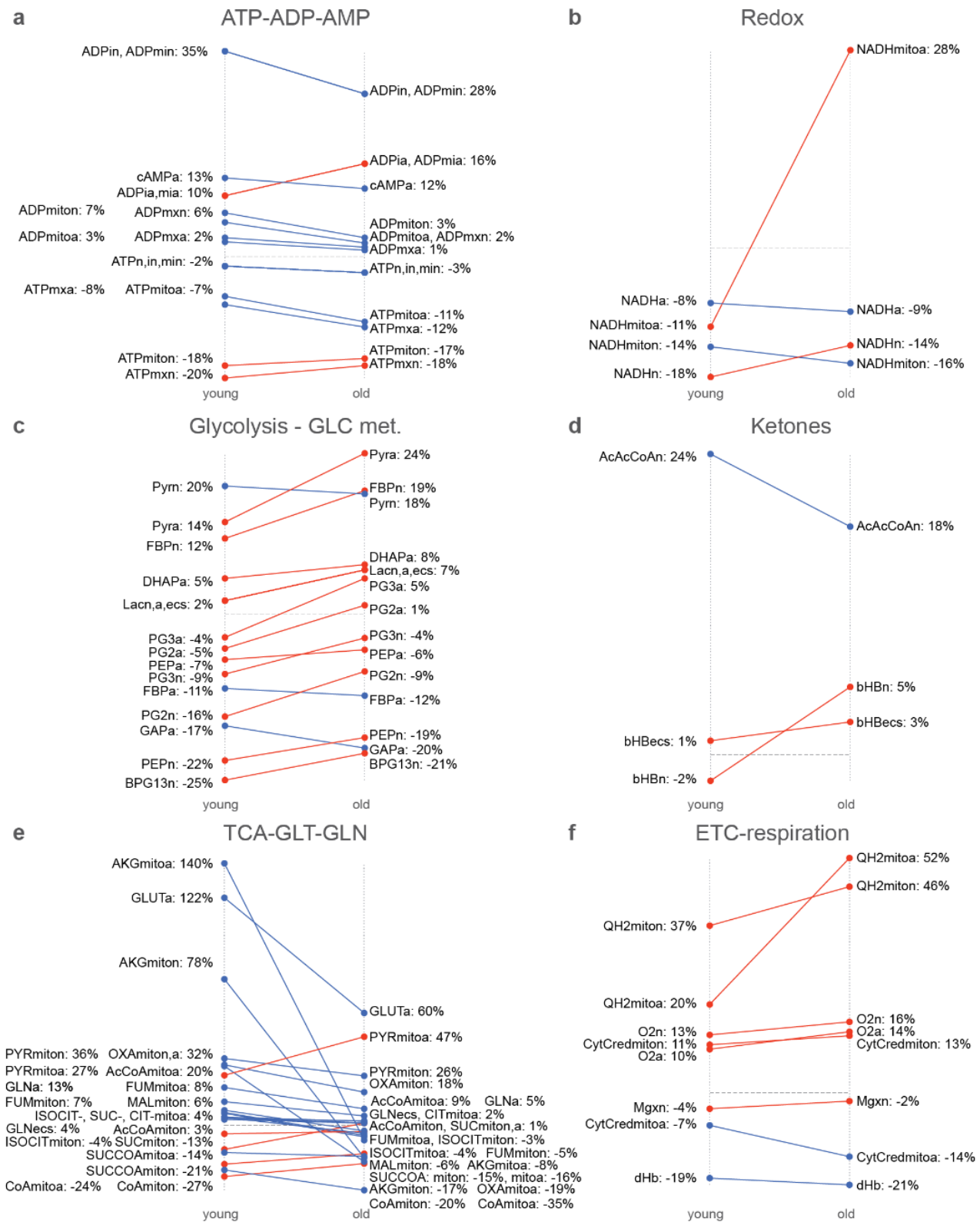
Supplementary Fig. 2. ATP production, glucose and lactate transport fluxes.



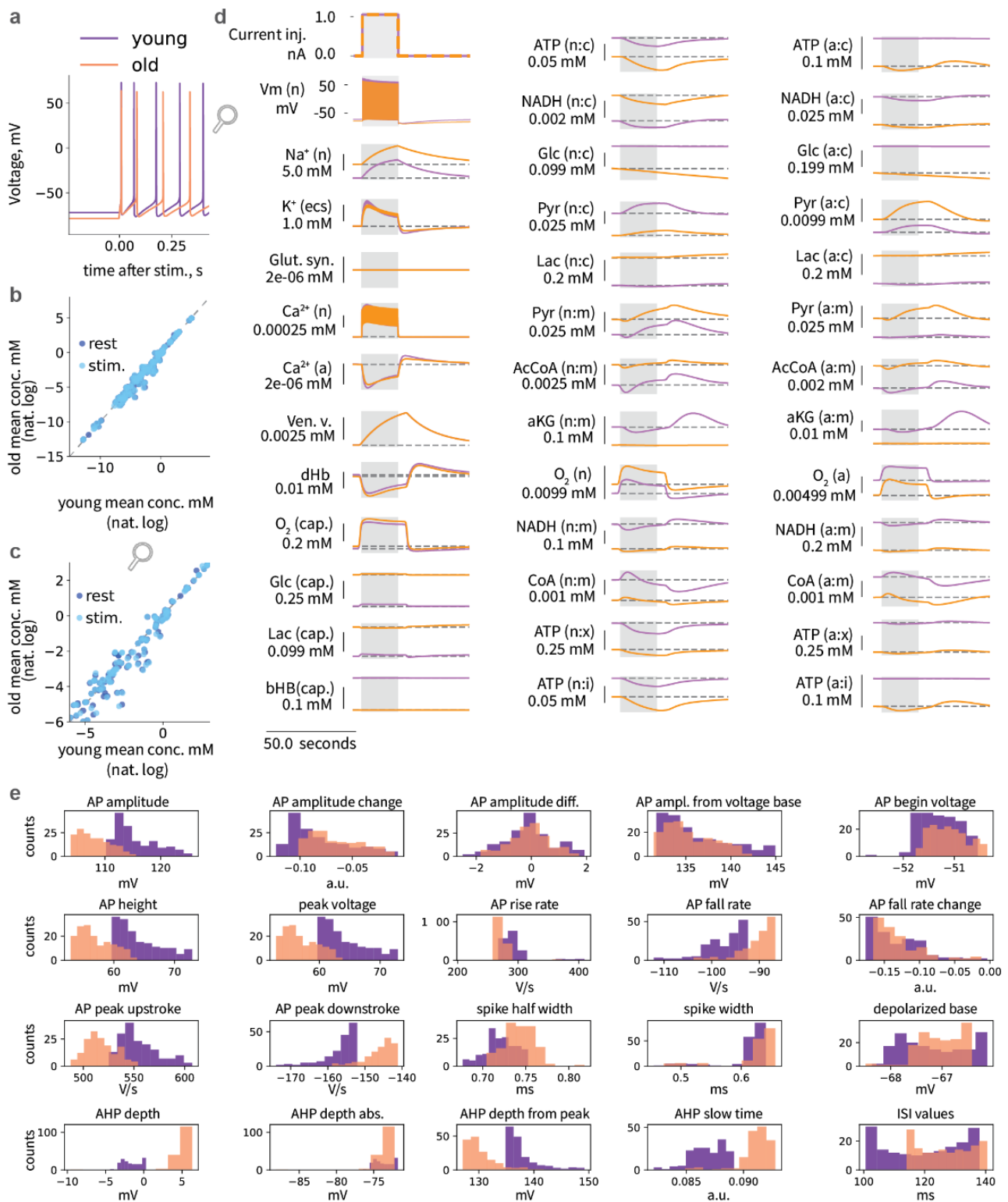
Supplementary Fig. 3. Differences between young and old in rest state concentrations (top) and in sum of relative deviations of concentration from rest (normalized by rest state) upon synaptic activation (bottom), both ranked by rest state differences (top), only top ranked are shown.



Supplementary Fig. 4. Comparison of amplitudes of metabolic response to synaptic activation in young and old ages (filtered by absolute values of deviations and difference in deviations of higher than 1%).

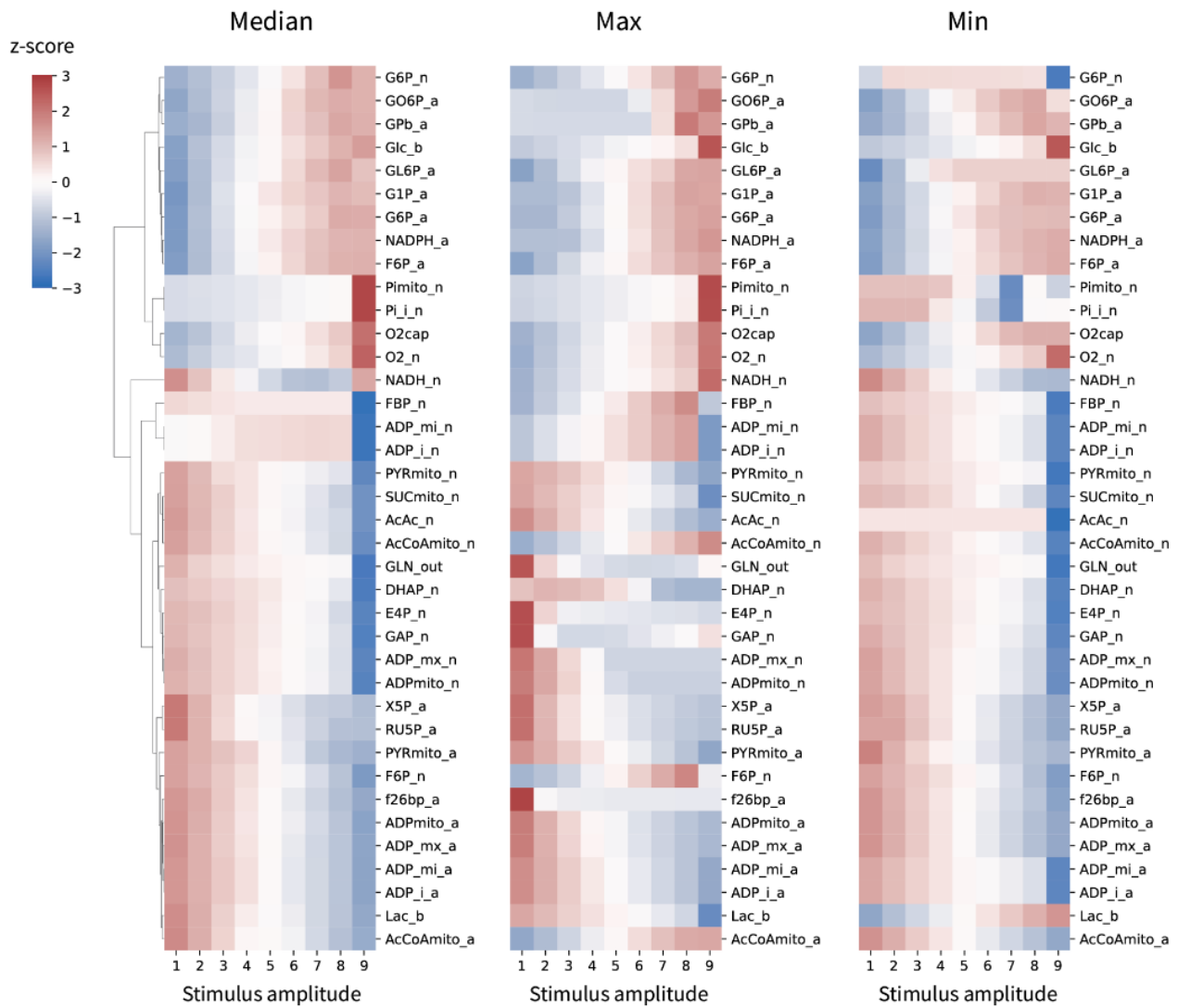


Supplementary Fig. 5. Train of APs evoked by 1 nA current injection simulations. **a**, Dynamics of metabolism in response to a train of APs evoked by current injection in different ages. **b**, Characteristics of neuronal firing in young and old ages evoked by current injection.

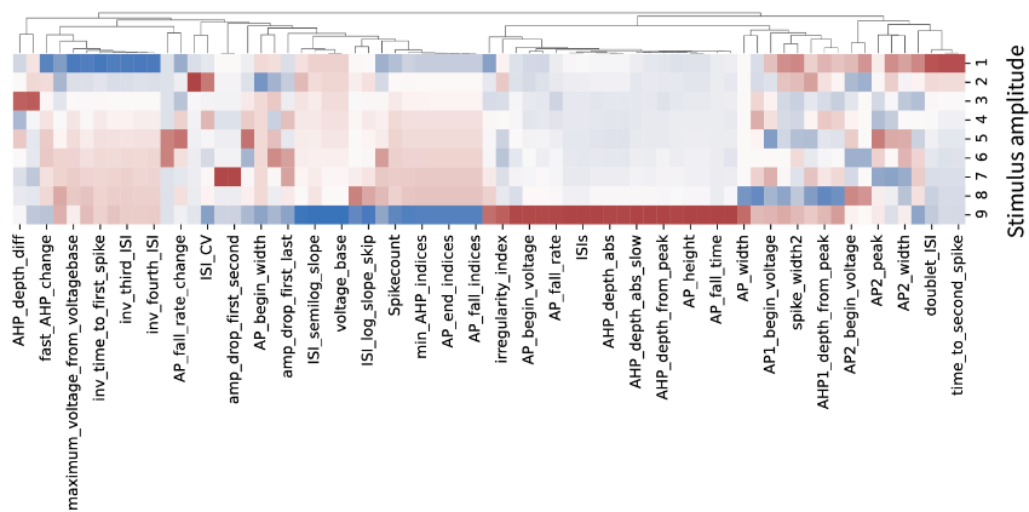


Supplementary Fig. 6. Aging-associated differences in range of response to the current injections of different amplitudes.

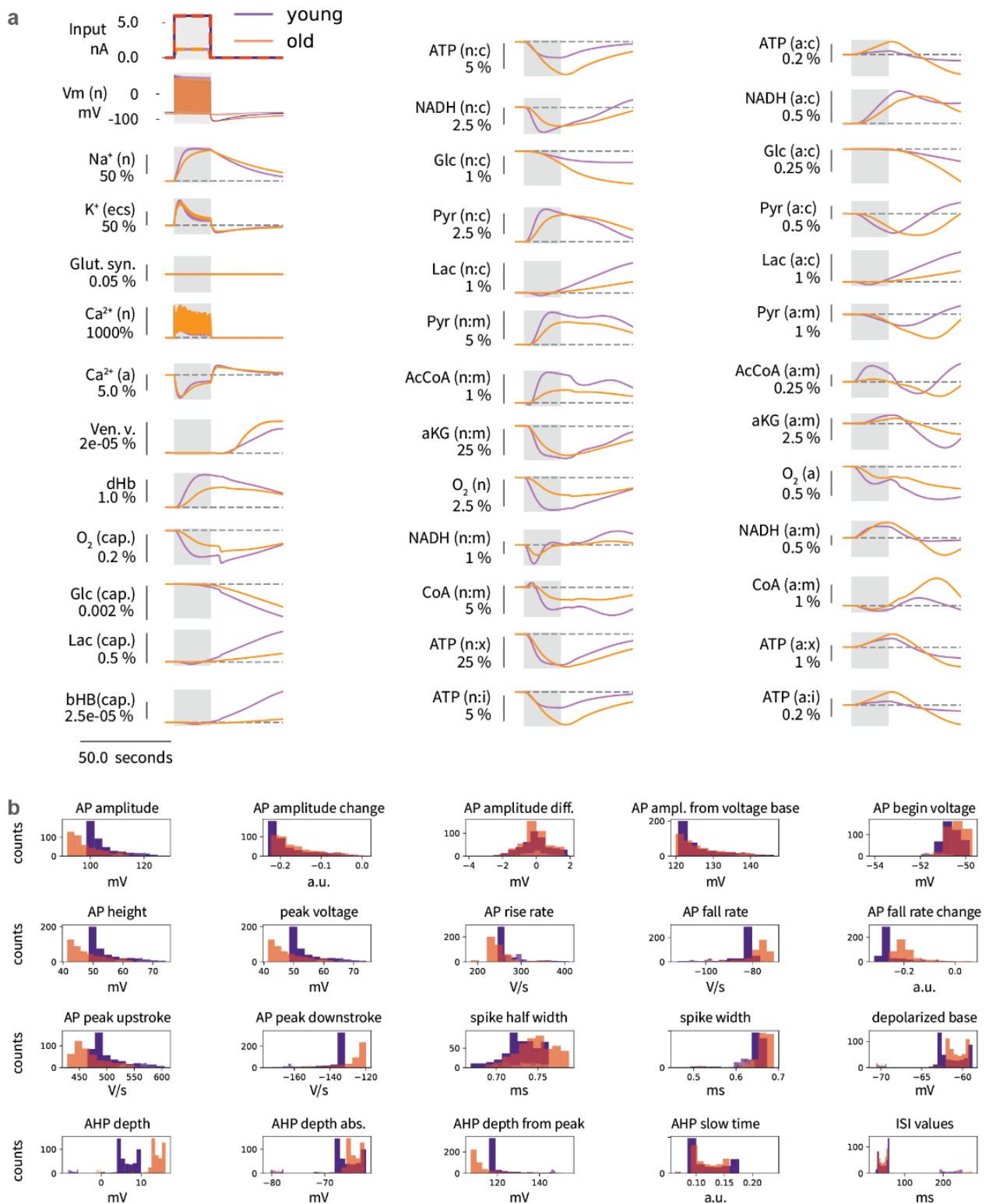
a Metabolic range of response



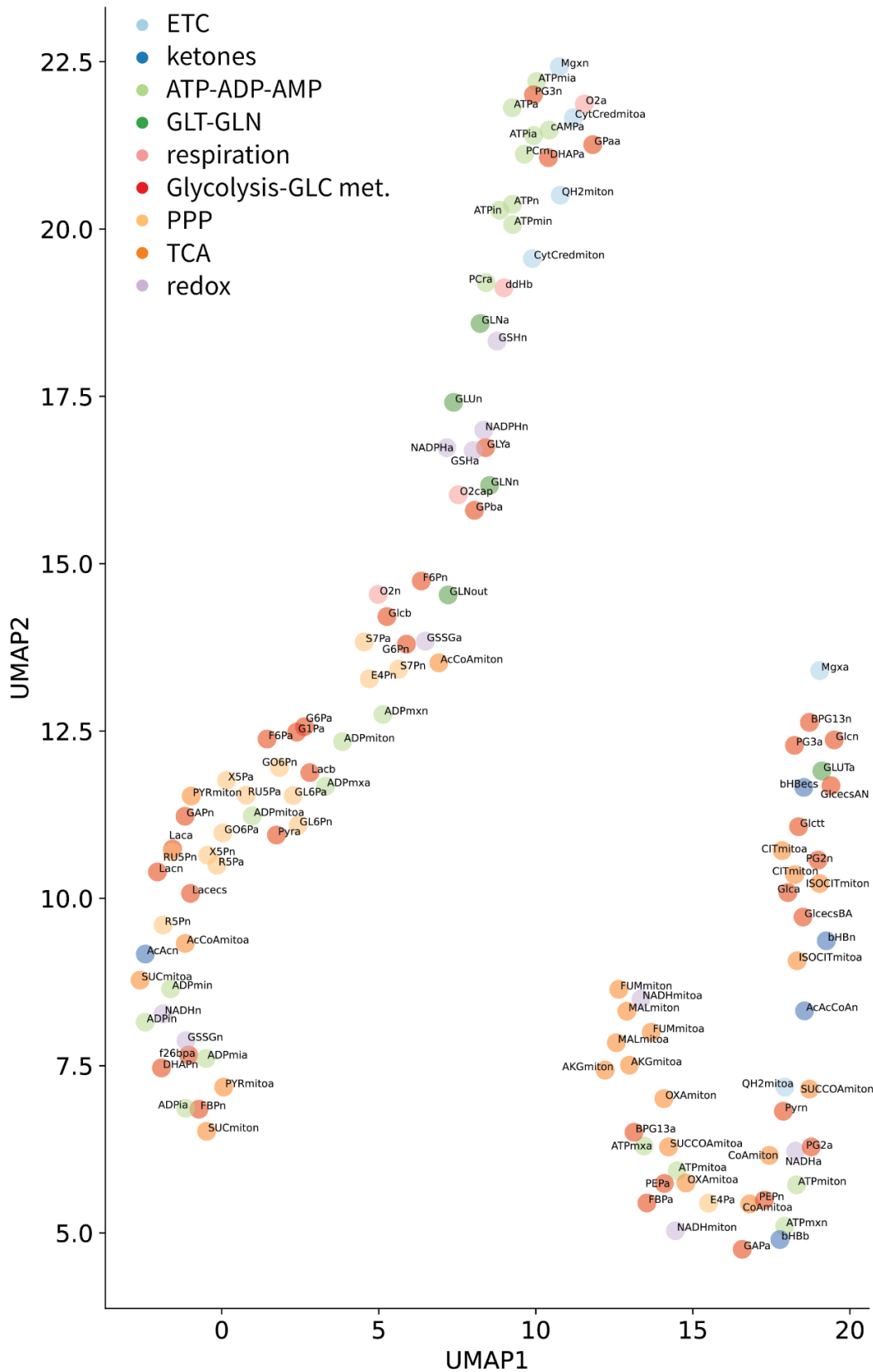
b Neuronal firing characteristics range of response



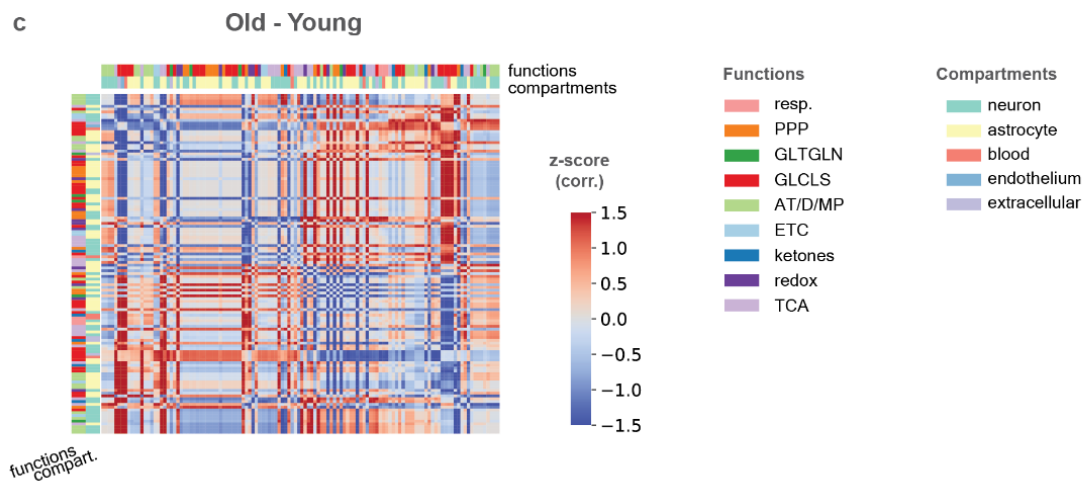
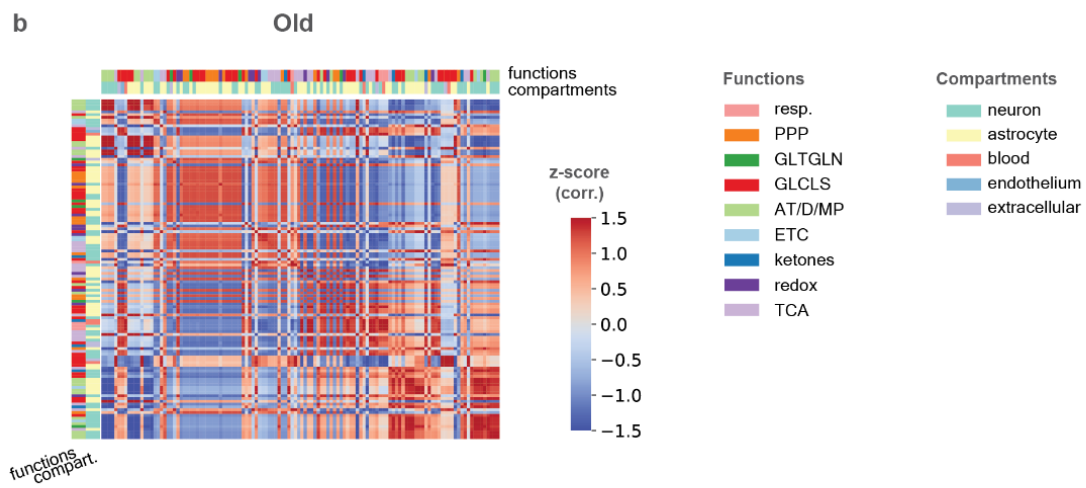
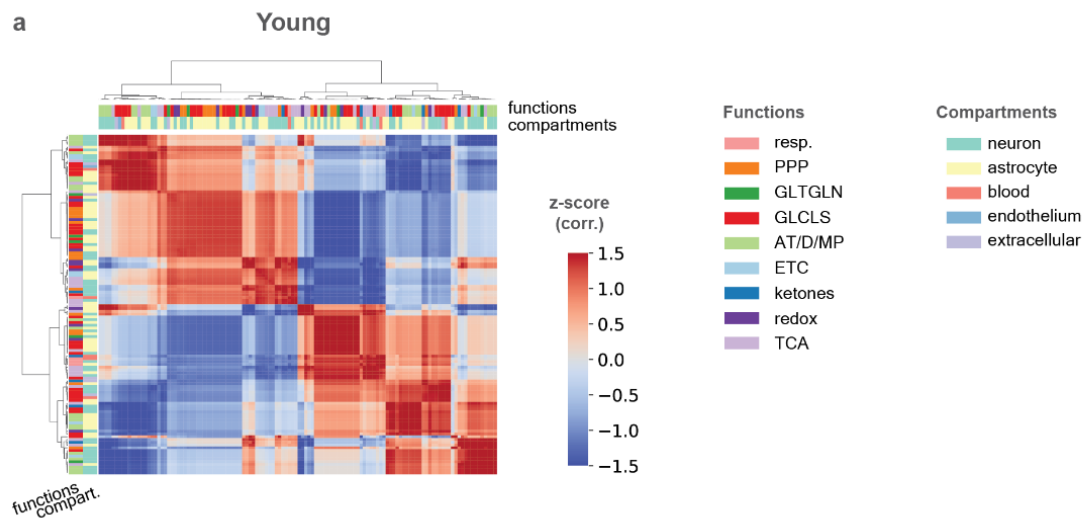
Supplementary Fig. 7. Dependence of metabolism and electrophysiology responses on the current injection amplitude in young and old ages. **a**, Young and old age responses to current injections of two different amplitudes: input current (top left in A), firing traces (left on second row in A), percent difference in metabolic response: $100 \cdot (m_{IinjHigh} - m_{IinjLow}) / m_{IinjLow}$ (all other figures in A). **b**, Characteristics of neuronal firing in young and old ages upon current injections of two different amplitudes.



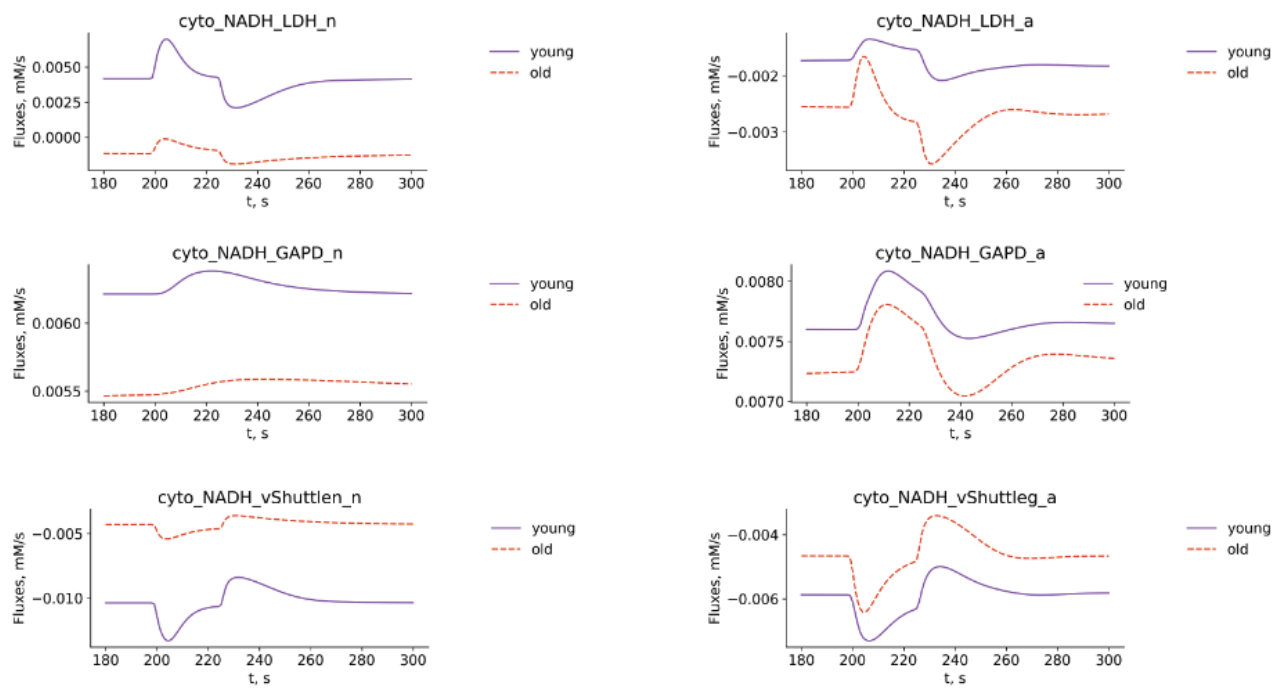
Supplementary Fig. 8. UMAP of relative differences in concentration traces in old compared to young.



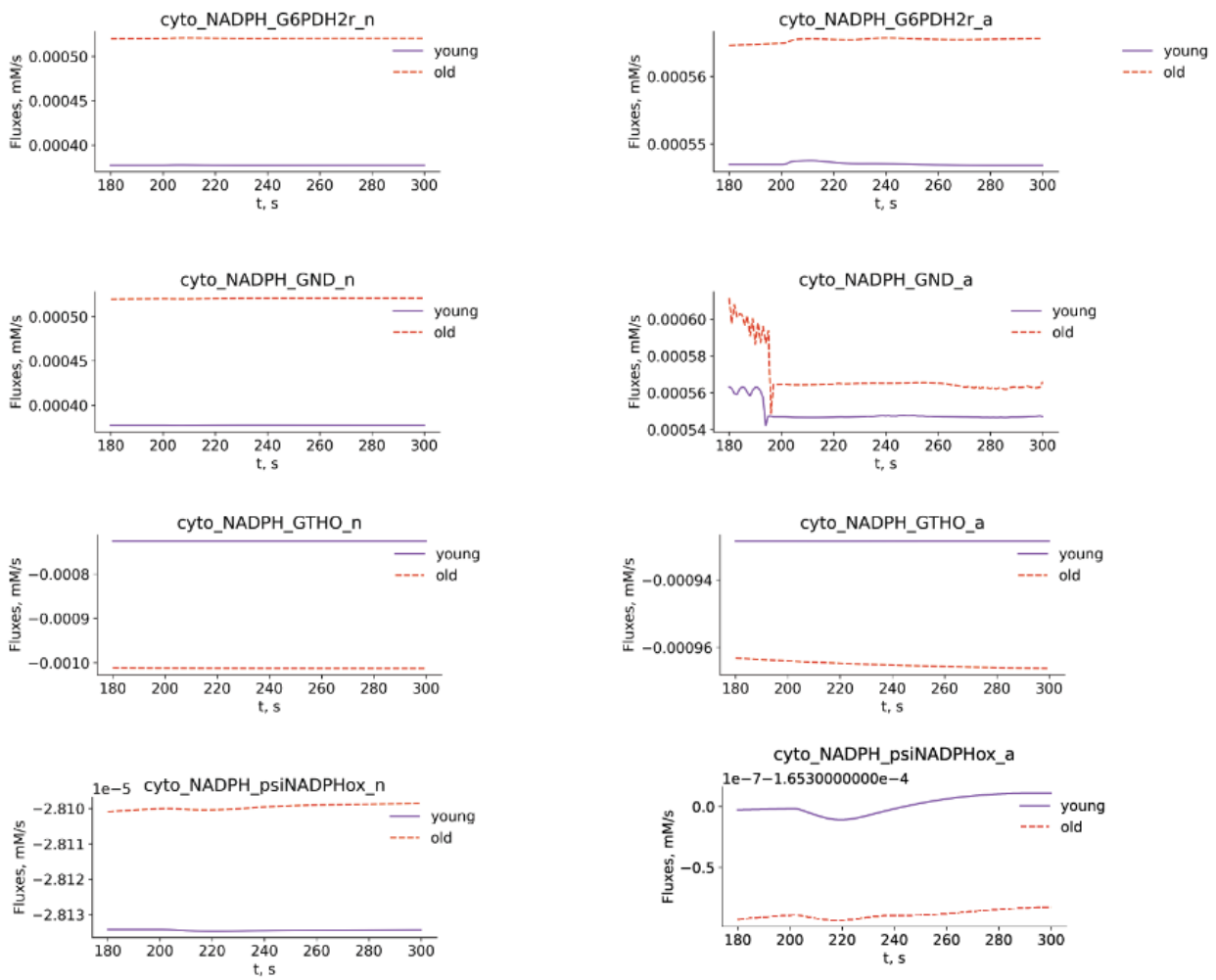
Supplementary Fig. 9. Kendall correlation of metabolite concentrations time series data in aging.



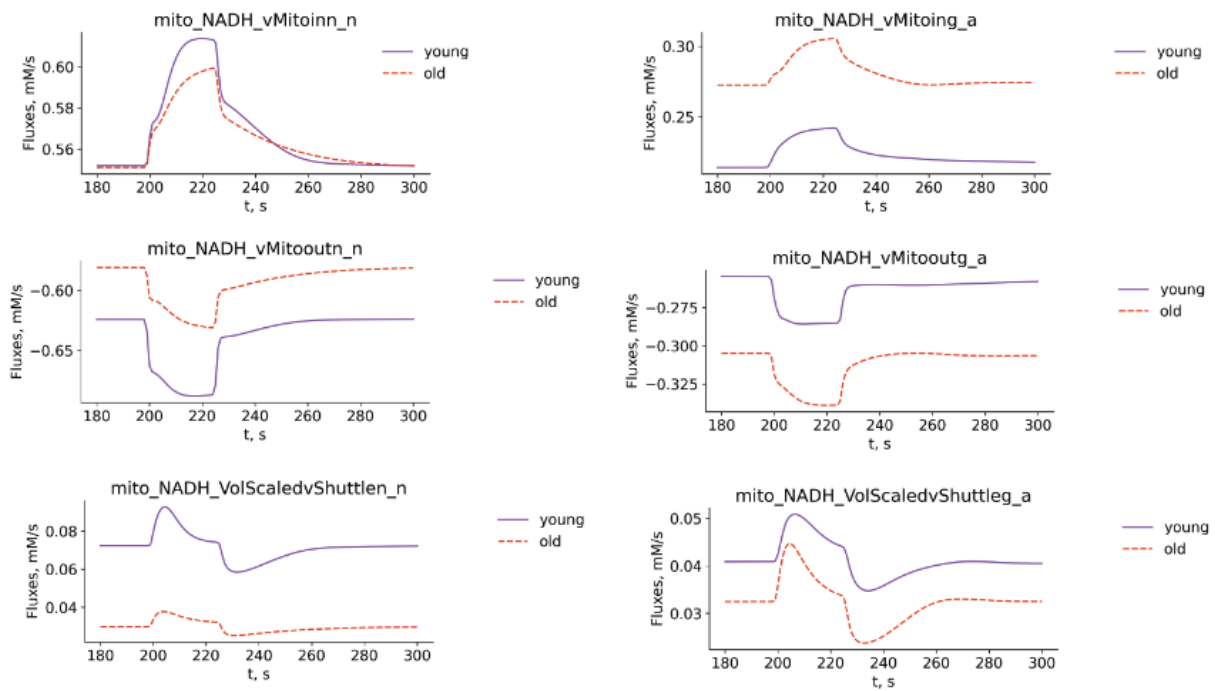
Supplementary Fig. 10. Cytosolic NADH fluxes.



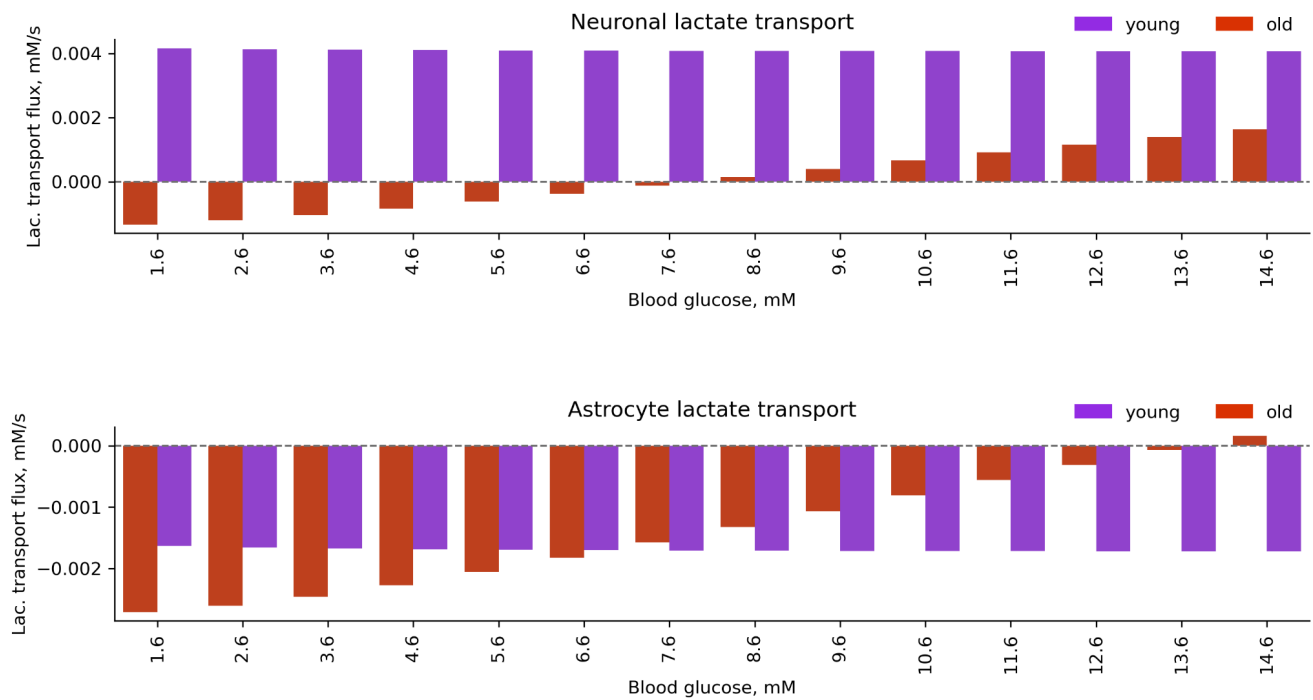
Supplementary Fig. 11. Cytosolic NADPH fluxes.



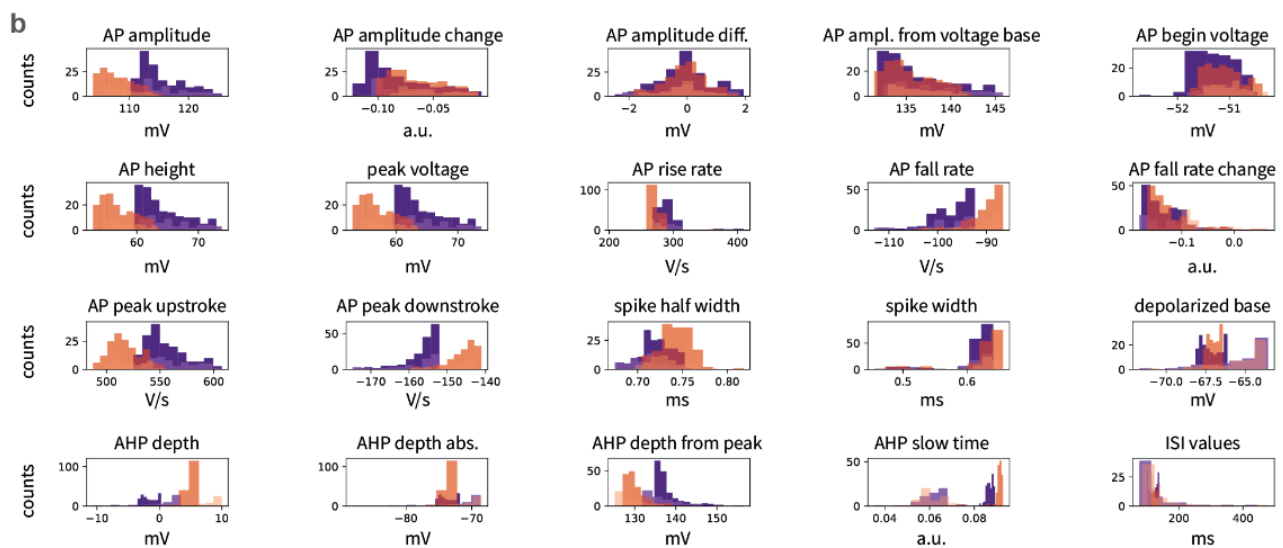
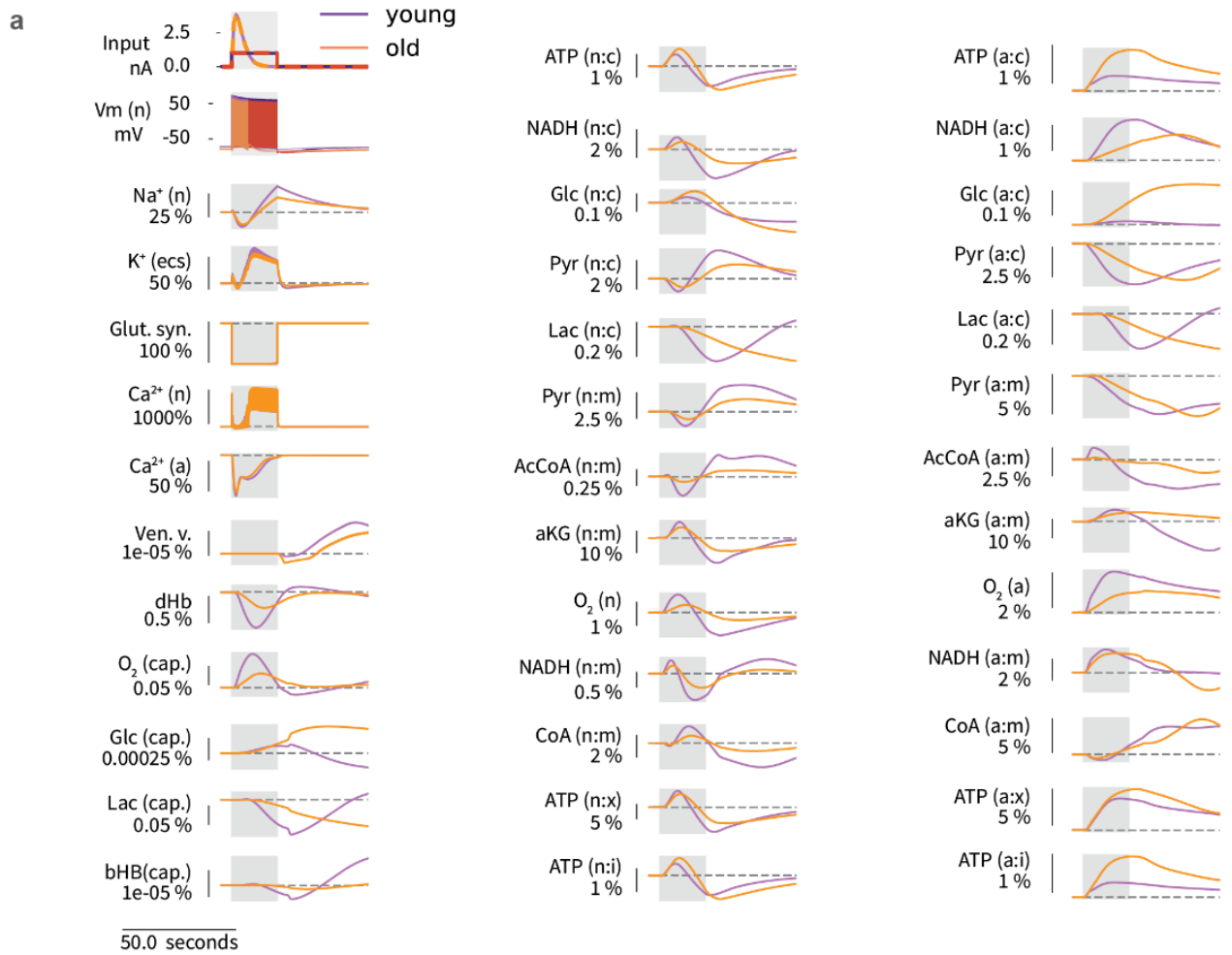
Supplementary Fig. 12. Mitochondrial NADH fluxes.



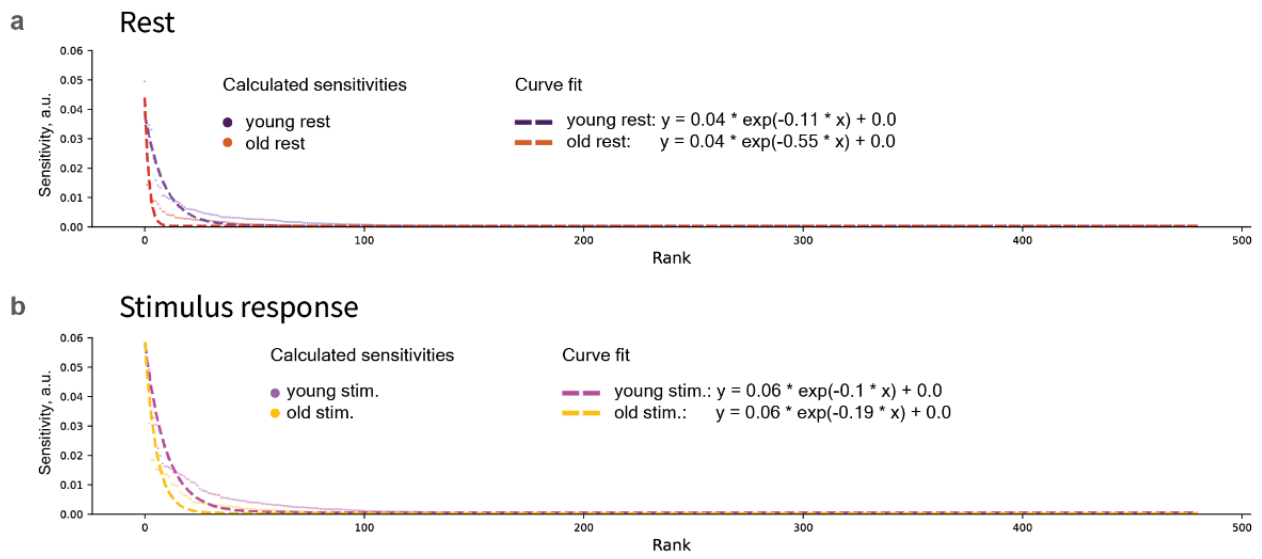
Supplementary Fig. 13. Lactate shuttle in conditions with different blood glucose levels.



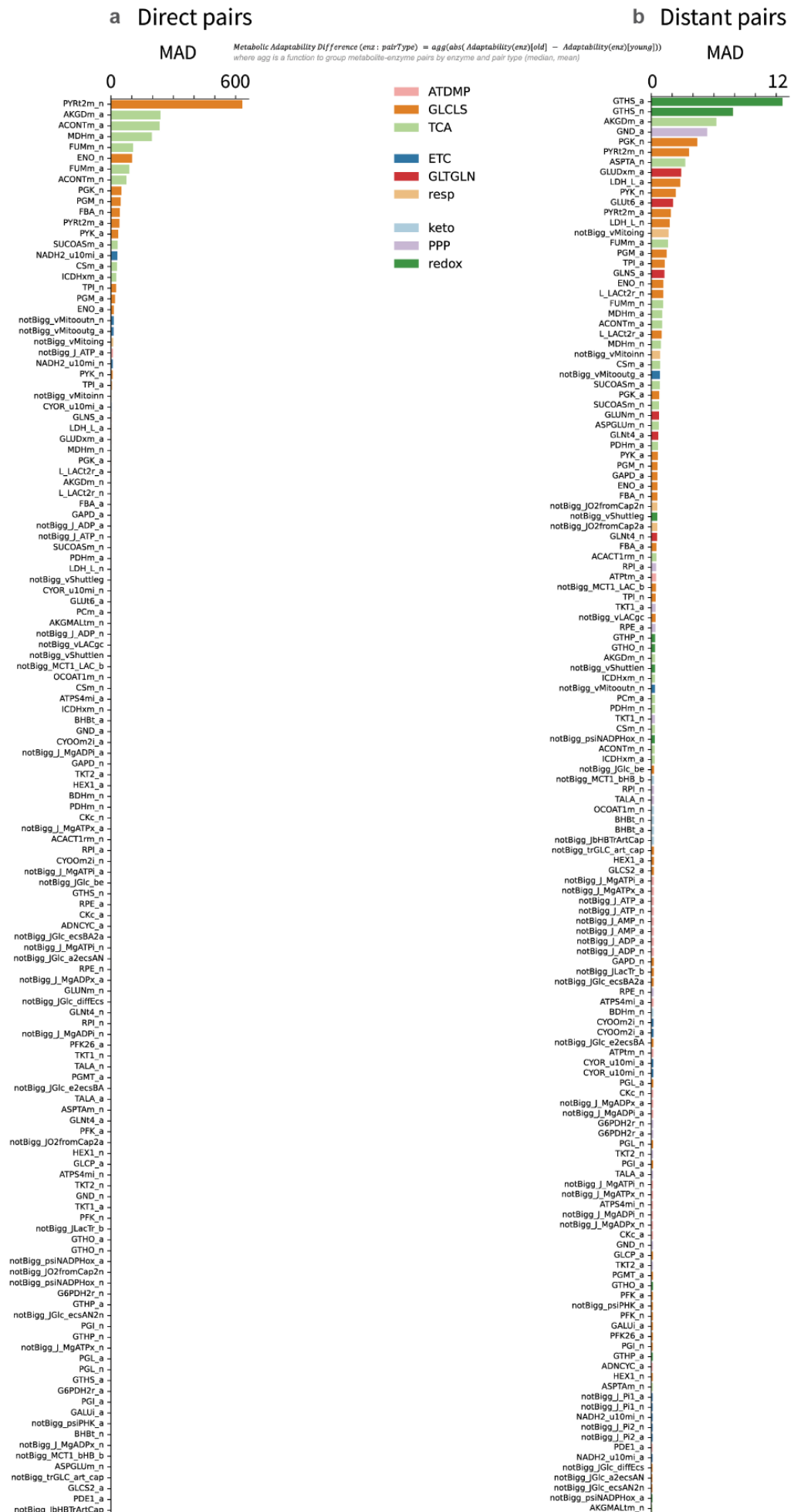
Supplementary Fig. 14. Comparison of synaptic activation and current injection evoked metabolic responses. **a**, Young and old age responses to synaptic input and current injection (approximately the same firing frequency): input current (top left in A), firing traces (left on second row in A), percent difference in metabolic response: $100 \cdot (m_{inj} - m_{syn}) / m_{syn}$ (all other figures in A). **b**, Characteristics of neuronal firing in young and old ages upon synaptic activation and current injection (approximately the same firing frequency).



Supplementary Fig. 15. Sensitivity curve fit.



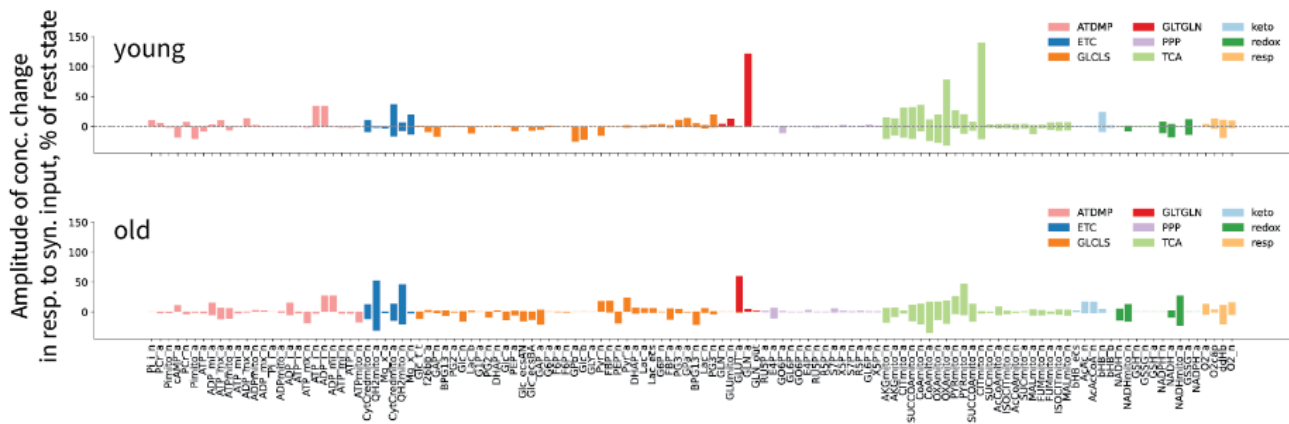
Supplementary Fig. 16. Metabolic adaptability difference.



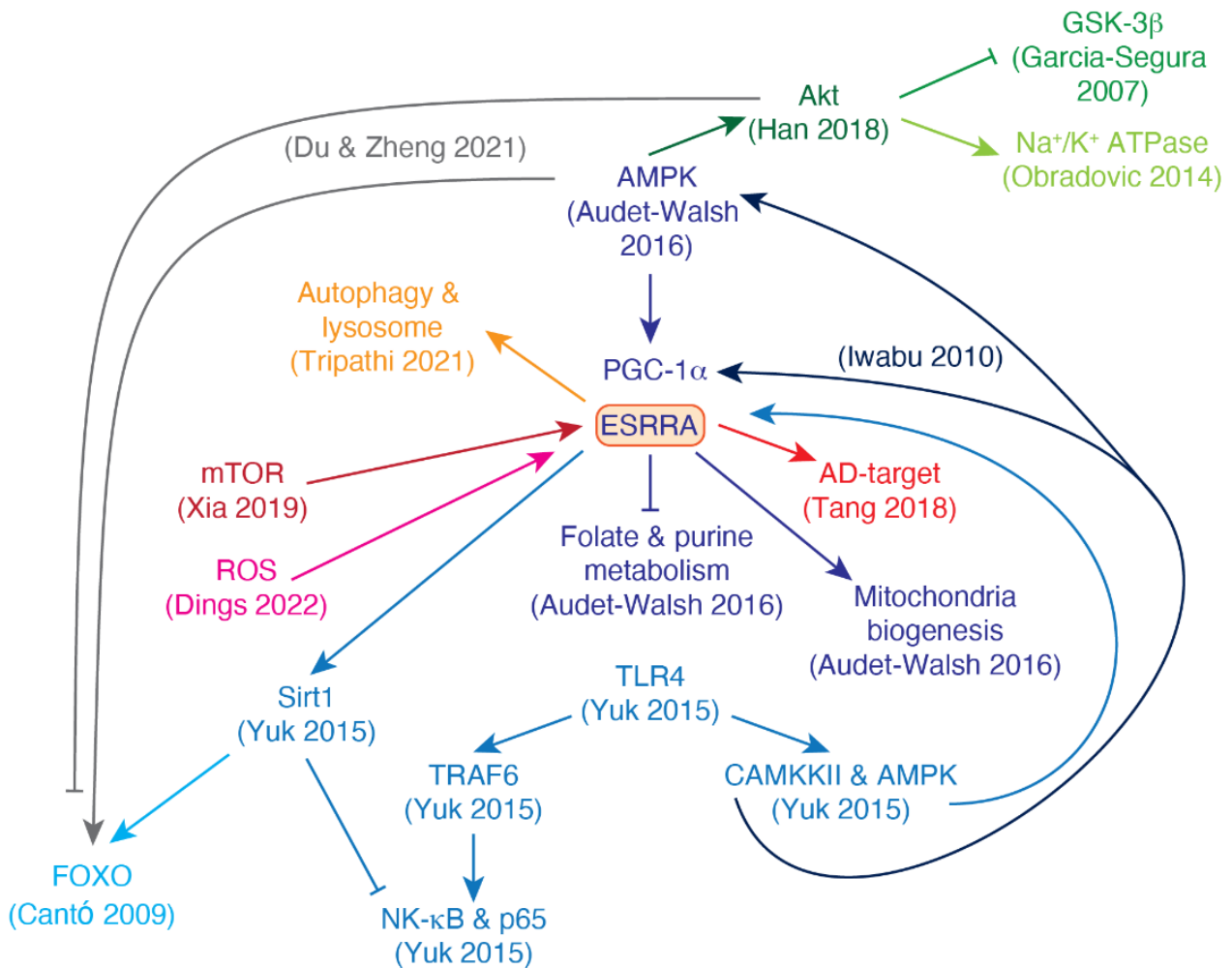
Supplementary Fig. 17. Bottom-up iterative model building workflow and the key considerations.



Supplementary Fig. 18. Labels of individual metabolites for **Fig. 3d**.



Supplementary Fig. 19. Literature evidence for ESRRA being a regulatory hub of aging-associated pathways (colored by reference).



Supplementary Information File 1.

Explanation of the Fruchterman-Reingold force-directed algorithm to position nodes

The Fruchterman-Reingold force-directed algorithm is used for a representation of the network. Edges correspond to springs which are holding nodes close, and nodes correspond to repelling objects. There are two types of forces which define the position of nodes as described below.

1. Attractive force, which acts between nodes that are connected by an edge. It is stronger for nodes connected by higher-weight edges, so these nodes are pulled closer together by the attractive force.
2. Repulsive force, which acts between all pairs of nodes (regardless of connecting edge presence). This force pushes nodes away from each other.

So the resulting edge lengths are not directly proportional to the weights. Instead, the edge weight affects the strength of the attractive force between connected nodes, where larger weight of edge (which in our case corresponds to smaller metabolic adaptability) means a stronger attractive force, and nodes being pulled together.

Centrality in context of metabolic adaptability

Centrality, or closeness centrality (CC), is calculated as a reciprocal of the sum of shortest path distances between the node and all other nodes. Higher centrality means smaller metabolic adaptability: CC is reciprocal to distance, while distance is reciprocal to weight, which makes CC proportional to the weight, while weight is defined as reciprocal of metabolic adaptability, which makes CC reciprocal of metabolic adaptability (Equation 1).

$$CC \sim \frac{1}{distance} = \frac{1}{\frac{1}{weight}} = weight = 1/Adaptability \quad (\text{Equation 1})$$

Supplementary Information File 2.

Changes in other characteristics of neuronal firing (related to Fig.3):

AHP1_depth_from_peak: -7.42%, old: 144.86, young: 156.48

AHP2_depth_from_peak: -7.23%, old: 140.48, young: 151.42

AP1_amp: -8.5%, old: 114.94, young: 125.62

AP1_begin_voltage: -0.35%, old: -51.64, young: -51.82

AP1_begin_width: 0.0%, old: 1.3, young: 1.3

AP1_peak: -14.23%, old: 63.3, young: 73.81
AP1_width: 3.59%, old: 0.76, young: 0.73
AP2_AP1_begin_width_diff: nan%, old: 0.0, young: 0.0
AP2_AP1_diff: -31.37%, old: -1.04, young: -1.52
AP2_AP1_peak_diff: -53.87%, old: -0.49, young: -1.05
AP2_amp: -8.22%, old: 113.9, young: 124.1
AP2_begin_voltage: -0.53%, old: -51.08, young: -51.35
AP2_begin_width: 0.0%, old: 1.3, young: 1.3
AP2_peak: -13.66%, old: 62.82, young: 72.75
AP2_width: 3.46%, old: 0.72, young: 0.7
APlast_amp: -6.17%, old: 105.99, young: 112.96
APlast_width: 3.5%, old: 0.79, young: 0.76
ISI_CV: -2.13%, old: 0.57, young: 0.58
ISI_log_slope: -0.57%, old: 0.16, young: 0.17
ISI_log_slope_skip: 0.24%, old: 0.22, young: 0.22
ISI_semilog_slope: 6.44%, old: 0.02, young: 0.02
Spikecount: -8.47%, old: 54, young: 59
Spikecount_stimint: -8.47%, old: 54, young: 59
adaptation_index: 11.23%, old: 0.01, young: 0.01
adaptation_index2: 11.31%, old: 0.01, young: 0.01
amp_drop_first_last: -29.32%, old: 8.64, young: 12.23
amp_drop_first_second: -53.87%, old: 0.49, young: 1.05
amp_drop_second_last: -27.0%, old: 8.16, young: 11.17
decay_time_constant_after_stim: -91.66%, old: 1603.71, young: 19220.41
doublet_ISI: 5.9%, old: 195.7, young: 184.8
inv_fifth_ISI: -6.26%, old: 8.94, young: 9.53
inv_first_ISI: -5.57%, old: 5.11, young: 5.41
inv_fourth_ISI: -6.06%, old: 8.31, young: 8.84
inv_last_ISI: -7.22%, old: 2.09, young: 2.26
inv_second_ISI: -5.68%, old: 6.53, young: 6.92
inv_third_ISI: -5.8%, old: 7.53, young: 7.99
inv_time_to_first_spike: -33.47%, old: 6.0, young: 9.02
irregularity_index: 16.38%, old: 8.87, young: 7.62
max_amp_difference: -16.07%, old: 1.14, young: 1.35

maximum_voltage: -14.23%, old: 63.3, young: 73.81
maximum_voltage_from_voltagebase: -2.75%, old: 141.84, young: 145.86
mean_AP_amplitude: -6.7%, old: 108.94, young: 116.76
mean_frequency: -8.46%, old: 7.55, young: 8.25
minimum_voltage: 3.33%, old: -85.43, young: -82.68
number_initial_spikes: -10.0%, old: 18, young: 20
steady_state_hyper: 6.37%, old: -85.14, young: -80.05
steady_state_voltage: 8.57%, old: -83.27, young: -76.7
time_to_first_spike: 50.32%, old: 166.7, young: 110.9
time_to_last_spike: -0.02%, old: 7150.2, young: 7151.4
time_to_second_spike: 22.56%, old: 362.4, young: 295.7
voltage_base: 9.0%, old: -78.54, young: -72.05

Statistical tests for comparison of characteristics of neuronal firing (Figure 3).

AP_amplitude

Sample sizes: 59,54

Levene statistic: 6.605499030481687 p-value: 0.011491236053743635

Levene: different variances (reject H0)

Fligner statistic: 6.630869011027655 p-value: 0.01002263560239055

Fligner: different variances (reject H0)

Wilcoxon-Mann-Whitney two-sided U test statistic: 3057.0 p-value: 4.0249411168018834e-17

Wilcoxon-Mann-Whitney two-sided U test: different distributions (reject H0)

Kolmogorov-Smirnov two-sided test statistic: 0.834902699309479 p-value: 6.661338147750939e-16

Kolmogorov-Smirnov two-sided test: different distributions (reject H0)

AP_amplitude_change

Sample sizes: 58,53

Levene statistic: 3.8760940845777174 p-value: 0.051516931692045034

Levene: same variances (fail to reject H0)

Fligner statistic: 4.545621778929398 p-value: 0.033003033701898096

Fligner: different variances (reject H0)

Wilcoxon-Mann-Whitney two-sided U test statistic: 920.0 p-value: 0.0002729809833335603

Wilcoxon-Mann-Whitney two-sided U test: different distributions (reject H0)

Kolmogorov-Smirnov two-sided test statistic: 0.42940793754066364 p-value:

3.8705542437011964e-05

Kolmogorov-Smirnov two-sided test: different distributions (reject H0)

AP_amplitude_diff

Sample sizes: 58,53

Levene statistic: 6.152257861376695 p-value: 0.014653671953606095

Levene: different variances (reject H0)

Fligner statistic: 5.75689520557301 p-value: 0.016424069262576897

Fligner: different variances (reject H0)

Wilcoxon-Mann-Whitney two-sided U test statistic: 1491.0 p-value: 0.7882208195357832

Wilcoxon-Mann-Whitney two-sided U test: same distribution (fail to reject H0)

Kolmogorov-Smirnov two-sided test statistic: 0.1486662329212752 p-value: 0.5084641118074855

Kolmogorov-Smirnov two-sided test: same distribution (fail to reject H0)

AP_amplitude_from_voltagebase

Sample sizes: 59,54

Levene statistic: 7.459710428818111 p-value: 0.007341447281952335

Levene: different variances (reject H0)

Fligner statistic: 7.391190337972734 p-value: 0.006554409829916771

Fligner: different variances (reject H0)

Wilcoxon-Mann-Whitney two-sided U test statistic: 1862.0 p-value: 0.12275003593521057

Wilcoxon-Mann-Whitney two-sided U test: same distribution (fail to reject H0)

Kolmogorov-Smirnov two-sided test statistic: 0.1864406779661017 p-value: 0.23771345375057895

Kolmogorov-Smirnov two-sided test: same distribution (fail to reject H0)

AP_begin_voltage

Sample sizes: 59,54

Levene statistic: 0.3716334196659708 p-value: 0.5433611341543954

Levene: same variances (fail to reject H0)

Fligner statistic: 0.3123751596228548 p-value: 0.5762263366963747

Fligner: same variances (fail to reject H0)

Wilcoxon-Mann-Whitney two-sided U test statistic: 1226.0 p-value: 0.03514923245426359

Wilcoxon-Mann-Whitney two-sided U test: different distributions (reject H0)

Kolmogorov-Smirnov two-sided test statistic: 0.21876961707470183 p-value: 0.1096654688128944

Kolmogorov-Smirnov two-sided test: same distribution (fail to reject H0)

AP_height

Sample sizes: 59,54

Levene statistic: 7.459710428818096 p-value: 0.007341447281952389

Levene: different variances (reject H0)

Fligner statistic: 7.391190337972734 p-value: 0.006554409829916771

Fligner: different variances (reject H0)

Wilcoxon-Mann-Whitney two-sided U test statistic: 3079.0 p-value: 1.3582777666804203e-17

Wilcoxon-Mann-Whitney two-sided U test: different distributions (reject H0)

Kolmogorov-Smirnov two-sided test statistic: 0.8549905838041432 p-value:
6.661338147750939e-16

Kolmogorov-Smirnov two-sided test: different distributions (reject H0)

peak_voltage

Sample sizes: 59,54

Levene statistic: 7.459710428818096 p-value: 0.007341447281952389

Levene: different variances (reject H0)

Fligner statistic: 7.391190337972734 p-value: 0.006554409829916771

Fligner: different variances (reject H0)

Wilcoxon-Mann-Whitney two-sided U test statistic: 3079.0 p-value: 1.3582777666804203e-17

Wilcoxon-Mann-Whitney two-sided U test: different distributions (reject H0)

Kolmogorov-Smirnov two-sided test statistic: 0.8549905838041432 p-value:
6.661338147750939e-16

Kolmogorov-Smirnov two-sided test: different distributions (reject H0)

AP_rise_rate

Sample sizes: 59,54

Levene statistic: 3.2120282887999094 p-value: 0.07582303196261797

Levene: same variances (fail to reject H0)

Fligner statistic: 8.500912633404996 p-value: 0.003549683927627355

Fligner: different variances (reject H0)

Wilcoxon-Mann-Whitney two-sided U test statistic: 3008.0 p-value: 4.274566678078413e-16

Wilcoxon-Mann-Whitney two-sided U test: different distributions (reject H0)

Kolmogorov-Smirnov two-sided test statistic: 0.8163841807909604 p-value:
6.661338147750939e-16

Kolmogorov-Smirnov two-sided test: different distributions (reject H0)

AP_fall_rate

Sample sizes: 59,54

Levene statistic: 3.066184321429485 p-value: 0.08269937892109969

Levene: same variances (fail to reject H0)

Fligner statistic: 6.71176089244189 p-value: 0.0095779100160061

Fligner: different variances (reject H0)

Wilcoxon-Mann-Whitney two-sided U test statistic: 442.0 p-value: 3.7647624938176844e-11

Wilcoxon-Mann-Whitney two-sided U test: different distributions (reject H0)

Kolmogorov-Smirnov two-sided test statistic: 0.7052730696798494 p-value:
3.952393967665557e-14

Kolmogorov-Smirnov two-sided test: different distributions (reject H0)

AP_fall_rate_change

Sample sizes: 58,53

Levene statistic: 0.6190034404678872 p-value: 0.433125124634122

Levene: same variances (fail to reject H0)

Fligner statistic: 3.187363730600531 p-value: 0.0742095978425819

Fligner: same variances (fail to reject H0)

Wilcoxon-Mann-Whitney two-sided U test statistic: 351.0 p-value: 2.5793688476458548e-12

Wilcoxon-Mann-Whitney two-sided U test: different distributions (reject H0)

Kolmogorov-Smirnov two-sided test statistic: 0.8103448275862069 p-value:
1.775156606426841e-20

Kolmogorov-Smirnov two-sided test: different distributions (reject H0)

AP_peak_upstroke

Sample sizes: 59,54

Levene statistic: 4.408526533521235 p-value: 0.038025854014361024

Levene: different variances (reject H0)

Fligner statistic: 4.601321053363534 p-value: 0.03194732985273627

Fligner: different variances (reject H0)

Wilcoxon-Mann-Whitney two-sided U test statistic: 3064.0 p-value: 2.853607187168821e-17

Wilcoxon-Mann-Whitney two-sided U test: different distributions (reject H0)

Kolmogorov-Smirnov two-sided test statistic: 0.7919020715630886 p-value:
6.661338147750939e-16

Kolmogorov-Smirnov two-sided test: different distributions (reject H0)

AP_peak_downstroke

Sample sizes: 59,54

Levene statistic: 1.2715834062751352 p-value: 0.2619014544184533

Levene: same variances (fail to reject H0)

Fligner statistic: 1.6194972442709932 p-value: 0.2031619039342202

Fligner: same variances (fail to reject H0)

Wilcoxon-Mann-Whitney two-sided U test statistic: 239.0 p-value: 7.258645224012553e-15

Wilcoxon-Mann-Whitney two-sided U test: different distributions (reject H0)

Kolmogorov-Smirnov two-sided test statistic: 0.834902699309479 p-value: 6.661338147750939e-16

Kolmogorov-Smirnov two-sided test: different distributions (reject H0)

spike_half_width

Sample sizes: 59,54

Levene statistic: 0.8356847163178224 p-value: 0.36261535212273177

Levene: same variances (fail to reject H0)

Fligner statistic: 0.9340883843599507 p-value: 0.3338028095263355

Fligner: same variances (fail to reject H0)

Wilcoxon-Mann-Whitney two-sided U test statistic: 716.0 p-value: 4.7016301099113494e-07

Wilcoxon-Mann-Whitney two-sided U test: different distributions (reject H0)

Kolmogorov-Smirnov two-sided test statistic: 0.5266792215944758 p-value:
1.0318489573890588e-07

Kolmogorov-Smirnov two-sided test: different distributions (reject H0)

spike_width2

Sample sizes: 58,53

Levene statistic: 0.4059195398968852 p-value: 0.5253838004179687

Levene: same variances (fail to reject H0)

Fligner statistic: 0.8000585301188278 p-value: 0.3710758705566992

Fligner: same variances (fail to reject H0)

Wilcoxon-Mann-Whitney two-sided U test statistic: 728.0 p-value: 1.8132084872745687e-06

Wilcoxon-Mann-Whitney two-sided U test: different distributions (reject H0)

Kolmogorov-Smirnov two-sided test statistic: 0.4362394274560833 p-value:
2.7784173407874313e-05

Kolmogorov-Smirnov two-sided test: different distributions (reject H0)

depolarized_base

Sample sizes: 58,53

Levene statistic: 0.21330792406056287 p-value: 0.6451074156436485

Levene: same variances (fail to reject H0)

Fligner statistic: 0.5099912340048506 p-value: 0.47514265083983753

Fligner: same variances (fail to reject H0)

Wilcoxon-Mann-Whitney two-sided U test statistic: 1622.0 p-value: 0.617871778194361

Wilcoxon-Mann-Whitney two-sided U test: same distribution (fail to reject H0)

Kolmogorov-Smirnov two-sided test statistic: 0.1724137931034483 p-value: 0.3298788555460255

Kolmogorov-Smirnov two-sided test: same distribution (fail to reject H0)

AHP_depth

Sample sizes: 59,54

Levene statistic: 0.08022401294287185 p-value: 0.7775216314033404

Levene: same variances (fail to reject H0)

Fligner statistic: 0.10770161746045517 p-value: 0.7427761389915951

Fligner: same variances (fail to reject H0)

Wilcoxon-Mann-Whitney two-sided U test statistic: 271.0 p-value: 3.055267399749676e-14

Wilcoxon-Mann-Whitney two-sided U test: different distributions (reject H0)

Kolmogorov-Smirnov two-sided test statistic: 0.8518518518518519 p-value:
6.661338147750939e-16

Kolmogorov-Smirnov two-sided test: different distributions (reject H0)

AHP_depth_abs

Sample sizes: 59,54

Levene statistic: 0.08022401294287124 p-value: 0.7775216314033404

Levene: same variances (fail to reject H0)

Fligner statistic: 0.10770132317169079 p-value: 0.7427764779807888

Fligner: same variances (fail to reject H0)

Wilcoxon-Mann-Whitney two-sided U test statistic: 1510.0 p-value: 0.6353512902776368

Wilcoxon-Mann-Whitney two-sided U test: same distribution (fail to reject H0)

Kolmogorov-Smirnov two-sided test statistic: 0.12962962962962962 p-value: 0.6655913571840438

Kolmogorov-Smirnov two-sided test: same distribution (fail to reject H0)

AHP_depth_from_peak

Sample sizes: 59,54

Levene statistic: 1.3399447901571637 p-value: 0.24952849723117262

Levene: same variances (fail to reject H0)

Fligner statistic: 2.424339978036405 p-value: 0.1194635491567324

Fligner: same variances (fail to reject H0)

Wilcoxon-Mann-Whitney two-sided U test statistic: 2893.0 p-value: 8.049943715324859e-14

Wilcoxon-Mann-Whitney two-sided U test: different distributions (reject H0)

Kolmogorov-Smirnov two-sided test statistic: 0.7777777777777778 p-value:
6.661338147750939e-16

Kolmogorov-Smirnov two-sided test: different distributions (reject H0)

AHP_slow_time

Sample sizes: 57,52

Levene statistic: 0.2773733483050493 p-value: 0.5995181094433077

Levene: same variances (fail to reject H0)

Fligner statistic: 0.3607862611307999 p-value: 0.5480698901731853

Fligner: same variances (fail to reject H0)

Wilcoxon-Mann-Whitney two-sided U test statistic: 1598.0 p-value: 0.48348010610693026

Wilcoxon-Mann-Whitney two-sided U test: same distribution (fail to reject H0)

Kolmogorov-Smirnov two-sided test statistic: 0.22604588394062078 p-value:
0.10176313080703958

Kolmogorov-Smirnov two-sided test: same distribution (fail to reject H0)

ISI_values

Sample sizes: 57,52

Levene statistic: 0.02132078025677348 p-value: 0.8841831976486665

Levene: same variances (fail to reject H0)

Fligner statistic: 0.07623370008066287 p-value: 0.7824677972955265

Fligner: same variances (fail to reject H0)

Wilcoxon-Mann-Whitney two-sided U test statistic: 1117.0 p-value: 0.027011518317369983

Wilcoxon-Mann-Whitney two-sided U test: different distributions (reject H0)

Kolmogorov-Smirnov two-sided test statistic: 0.3684210526315789 p-value:

0.0007881130606729458

Kolmogorov-Smirnov two-sided test: different distributions (reject H0)

Supplementary Information File 3.

The top-scoring TF was ESRRA (estrogen-related receptor alpha). This TF regulates expression of multiple metabolism-related genes, including those of mitochondrial function, biogenesis and turnover, as well as lipid catabolism (Tripathi et al., 2020). It is also linked to autophagy and NF- κ B inflammatory response via Sirt1 signaling (Cantó et al., 2009; Yuk et al., 2015; Kim et al., 2018; Suresh et al., 2018). Mitochondrial dysfunction and autophagy impairments are consistently among the hallmarks of aging (López-Otín et al., 2013, 2023; Mattson and Arumugam, 2018). Notably, ESRRA expression is downregulated in aging according to various studies (Schaum et al., 2020; Tripathi et al., 2020).

The second-scoring TF was Nkx2-5 (NK2 homeobox 5), which is highly conserved among species and mostly studied in development and cardiac function (Takeda et al., 2009). Reduction of Nkx2-5 cardiac expression has been reported in aging (Volkova et al., 2005).

The third-ranked TF was the evolutionary conserved energy sensor NFE2L1 (nuclear factor erythroid 2-related factor 1, also called Nrf1 or nuclear respiratory factor 1). It is one of the key regulators of redox signaling and homeostasis. Dysfunction of this TF is associated with glucose metabolism

reprogramming via AMPK signaling (Yang et al., 2021). NFE2L1 also upregulates expression of proteasomal genes in an ERK-signaling dependent manner (Zhang et al., 2021b), which is suggested to contribute to the development of neurodegenerative diseases (Lee et al., 2011).

The next TF was ZBED1 (zinc finger BED domain-containing protein 1). It acts as a small ubiquitin-like modifier (SUMO) ligase by SUMOylating Mi2-alpha during nucleosome remodeling and deacetylation (Yamashita et al., 2016).

The fifth TF, THAP4 (nitrobindin), detoxifies reactive nitrogen and oxygen species and scavenges peroxynitrite (De Simone et al., 2018).

The next TF was PREB (prolactin regulatory element binding). Interestingly, it has been reported as one of the links between aging and Alzheimer's disease (Zhou et al., 2019).

The next TF was HIF1A (hypoxia inducible factor 1), which serves as a key regulator of the hypoxia response at both cellular and system scale. The role of HIF1a in brain aging and neurodegenerative diseases is convoluted, multifaceted and incompletely understood. On one hand, HIF1a promotes erythropoiesis, angiogenesis and exerts neuroprotection (Majmundar et al., 2010; Burtscher et al., 2021). On the other hand, there are contradictory reports on either the detrimental (Sun et al., 2006; March-Diaz et al., 2021; Lee et al., 2023) or protective (Ashok et al., 2017) role of HIF1a in neurodegeneration, Alzheimer's disease in particular. To add the complexity, HIF1a is involved in inflammatory response and metabolism regulation (McGettrick and O'Neill, 2020; Taylor and Scholz, 2022). Even though mechanisms of HIF1a are so multifaceted, therapeutic potential of this TF has been recognized (Lee et al., 2019; Luo et al., 2022).

The next TF was MYRFL (myelin regulatory factor-like protein). Its biological function (and that of some other myelin regulatory factors, such as MYRF) is poorly understood, which is surprising given the importance of myelin for neuronal health (Huang et al., 2021).

The next TF was ZNF878 (zinc finger protein 878), which is one of the hundreds in the rapidly evolved KRAB-domain containing family (Shen et al., 2021).

The last out of top-10 TFs was SALL3 (spalt-like transcription factor 3). It modulates DNA methyltransferase activity and influences human induced pluripotent stem cell differentiation (Kuroda et al., 2019).

We further searched the STRING database (Szklarczyk et al., 2019) for the protein-protein associations of the top TF ESRRA (Fig. 5c), following which we performed a literature search for the top-10 proteins from this search: Hif1a, Sirt1, Hdac8, Ppargc1a, Ppargc1b, Mef2c, Nrip1, Ncoa1, Tfam, Perm1. Interestingly, numerous reports attribute roles in aging and neurodegeneration to these proteins as detailed below.

Hif1a is a common hit in the top-10 of STRING associations and ChEA3 enrichment with its implications in brain aging and neurodegeneration described above.

Sirt1 is a NAD⁺-dependent deacetylase, a member of the sirtuin family of proteins. It is largely studied for its role in aging, longevity, apoptosis, stress resistance, inflammation, linking nutrition and chromatin regulation, energy homeostasis and caloric restriction (Rodgers et al., 2005; Guarente, 2006; Milne et al., 2007; Cantó et al., 2009; Finkel et al., 2009; Bishop et al., 2010; Ledford, 2010; Gut and Verdin, 2013; O'Neill and Hardie, 2013; Ng et al., 2015; Shin et al., 2016; Satoh et al., 2017; Katsyuba et al., 2018; Yang et al., 2018).

Another protein found in STRING associations of ESRRA is HDAC8 (histone deacetylase 8), closely related to the sirtuins signaling. It is largely recognised as a promising drug target in several disorders (Chakrabarti et al., 2015; Mormino et al., 2021; Zhao et al., 2021; Emmons et al., 2022).

Another protein in our list, Ppargc1a (peroxisome proliferator-activated receptor gamma coactivator 1-alpha, also called PGC-1alpha), is an important regulator of energy metabolism and is implicated in aging (Rodgers et al., 2005; Anderson and Prolla, 2009; Garcia et al., 2018). It is associated with Parkinson's (Li et al., 2022) and Huntington's diseases (Cui et al., 2006).

Closely related to PGC-1alpha is the other protein on our list, Ppargc1b (peroxisome proliferator-activated receptor gamma coactivator 1-alpha, also called PGC-1beta), which is also involved in energy metabolism regulation, but less well studied and is an active area of research (Thiebold et al., 2017; Thibonnier et al., 2020).

The next protein on our list is Tfam (mitochondrial transcription factor 1), which is regulated by PGC-1alpha and is implicated in brain aging and neurodegeneration (Grimm and Eckert, 2017; Kang et al., 2018).

Another protein on the list is Perm1 (PGC-1 And ERR-Induced Regulator In Muscle Protein 1) is mostly studied in cardiac mitochondrial metabolism regulation (Huang et al., 2022).

The next on the list is Nrip1 (nuclear receptor interacting protein 1). It is an oxidative metabolism regulator and a potential therapeutic target in Down syndrome (Izzo et al., 2014).

The other protein on the list is Nco1 (nuclear receptor coactivator 1), which is involved in hormonal regulation, learning, memory and neurogenesis (Nishihara et al., 2007; Sun and Xu, 2020).

Next, brain-expressed Mef2c (myocyte enhancer factor 2C) is a TF downregulated in aging in an interferon signaling-dependent way (Deczkowska et al., 2017). Furthermore, therapeutic potential of this TF in neurodegeneration and aging has been recently shown with its effects in promoting cognitive resilience (Barker et al., 2021).

To sum up, our identified anti-aging targets largely align with the literature data on therapeutics for healthy aging (Campisi et al., 2019), but also suggest a role of a few poorly studied TFs in the brain energy metabolism aging and provide the insights on the links between molecular mechanisms implicated in aging and neurodegeneration.

Supplementary Information File 4.

This information will be available after peer-reviewed publication.

Supplementary Information File 5.

This information will be available after peer-reviewed publication.

Supplementary Information File 6.

This information will be available after peer-reviewed publication.

Supplementary Information File 7.

Mapping of model variables indexes to descriptive names and Bigg (King et al., 2016) nomenclature (where available).

#idx	id	u_ + bigg_id (if available) + compartment_id	descriptive name
1	K_x_n	u_k_m_n	Potassium ion in neuronal mito. matrix
2	Mg_x_n	u_mg2_m_n	Magnesium ion in neuronal mito. matrix
3	NADHmito_n	u_nadh_m_n	NADH in neuronal mito.
4	QH2mito_n	u_q10h2_m_n	Reduced ubiquinol in neuronal mito. matrix
5	CytCredmito_n	u_focytC_m_n	Reduced cytochrome c in neuronal mito. matrix
6	O2_n	u_o2_c_n	Oxygen in neuronal cytosol
7	ATPmito_n	u_atp_m_n	Free ATP in neuronal mito. matrix
8	ADPmito_n	u_adp_m_n	Free ADP in neuronal mito. matrix
9	ATP_mx_n	u_notBigg_ATP_mx_m_n	Magnesium-bound ATP in neuronal mito. matrix
10	ADP_mx_n	u_notBigg_ADp_mx_m_n	Magnesium-bound ADP in neuronal mito. matrix
11	Pimito_n	u_pi_m_n	Phosphate in neuronal mito. matrix
12	ATP_i_n	u_atp_i_n	Free ATP in neuronal mito. IMS
13	ADP_i_n	u_adp_i_n	Free ADP in neuronal mito. IMS
14	ATP_mi_n	u_notBigg_ATP_mi_i_n	Magnesium-bound ATP in neuronal mito. IMS

15	ADP_mito_n	u_notBigg_ADp_mi_i_n	Magnesium-bound ADP in neuronal mito. IMS
16	Pi_i_n	u_pi_i_n	Phosphate in neuronal mito. IMS
17	MitoMembrPotent_n	u_notBigg_MitoMembrPotent_m_n	Neuronal mitochondrial membrane potential
18	ATP_n	u_atp_c_n	ATP in neuronal cytosol
19	FUMmito_n	u_fum_m_n	Fumarate in neuronal mito.
20	MALmito_n	u_mal_L_m_n	L-Malate in neuronal mito.
21	OXAmito_n	u_oaa_m_n	Oxaloacetate in neuronal mito.
22	SUCmito_n	u_succ_m_n	Succinate in neuronal mito.
23	SUCCOAmito_n	u_succoa_m_n	Succinyl-CoA in neuronal mito.
24	CoAmito_n	u_coa_m_n	Coenzyme A in neuronal mito.
25	AKGmito_n	u_akg_m_n	Alpha-ketoglutarate in neuronal mito.
26	ISOCITmito_n	u_icit_m_n	Isocitrate in neuronal mito.
27	CITmito_n	u_cit_m_n	Citrate in neuronal mito.
28	AcCoAmito_n	u_accoa_m_n	Acetyl-CoA in neuronal mito.
29	AcAc_n	u_acac_c_n	Acetoacetate in neuron (only mito., no cytosolic AcAc in the model)
30	AcAcCoA_n	u_aacoa_m_n	Acetoacetyl-CoA in neuronal mito.
31	PYRmito_n	u_pyr_m_n	Pyruvate in neuronal mito.
32	bHB_n	u_bhb_c_n	beta-Hydroxybutyrate in neuronal cytosol

33	bHB_ecs	u_bhb_e_e	beta-Hydroxybutyrate in extracellular space
34	bHB_b	u_bhb_b_b	beta-Hydroxybutyrate in capillaries
35	GLUmito_n	u_glu_L_m_n	L-Glutamate in neuronal mito.
36	GLU_n	u_glu_L_c_n	L-Glutamate in neuronal cytosol
37	NADH_n	u_nadh_c_n	NADH in neuronal cytosol
38	K_x_a	u_k_m_a	Potassium ion in astrocytic mito. matrix
39	Mg_x_a	u_mg2_m_a	Magnesium ion in astrocytic mito. matrix
40	NADHmito_a	u_nadh_m_a	NADH in astrocytic mito.
41	QH2mito_a	u_q10h2_m_a	Reduced ubiquinol in astrocytic mito. matrix
42	CytCredmito_a	u_focytC_m_a	Reduced cytochrome c in astrocytic mito. matrix
43	O2_a	u_o2_c_a	Oxygen in astrocytic cytosol
44	ATPmito_a	u_atp_m_a	Free ATP in astrocytic mito. matrix
45	ADPmito_a	u_adp_m_a	Free ADP in astrocytic mito. matrix
46	ATP_mx_a	u_notBigg_ATP_mx_m_a	Magnesium-bound ATP in astrocytic mito. matrix
47	ADP_mx_a	u_notBigg_ADp_mx_m_a	Magnesium-bound ADP in astrocytic mito. matrix
48	Pimito_a	u_pi_m_a	Phosphate in astrocytic mito. matrix
49	ATP_i_a	u_atp_i_a	Free ATP in astrocytic mito. IMS
50	ADP_i_a	u_adp_i_a	Free ADP in astrocytic mito. IMS

51	ATP_mi_a	u_notBigg_ATP_mi_i_a	Magnesium-bound ATP in astrocytic mito. IMS
52	ADP_mi_a	u_notBigg_ADP_mi_i_a	Magnesium-bound ADP in astrocytic mito. IMS
53	Pi_i_a	u_pi_i_a	Phosphate in astrocytic mito. IMS
54	MitoMembrPotent_a	u_notBigg_MitoMembrPotential_m_a	Astrocytic mitochondrial membrane potential
55	ATP_a	u_atp_c_a	ATP in astrocytic cytosol
56	FUMmito_a	u_fum_m_a	Fumarate in astrocytic mito.
57	MALmito_a	u_mal_L_m_a	L-Malate in astrocytic mito.
58	OXAmito_a	u_oaa_m_a	Oxaloacetate in astrocytic mito.
59	SUCmito_a	u_succ_m_a	Succinate in astrocytic mito.
60	SUCCOAmito_o_a	u_succoa_m_a	Succinyl-CoA in astrocytic mito.
61	CoAmito_a	u_coa_m_a	Coenzyme A in astrocytic mito.
62	AKGmito_a	u_akg_m_a	Alpha-ketoglutarate in astrocytic mito.
63	ISOCITmito_a	u_icit_m_a	Isocitrate in astrocytic mito.
64	CITmito_a	u_cit_m_a	Citrate in astrocytic mito.
65	AcCoAmito_a	u_accoa_m_a	Acetyl-CoA in astrocytic mito.
66	PYRmito_a	u_pyr_m_a	Pyruvate in astrocytic mito.
67	GLN_n	u_gln_L_c_n	Glutamine in neuron
68	GLN_out	u_gln_L_e_e	Glutamine in extracellular space
69	GLN_a	u_gln_L_c_a	Glutamine in astrocytic cytosol
70	GLUT_a	u_glu_L_c_a	Glutamate in astrocytic cytosol
71	Va	u_notBigg_Va_c_a	Astrocytic membrane potential

72	Na_a	u_na1_c_a	Sodium ion in astrocytic cytosol
73	K_a	u_k_c_a	Potassium ion in astrocytic cytosol
74	K_out	u_k_e_e	Potassium ion in extracellular space
75	GLUT_syn	u_glu_L_syn_syn	Synaptic glutamate
76	VNeu (also referred as V)	u_notBigg_VNeu_c_n	Neuronal membrane potential
77	Na_n	u_na1_c_n	Sodium ion in neuronal cytosol
78	h	u_notBigg_hgate_c_n	Gating variable h of Hodgkin-Huxley model in neuron
79	n	u_notBigg_ngate_c_n	Gating variable n of Hodgkin-Huxley model in neuron
80	Ca_n	u_ca2_c_n	Calcium in neuronal cytosol
81	pgate	u_notBigg_pgate_c_n	Gating variable of M-current in neuron
82	nBK_a	u_notBigg_nBK_c_a	Gating variable of BK channels in astrocyte
83	mGluRbound Ratio_a	u_notBigg_mGluRboundRatio_c_a	Ratio of bound metabotropic glutamate receptors in astrocyte
84	IP3_a	u_notBigg_IP3_c_a	IP3 in astrocytic cytosol
85	hIP3Ca_a	u_notBigg_hIP3Ca_c_a	Gating variable of IP3-dependent calcium flow in astrocytic cytosol
86	Ca_a	u_ca2_c_a	Calcium in astrocytic cytosol
87	sTRP_a	u_notBigg_sTRP_c_a	Astrocytic TRPV4 channel open probability
88	vV	u_notBigg_vV_b_b	Venous volume
89	EET_a	u_notBigg_EET_c_a	Epoxyeicosatrienoic acid

90	ddHb	u_notBigg_ddHb_b_b	Deoxyhemoglobin
91	O2cap	u_o2_b_b	Oxygen in capillaries
92	Glc_b	u_glc_D_b_b	D-Glucose in capillaries
93	Glc_t_t	u_glc_D_ecsEndothelium_ecsEndothelium	D-Glucose in endothelium
94	Glc_ecsBA	u_glc_D_ecsBA_ecsBA	D-Glucose in basal lamina
95	Glc_a	u_glc_D_c_a	D-Glucose in astrocytic cytosol
96	Glc_ecsAN	u_glc_D_ecsAN_ecsAN	D-Glucose in interstitial space
97	Glc_n	u_glc_D_c_n	D-Glucose in neuronal cytosol
98	G6P_n	u_g6p_c_n	D-Glucose 6-phosphate in neuronal cytosol
99	G6P_a	u_g6p_c_a	D-Glucose 6-phosphate in astrocytic cytosol
100	F6P_n	u_f6p_c_n	D-Fructose 6-phosphate in neuronal cytosol
101	F6P_a	u_f6p_c_a	D-Fructose 6-phosphate in astrocytic cytosol
102	FBP_n	u_fdp_c_n	D-Fructose 1,6-bisphosphate in neuronal cytosol
103	FBP_a	u_fdp_c_a	D-Fructose 1,6-bisphosphate in astrocytic cytosol
104	f26bp_a	u_f26bp_c_a	D-Fructose 2,6-bisphosphate in astrocytic cytosol
105	GLY_a	u_glycogen_c_a	Glycogen in astrocytic cytosol
106	G1P_a	u_g1p_c_a	D-Glucose 1-phosphate in astrocytic cytosol
107	GAP_n	u_g3p_c_n	Glyceraldehyde 3-phosphate in neuronal cytosol

108	GAP_a	u_g3p_c_a	Glyceraldehyde 3-phosphate in astrocytic cytosol
109	DHAP_n	u_dhap_c_n	Dihydroxyacetone phosphate in neuronal cytosol
110	DHAP_a	u_dhap_c_a	Dihydroxyacetone phosphate in astrocytic cytosol
111	BPG13_n	u_13dpg_c_n	3-Phospho-D-glyceroyl phosphate in neuronal cytosol
112	BPG13_a	u_13dpg_c_a	3-Phospho-D-glyceroyl phosphate in astrocytic cytosol
113	NADH_a	u_nadh_c_a	NADH in astrocytic cytosol
114	PG3_n	u_3pg_c_n	3-Phospho-D-glycerate in neuronal cytosol
115	PG3_a	u_3pg_c_a	3-Phospho-D-glycerate in astrocytic cytosol
116	PG2_n	u_2pg_c_n	D-Glycerate 2-phosphate in neuronal cytosol
117	PG2_a	u_2pg_c_a	D-Glycerate 2-phosphate in astrocytic cytosol
118	PEP_n	u_pep_c_n	Phosphoenolpyruvate in neuronal cytosol
119	PEP_a	u_pep_c_a	Phosphoenolpyruvate in astrocytic cytosol
120	Pyr_n	u_pyr_c_n	Pyruvate in neuronal cytosol
121	Pyr_a	u_pyr_c_a	Pyruvate in astrocytic cytosol
122	Lac_b	u_lac_L_b_b	L-Lactate in capillaries
123	Lac_ecs	u_lac_L_e_e	L-Lactate in extracellular space
124	Lac_a	u_lac_L_c_a	L-Lactate in astrocytic cytosol

125	Lac_n	u_lac_L_c_n	L-Lactate in neuronal cytosol
126	NADPH_n	u_nadph_c_n	NADPH in neuronal cytosol
127	NADPH_a	u_nadph_c_a	NADPH in astrocytic cytosol
128	GL6P_n	u_6pgl_c_n	6-phospho-D-glucono-1,5-lactone in neuronal cytosol
129	GL6P_a	u_6pgl_c_a	6-phospho-D-glucono-1,5-lactone in astrocytic cytosol
130	GO6P_n	u_6pgc_c_n	6-Phospho-D-gluconate in neuronal cytosol
131	GO6P_a	u_6pgc_c_a	6-Phospho-D-gluconate in astrocytic cytosol
132	RU5P_n	u_ru5p_D_c_n	D-Ribulose 5-phosphate in neuronal cytosol
133	RU5P_a	u_ru5p_D_c_a	D-Ribulose 5-phosphate in astrocytic cytosol
134	R5P_n	u_r5p_c_n	D-Ribose 5-phosphate in neuronal cytosol
135	R5P_a	u_r5p_c_a	D-Ribose 5-phosphate in astrocytic cytosol
136	X5P_n	u_xu5p_D_c_n	D-Xylulose 5-phosphate in neuronal cytosol
137	X5P_a	u_xu5p_D_c_a	D-Xylulose 5-phosphate in astrocytic cytosol
138	S7P_n	u_s7p_c_n	Sedoheptulose 7-phosphate in neuronal cytosol
139	S7P_a	u_s7p_c_a	Sedoheptulose 7-phosphate in astrocytic cytosol

140	E4P_n	u_e4p_c_n	D-Erythrose 4-phosphate in neuronal cytosol
141	E4P_a	u_e4p_c_a	D-Erythrose 4-phosphate in astrocytic cytosol
142	GSH_n	u_gthrd_c_n	Reduced glutathione in neuronal cytosol
143	GSH_a	u_gthrd_c_a	Reduced glutathione in astrocytic cytosol
144	GSSG_n	u_gthox_c_n	Oxidized glutathione in neuronal cytosol
145	GSSG_a	u_gthox_c_a	Oxidized glutathione in astrocytic cytosol
146	PCr_n	u_pcreat_c_n	Phosphocreatine in neuronal cytosol
147	PCr_a	u_pcreat_c_a	Phosphocreatine in astrocytic cytosol
148	cAMP_a	u_camp_c_a	Cyclic AMP in astrocytic cytosol
149	NE_neuromod	u_nrpphr_e_e	Norepinephrine in extracellular space
150	GPa_a	u_notBigg_GPa_c_a	Active glycogen phosphorylase in astrocytic cytosol
151	GPb_a	u_notBigg_GPb_c_a	Inactive glycogen phosphorylase in astrocytic cytosol

Supplementary Information File 8.

Model variables initial values.

#	Variable	Initial value	Units
---	----------	---------------	-------

1	K_x_n	54.88513909303930	mM
2	Mg_x_n	0.6405401937956020	mM
3	NADHmito_n	0.3146584474671010	mM
4	QH2mito_n	0.0155067120830932	mM
5	CytCredmito_n	0.1318502545732710	mM
6	O2_n	0.0314865025158087	mM
7	ATPmito_n	0.7487433393982620	mM
8	ADPmito_n	1.8512566606017400	mM
9	ATP_mx_n	0.2084517745966100	mM
10	ADP_mx_n	1.129008031715840	mM
11	Pimito_n	17.22873019667990	mM
12	ATP_i_n	1.385172099080790	mM
13	ADP_i_n	0.0572067246036489	mM
14	ATP_mi_n	1.2787221400985900	mM
15	ADP_mi_n	0.0560549944512344	mM
16	Pi_i_n	19.999860977665800	mM
17	MitoMembrPotent_n	152.33918637408700	mV
18	ATP_n	1.3846374147608100	mM
19	FUMmito_n	0.0703303834778912	mM
20	MALmito_n	0.3877284278881230	mM
21	OXAmito_n	0.0113308326310003	mM
22	SUCmito_n	0.3913984292428140	mM
23	SUCCOAmito_n	0.0027652024434962	mM
24	CoAmito_n	0.0027278355391079	mM
25	AKGmito_n	0.0730279198447203	mM
26	ISOCITmito_n	0.0331278125743512	mM
27	CITmito_n	0.3414510962627290	mM
28	AcCoAmito_n	0.040486317761993	mM
29	AcAc_n	0.0008938613668892	mM
30	AcAcCoA_n	3.47172557254032E-05	mM
31	PYRmito_n	0.0459280204781883	mM
32	bHB_n	0.0020508302306412	mM
33	bHB_ecs	0.0028617229372728	mM
34	bHB_b	0.2981203841045340	mM

35	GLUmito_n	10.001887920296100	mM
36	GLU_n	10.000000420931500	mM
37	NADH_n	0.0041407804365102	mM
38	K_x_a	54.88513909303930	mM
39	Mg_x_a	0.6254020744170420	mM
40	NADHmito_a	0.3622495632039700	mM
41	QH2mito_a	0.0106589284924907	mM
42	CytCredmito_a	0.1075501448904180	mM
43	O2_a	0.0390586574723978	mM
44	ATPmito_a	0.8554395319513810	mM
45	ADPmito_a	1.7445604680486200	mM
46	ATP_mx_a	0.2082789745472760	mM
47	ADP_mx_a	1.1443189511420600	mM
48	Pimito_a	17.625288473162200	mM
49	ATP_i_a	1.29745793823728	mM
50	ADP_i_a	0.0443466995414318	mM
51	ATP_mi_a	1.1823280190768100	mM
52	ADP_mi_a	0.0436294958926607	mM
53	Pi_i_a	19.999931107524700	mM
54	MitoMembrPotent_a	155.39201516889300	mV
55	ATP_a	1.2971907639974400	mM
56	FUMmito_a	0.0500591772559637	mM
57	MALmito_a	0.2552499695609830	mM
58	OXAmito_a	0.0044682268709836	mM
59	SUCmito_a	0.5865999694835420	mM
60	SUCCOAmityo_a	0.0016699868314113	mM
61	CoAmityo_a	0.0025413688391748	mM
62	AKGmito_a	0.0151591579926322	mM
63	ISOCITmito_a	0.0360692382798456	mM
64	CITmito_a	0.358985824746709	mM
65	AcCoAmityo_a	0.0042886443294129	mM
66	PYRmito_a	0.0129832531511687	mM
67	GLN_n	0.4001678075113440	mM
68	GLN_out	0.1999103267772770	mM

69	GLN_a	0.2497981926884060	mM
70	GLUT_a	0.2994675379035370	mM
71	Va	-94.73739998434870	mV
72	Na_a	16.27886560396610	mM
73	K_a	100.79307843484200	mM
74	K_out	3.1104211426858500	mM
75	GLUT_syn	2.5E-05	mM
76	VNeu	-68.00932293426200	mV
77	Na_n	8.473759755301560	mM
78	h	0.9811237297560300	a.u.
79	n	0.0346735745461176	a.u.
80	Ca_n	5.43668920573349E-05	mM
81	pgate	0.0355392388163259	a.u.
82	nBK_a	7.45614720951229E-06	a.u.
83	mGluRboundRatio_a	0.0	a.u.
84	IP3_a	1.18523405898429E-06	mM
85	hIP3Ca_a	0.6531565346093100	a.u.
86	Ca_a	5.31000955574647E-05	mM
87	sTRP_a	0.0012469723667279	a.u.
88	vV	0.0237000024973173	ml
89	EET_a	3.14387167003372E-05	mM
90	ddHb	0.0585277029194496	mM
91	O2cap	7.105220869902980	mM
92	Glc_b	4.555436497117540	mM
93	Glc_t_t	1.4036921120261500	mM
94	Glc_ecsBA	1.302331013714970	mM
95	Glc_a	1.2215129412034000	mM
96	Glc_ecsAN	1.0034276408975700	mM
97	Glc_n	0.9117230433328600	mM
98	G6P_n	0.0451803110921908	mM
99	G6P_a	0.0614224256490154	mM
100	F6P_n	0.0073671881089935	mM
101	F6P_a	0.0101391530037056	mM
102	FBP_n	0.0094588621787074	mM

103	FBP_a	0.0299767447273059	mM
104	f26bp_a	0.0121698969225108	mM
105	GLY_a	13.99969995417290	mM
106	G1P_a	0.0128112803617315	mM
107	GAP_n	0.0012351454067088	mM
108	GAP_a	0.0022568560606488	mM
109	DHAP_n	0.0032208035336226	mM
110	DHAP_a	0.0037897580104066	mM
111	BPG13_n	0.0060805407271592	mM
112	BPG13_a	0.0080305626199569	mM
113	NADH_a	0.10927809092221	mM
114	PG3_n	0.0176506715347894	mM
115	PG3_a	0.0214636041341032	mM
116	PG2_n	0.0019612387455003	mM
117	PG2_a	0.0023600313501276	mM
118	PEP_n	0.0011299114036925	mM
119	PEP_a	0.0013498159787353	mM
120	Pyr_n	0.0988456289470794	mM
121	Pyr_a	0.0294824423032595	mM
122	Lac_b	0.6887631395085970	mM
123	Lac_ecs	0.6223377821910430	mM
124	Lac_a	0.6224222941358750	mM
125	Lac_n	0.62189156291357	mM
126	NADPH_n	0.0300300281880248	mM
127	NADPH_a	0.0300061794837243	mM
128	GL6P_n	2.72238586697895E-06	mM
129	GL6P_a	3.01982377401018E-06	mM
130	GO6P_n	0.0026154588421574	mM
131	GO6P_a	0.0018252228026121	mM
132	RU5P_n	0.0005499402428921	mM
133	RU5P_a	0.0006682285740983	mM
134	R5P_n	1.56498486886425E-05	mM
135	R5P_a	2.60658832155385E-05	mM
136	X5P_n	0.0168344242629796	mM

137	X5P_a	0.0204705104083548	mM
138	S7P_n	0.0198078394367428	mM
139	S7P_a	0.249543115567966	mM
140	E4P_n	0.0066329544563609	mM
141	E4P_a	0.0061388697486627	mM
142	GSH_n	1.200006238770550	mM
143	GSH_a	4.300000202932420	mM
144	GSSG_n	0.0119968806147281	mM
145	GSSG_a	0.0429998985338233	mM
146	PCr_n	4.98986852470732	mM
147	PCr_a	4.927691727614910	mM
148	cAMP_a	0.0391827032589541	mM
149	NE_neuromod	0.0	mM
150	GPa_a	0.0013314628973952	mM
151	GPb_a	0.0686685371026043	mM

References

- Acevedo, A., Torres, F., Kiwi, M., Baeza-Lehnert, F., Barros, L. F., Lee-Liu, D., et al. (2023). Metabolic switch in the aging astrocyte supported via integrative approach comprising network and transcriptome analyses. *Aging* 15. doi: 10.18632/aging.204663.
- Achanta, L. B., and Rae, C. D. (2017). β -Hydroxybutyrate in the Brain: One Molecule, Multiple Mechanisms. *Neurochem. Res.* 42, 35–49. doi: 10.1007/s11064-016-2099-2.
- Amorim, J. A., Coppotelli, G., Rolo, A. P., Palmeira, C. M., Ross, J. M., and Sinclair, D. A. (2022). Mitochondrial and metabolic dysfunction in ageing and age-related diseases. *Nat. Rev. Endocrinol.* 18, 243–258. doi: 10.1038/s41574-021-00626-7.
- Anderson, P. J., and Wright, B. E. (1980). Kinetic models of glycogen metabolism in normal rat liver, morris Hepatom 7787 and host liver. *Int. J. Biochem.* 12, 361–369. doi: 10.1016/0020-711X(80)90115-9.
- Anderson, R., and Prolla, T. (2009). PGC-1 α in aging and anti-aging interventions. *Biochim. Biophys. Acta* 1790, 1059–1066. doi: 10.1016/j.bbagen.2009.04.005.
- Antononkov, V. D., Croes, K., Waelkens, E., Van Veldhoven, P. P., and Mannaerts, G. P. (2000). Identification, purification and characterization of an acetoacetyl-CoA thiolase from rat liver peroxisomes: Acetoacetyl-CoA thiolase from liver peroxisomes. *Eur. J. Biochem.* 267, 2981–2990. doi: 10.1046/j.1432-1033.2000.01314.x.
- Arce-Molina, R., Cortés-Molina, F., Sandoval, P. Y., Galaz, A., Alegría, K., Schirmeier, S., et al. (2020). A highly responsive pyruvate sensor reveals pathway-regulatory role of the mitochondrial pyruvate carrier MPC. *eLife* 9, e53917. doi: 10.7554/eLife.53917.

- Ashok, B. S., Ajith, T. A., and Sivanesan, S. (2017). Hypoxia-inducible factors as neuroprotective agent in Alzheimer's disease. *Clin. Exp. Pharmacol. Physiol.* 44, 327–334. doi: 10.1111/1440-1681.12717.
- Atkinson, D. E. (1968). Energy charge of the adenylate pool as a regulatory parameter. Interaction with feedback modifiers. *Biochemistry* 7, 4030–4034. doi: 10.1021/bi00851a033.
- Aubert, A., Costalat, R., and Valabrègue, R. (2001). Modelling of the coupling between brain electrical activity and metabolism. *Acta Biotheor.* 49, 301–326. doi: 10.1023/a:1014286728421.
- Baeza-Lehnert, F., Saab, A. S., Gutiérrez, R., Larenas, V., Díaz, E., Horn, M., et al. (2019). Non-Canonical Control of Neuronal Energy Status by the Na⁺ Pump. *Cell Metab.* 29, 668–680.e4. doi: 10.1016/j.cmet.2018.11.005.
- Barbagallo, M., Belvedere, M., and Dominguez, L. J. (2009). Magnesium homeostasis and aging. *Magnes. Res.* 22, 235–246. doi: 10.1684/mrh.2009.0187.
- Barbagallo, M., and Dominguez, L. (2010). Magnesium and Aging. *Curr. Pharm. Des.* 16, 832–839. doi: 10.2174/138161210790883679.
- Barbagallo, M., Veronese, N., and Dominguez, L. J. (2021). Magnesium in Aging, Health and Diseases. *Nutrients* 13, 463. doi: 10.3390/nu13020463.
- Barden, R. E., Fung, C. H., Utter, M. F., and Scrutton, M. C. (1972). Pyruvate carboxylase from chicken liver. Steady state kinetic studies indicate a “two-site” ping-pong mechanism. *J. Biol. Chem.* 247, 1323–1333.
- Barker, S. J., Raju, R. M., Milman, N. E. P., Wang, J., Davila-Velderrain, J., Gunter-Rahman, F., et al. (2021). MEF2 is a key regulator of cognitive potential and confers resilience to neurodegeneration. *Sci. Transl. Med.* 13, eabd7695. doi: 10.1126/scitranslmed.abd7695.
- Barros, L. (2022). How expensive is the astrocyte? *J. Cereb. Blood Flow Metab.* 42, 738–745. doi: 10.1177/0271678X221077343.
- Barros, L. F., Bittner, C. X., Loaiza, A., and Porras, O. H. (2007). A quantitative overview of glucose dynamics in the gliovascular unit. *Glia* 55, 1222–1237. doi: 10.1002/glia.20375.
- Barros, L. F., San Martín, A., Ruminot, I., Sandoval, P. Y., Fernández-Moncada, I., Baeza-Lehnert, F., et al. (2017). Near-critical GLUT1 and Neurodegeneration: Glucose Transport and Neurodegeneration. *J. Neurosci. Res.* 95, 2267–2274. doi: 10.1002/jnr.23998.
- Bélanger, M., Allaman, I., and Magistretti, P. J. (2011). Brain energy metabolism: focus on astrocyte-neuron metabolic cooperation. *Cell Metab.* 14, 724–738. doi: 10.1016/j.cmet.2011.08.016.
- Bennett, M. R., Farnell, L., and Gibson, W. G. (2008). Origins of blood volume change due to glutamatergic synaptic activity at astrocytes abutting on arteriolar smooth muscle cells. *J. Theor. Biol.* 250, 172–185. doi: 10.1016/j.jtbi.2007.08.024.
- Benton, D., Parker, P. Y., and Donohoe, R. T. (1996). The supply of glucose to the brain and cognitive functioning. *J. Biosoc. Sci.* 28, 463–479. doi: 10.1017/S0021932000022537.
- Berndt, N., Bulik, S., and Holzhütter, H.-G. (2012). Kinetic Modeling of the Mitochondrial Energy Metabolism of Neuronal Cells: The Impact of Reduced α -Ketoglutarate Dehydrogenase Activities on ATP Production and Generation of Reactive Oxygen Species. *Int. J. Cell Biol.* 2012, 757594. doi: 10.1155/2012/757594.
- Berndt, N., Bulik, S., Wallach, I., Wünsch, T., König, M., Stockmann, M., et al. (2018). HEPATOKIN1 is a biochemistry-based model of liver metabolism for applications in medicine and pharmacology. *Nat. Commun.* 9, 2386. doi: 10.1038/s41467-018-04720-9.
- Berndt, N., Kann, O., and Holzhütter, H.-G. (2015). Physiology-Based Kinetic Modeling of Neuronal Energy Metabolism Unravels the Molecular Basis of NAD(P)H Fluorescence Transients. *J. Cereb. Blood Flow Metab.* 35, 1494–1506. doi: 10.1038/jcbfm.2015.70.
- Bezanson, J., Edelman, A., Karpinski, S., and Shah, V. B. (2017). Julia: A Fresh Approach to Numerical Computing. *SIAM Rev.* 59, 65–98. doi: 10.1137/141000671.
- Bishop, N. A., Lu, T., and Yankner, B. A. (2010). Neural mechanisms of ageing and cognitive decline. *Nature* 464, 529–535. doi: 10.1038/nature08983.

- Błaszczuk, J. W. (2020). Energy Metabolism Decline in the Aging Brain—Pathogenesis of Neurodegenerative Disorders. *Metabolites* 10, 450. doi: 10.3390/metabo10110450.
- Bonvento, G., and Bolaños, J. P. (2021). Astrocyte-neuron metabolic cooperation shapes brain activity. *Cell Metab.* 33, 1546–1564. doi: 10.1016/j.cmet.2021.07.006.
- Borst, P. (2020). The malate–aspartate shuttle (Borst cycle): How it started and developed into a major metabolic pathway. *IUBMB Life* 72, 2241–2259. doi: 10.1002/iub.2367.
- Botman, D., Tigchelaar, W., and Van Noorden, C. J. F. (2014). Determination of glutamate dehydrogenase activity and its kinetics in mouse tissues using metabolic mapping (quantitative enzyme histochemistry). *J. Histochem. Cytochem. Off. J. Histochem. Soc.* 62, 802–812. doi: 10.1369/0022155414549071.
- Bouzier-Sore, A.-K., and Bolaños, J. P. (2015). Uncertainties in pentose-phosphate pathway flux assessment underestimate its contribution to neuronal glucose consumption: relevance for neurodegeneration and aging. *Front. Aging Neurosci.* 7. doi: 10.3389/fnagi.2015.00089.
- Bouzier-Sore, A.-K., Voisin, P., Bouchaud, V., Bezancon, E., Franconi, J.-M., and Pellerin, L. (2006). Competition between glucose and lactate as oxidative energy substrates in both neurons and astrocytes: a comparative NMR study. *Eur. J. Neurosci.* 24, 1687–1694. doi: 10.1111/j.1460-9568.2006.05056.x.
- Bradshaw, P. (2019). Cytoplasmic and Mitochondrial NADPH-Coupled Redox Systems in the Regulation of Aging. *Nutrients* 11, 504. doi: 10.3390/nu11030504.
- Braidy, N., Poljak, A., Grant, R., Jayasena, T., Mansour, H., Chan-Ling, T., et al. (2014). Mapping NAD⁺ metabolism in the brain of ageing Wistar rats: potential targets for influencing brain senescence. *Biogerontology* 15, 177–198. doi: 10.1007/s10522-013-9489-5.
- Breslin, K., Wade, J. J., Wong-Lin, K., Harkin, J., Flanagan, B., Van Zalinge, H., et al. (2018). Potassium and sodium microdomains in thin astroglial processes: A computational model study. *PLOS Comput. Biol.* 14, e1006151. doi: 10.1371/journal.pcbi.1006151.
- Brilkova, M., Nigri, M., Kumar, H. S., Moore, J., Mantovani, M., Keller, C., et al. (2022). Error-prone protein synthesis recapitulates early symptoms of Alzheimer disease in aging mice. *Cell Rep.* 40, 111433. doi: 10.1016/j.celrep.2022.111433.
- Brocard, J. B., Tassetto, M., and Reynolds, I. J. (2001). Quantitative evaluation of mitochondrial calcium content in rat cortical neurones following a glutamate stimulus. *J. Physiol.* 531, 793–805. doi: 10.1111/j.1469-7793.2001.0793h.x.
- Bröer, S., and Brookes, N. (2001). Transfer of glutamine between astrocytes and neurons: Glutamine transfer between astrocytes and neurons. *J. Neurochem.* 77, 705–719. doi: 10.1046/j.1471-4159.2001.00322.x.
- Brunk, E., Sahoo, S., Zielinski, D. C., Altunkaya, A., Dräger, A., Mih, N., et al. (2018). Recon3D enables a three-dimensional view of gene variation in human metabolism. *Nat. Biotechnol.* 36, 272–281. doi: 10.1038/nbt.4072.
- Burtscher, J., Mallet, R. T., Burtscher, M., and Millet, G. P. (2021). Hypoxia and brain aging: Neurodegeneration or neuroprotection? *Ageing Res. Rev.* 68, 101343. doi: 10.1016/j.arr.2021.101343.
- Byrne, J. H., Heidelberger, R., and Waxham, M. N. eds. (2014). *From molecules to networks: an introduction to cellular and molecular neuroscience*. Third edition. Amsterdam ; Boston: Elsevier/AP, Academic Press is an imprint of Elsevier.
- Cai, L., Sutter, B. M., Li, B., and Tu, B. P. (2011). Acetyl-CoA Induces Cell Growth and Proliferation by Promoting the Acetylation of Histones at Growth Genes. *Mol. Cell* 42, 426–437. doi: 10.1016/j.molcel.2011.05.004.
- Calveti, D., Capo Rangel, G., Gerardo Giorda, L., and Somersalo, E. (2018). A computational model integrating brain electrophysiology and metabolism highlights the key role of extracellular potassium and oxygen. *J. Theor. Biol.* 446, 238–258. doi: 10.1016/j.jtbi.2018.02.029.
- Calveti, D., and Somersalo, E. (2011). Dynamic activation model for a glutamatergic neurovascular unit. *J. Theor. Biol.* 274, 12–29. doi: 10.1016/j.jtbi.2010.12.007.

- Campisi, J., Kapahi, P., Lithgow, G. J., Melov, S., Newman, J. C., and Verdin, E. (2019). From discoveries in ageing research to therapeutics for healthy ageing. *Nature* 571, 183–192. doi: 10.1038/s41586-019-1365-2.
- Cantó, C., Gerhart-Hines, Z., Feige, J. N., Lagouge, M., Noriega, L., Milne, J. C., et al. (2009). AMPK regulates energy expenditure by modulating NAD⁺ metabolism and SIRT1 activity. *Nature* 458, 1056–1060. doi: 10.1038/nature07813.
- Chakrabarti, A., Oehme, I., Witt, O., Oliveira, G., Sippl, W., Romier, C., et al. (2015). HDAC8: a multifaceted target for therapeutic interventions. *Trends Pharmacol. Sci.* 36, 481–492. doi: 10.1016/j.tips.2015.04.013.
- Chang, A., Jeske, L., Ulbrich, S., Hofmann, J., Koblit, J., Schomburg, I., et al. (2021). BRENDA, the ELIXIR core data resource in 2021: new developments and updates. *Nucleic Acids Res.* 49, D498–D508. doi: 10.1093/nar/gkaa1025.
- Chaudhry, F. A., Reimer, R. J., Krizaj, D., Barber, D., Storm-Mathisen, J., Copenhagen, D. R., et al. (1999). Molecular Analysis of System N Suggests Novel Physiological Roles in Nitrogen Metabolism and Synaptic Transmission. *Cell* 99, 769–780. doi: 10.1016/S0092-8674(00)81674-8.
- Choi, I.-Y., and Gruetter, R. eds. (2012). *Neural Metabolism In Vivo*. Boston, MA: Springer US doi: 10.1007/978-1-4614-1788-0.
- Chowdhury, G. M., Jiang, L., Rothman, D. L., and Behar, K. L. (2014). The Contribution of Ketone Bodies to Basal and Activity-Dependent Neuronal Oxidation in Vivo. *J. Cereb. Blood Flow Metab.* 34, 1233–1242. doi: 10.1038/jcbfm.2014.77.
- Cloutier, M., Bolger, F. B., Lowry, J. P., and Wellstead, P. (2009). An integrative dynamic model of brain energy metabolism using in vivo neurochemical measurements. *J. Comput. Neurosci.* 27, 391–414. doi: 10.1007/s10827-009-0152-8.
- Coggan, J. S., Keller, D., Cali, C., Lehvälaiho, H., Markram, H., Schürmann, F., et al. (2018). Norepinephrine stimulates glycogenolysis in astrocytes to fuel neurons with lactate. *PLOS Comput. Biol.* 14, e1006392. doi: 10.1371/journal.pcbi.1006392.
- Coggan, J. S., Keller, D., Markram, H., Schürmann, F., and Magistretti, P. J. (2020). Excitation states of metabolic networks predict dose-response fingerprinting and ligand pulse phase signalling. *J. Theor. Biol.* 487, 110123. doi: 10.1016/j.jtbi.2019.110123.
- Cox, M. F., Hascup, E. R., Bartke, A., and Hascup, K. N. (2022). Friend or Foe? Defining the Role of Glutamate in Aging and Alzheimer’s Disease. *Front. Aging* 3, 929474. doi: 10.3389/fragi.2022.929474.
- Cui, L., Jeong, H., Borovecki, F., Parkhurst, C. N., Tanese, N., and Krainc, D. (2006). Transcriptional repression of PGC-1 α by mutant huntingtin leads to mitochondrial dysfunction and neurodegeneration. *Cell* 127, 59–69. doi: 10.1016/j.cell.2006.09.015.
- Curtis, W. M., Seeds, W. A., Mattson, M. P., and Bradshaw, P. C. (2022). NADPH and Mitochondrial Quality Control as Targets for a Circadian-Based Fasting and Exercise Therapy for the Treatment of Parkinson’s Disease. *Cells* 11, 2416. doi: 10.3390/cells11152416.
- Datta, S., and Chakrabarti, N. (2018). Age related rise in lactate and its correlation with lactate dehydrogenase (LDH) status in post-mitochondrial fractions isolated from different regions of brain in mice. *Neurochem. Int.* 118, 23–33. doi: 10.1016/j.neuint.2018.04.007.
- De Simone, G., di Masi, A., Polticelli, F., and Ascenzi, P. (2018). Human nitrobindin: the first example of an all- β -barrel ferric heme-protein that catalyzes peroxynitrite detoxification. *FEBS Open Bio* 8, 2002–2010. doi: 10.1002/2211-5463.12534.
- Deczkowska, A., Matcovitch-Natan, O., Tsitsou-Kampeli, A., Ben-Hamo, S., Dvir-Szternfeld, R., Spinrad, A., et al. (2017). Mef2C restrains microglial inflammatory response and is lost in brain ageing in an IFN- γ -dependent manner. *Nat. Commun.* 8, 717. doi: 10.1038/s41467-017-00769-0.
- Dienel, G. A. (2012). Brain Lactate Metabolism: The Discoveries and the Controversies. *J. Cereb. Blood Flow Metab.* 32, 1107–1138. doi: 10.1038/jcbfm.2011.175.

- DiNuzzo, M., Mangia, S., Maraviglia, B., and Giove, F. (2010). Glycogenolysis in astrocytes supports blood-borne glucose channeling not glycogen-derived lactate shuttling to neurons: evidence from mathematical modeling. *J. Cereb. Blood Flow Metab. Off. J. Int. Soc. Cereb. Blood Flow Metab.* 30, 1895–1904. doi: 10.1038/jcbfm.2010.151.
- Disterhoft, J. F., and Oh, M. M. (2007). Alterations in intrinsic neuronal excitability during normal aging. *Aging Cell* 6, 327–336. doi: 10.1111/j.1474-9726.2007.00297.x.
- Dombrowski, G. J., Cheung, G. P., and Swiatek, K. R. (1977). Evidence for the existence of enzymatic variants of β -hydroxybutyrate dehydrogenase from rat liver and brain mitochondria. *Life Sci.* 21, 1821–1829. doi: 10.1016/0024-3205(77)90164-3.
- Dong, Y., and Brewer, G. J. (2019). Global Metabolic Shifts in Age and Alzheimer’s Disease Mouse Brains Pivot at NAD⁺/NADH Redox Sites. *J. Alzheimers Dis.* 71, 119–140. doi: 10.3233/JAD-190408.
- Duarte, J. M. N., and Gruetter, R. (2013). Glutamatergic and GABAergic energy metabolism measured in the rat brain by ¹³C NMR spectroscopy at 14.1 T. *J. Neurochem.* 126, 579–590. doi: 10.1111/jnc.12333.
- Dyson, F. (2004). A meeting with Enrico Fermi. *Nature* 427, 297–297. doi: 10.1038/427297a.
- Eap, B., Nomura, M., Panda, O., Garcia, T. Y., King, C. D., Rose, J. P., et al. (2022). Ketone body metabolism declines with age in mice in a sex-dependent manner. *Physiology* doi: 10.1101/2022.10.05.511032.
- Emmons, M. F., Bennett, R. L., Riva, A., Zhang, C., Macaulay, R., Dupéré-Riché, D., et al. (2022). HDAC8-mediated inhibition of EP300 drives a neural crest-like transcriptional state that increases melanoma brain metastasis. *Cancer Biology* doi: 10.1101/2022.10.12.511971.
- Erecińska, M., and Silver, I. A. (1989). ATP and brain function. *J. Cereb. Blood Flow Metab. Off. J. Int. Soc. Cereb. Blood Flow Metab.* 9, 2–19. doi: 10.1038/jcbfm.1989.2.
- Erecińska, M., and Silver, I. A. (1994). Ions and energy in mammalian brain. *Prog. Neurobiol.* 43, 37–71. doi: 10.1016/0301-0082(94)90015-9.
- Fang, E. F., Lautrup, S., Hou, Y., Demarest, T. G., Croteau, D. L., Mattson, M. P., et al. (2017). NAD⁺ in Aging: Molecular Mechanisms and Translational Implications. *Trends Mol. Med.* 23, 899–916. doi: 10.1016/j.molmed.2017.08.001.
- Featherstone, D. E. (2010). Intercellular Glutamate Signaling in the Nervous System and Beyond. *ACS Chem. Neurosci.* 1, 4–12. doi: 10.1021/cn900006n.
- Fillenz, M., and Lowry, J. P. (1998). Studies of the source of glucose in the extracellular compartment of the rat brain. *Dev. Neurosci.* 20, 365–368. doi: 10.1159/000017332.
- Fink, B. D., Bai, F., Yu, L., Sheldon, R. D., Sharma, A., Taylor, E. B., et al. (2018). Oxaloacetic acid mediates ADP-dependent inhibition of mitochondrial complex II-driven respiration. *J. Biol. Chem.* 293, 19932–19941. doi: 10.1074/jbc.RA118.005144.
- Finkel, T., Deng, C.-X., and Mostoslavsky, R. (2009). Recent progress in the biology and physiology of sirtuins. *Nature* 460, 587–591. doi: 10.1038/nature08197.
- Flanagan, B., McDaid, L., Wade, J., Wong-Lin, K., and Harkin, J. (2018). A computational study of astrocytic glutamate influence on post-synaptic neuronal excitability. *PLoS Comput. Biol.* 14, e1006040. doi: 10.1371/journal.pcbi.1006040.
- Fraser, C. L., and Arieff, A. I. (2001). Na-K-ATPase activity decreases with aging in female rat brain synaptosomes. *Am. J. Physiol. Renal Physiol.* 281, F674–678. doi: 10.1152/ajprenal.2001.281.4.F674.
- Frezza, C. (2017). Mitochondrial metabolites: undercover signalling molecules. *Interface Focus* 7, 20160100. doi: 10.1098/rsfs.2016.0100.
- Gaitonde, M. K., Murray, E., and Cunningham, V. J. (1989). Effect of 6-phosphogluconate on phosphoglucose isomerase in rat brain in vitro and in vivo. *J. Neurochem.* 52, 1348–1352. doi: 10.1111/j.1471-4159.1989.tb09178.x.
- Garcia, S., Nissanka, N., Mareco, E. A., Rossi, S., Peralta, S., Diaz, F., et al. (2018). Overexpression of PGC-1 α in aging muscle enhances a subset of young-like molecular patterns. *Aging Cell* 17,

- e12707. doi: 10.1111/accel.12707.
- Garrett, R., and Grisham, C. M. (2013). *Biochemistry*. 5th ed. Belmont, CA: Brooks/Cole, Cengage Learning.
- Ge, I., Kirschen, G. W., and Wang, X. (2021). Shifted Dynamics of Glucose Metabolism in the Hippocampus During Aging. *Front. Aging Neurosci.* 13, 700306. doi: 10.3389/fnagi.2021.700306.
- Ghosh, D., Levault, K. R., and Brewer, G. J. (2014). Relative importance of redox buffers GSH and NAD(P)H in age-related neurodegeneration and Alzheimer disease-like mouse neurons. *Aging Cell* 13, 631–640. doi: 10.1111/accel.12216.
- Gilbert, H. F., Lennox, B. J., Mossman, C. D., and Carle, W. C. (1981). The relation of acyl transfer to the overall reaction of thiolase I from porcine heart. *J. Biol. Chem.* 256, 7371–7377.
- Grimm, A., and Eckert, A. (2017). Brain aging and neurodegeneration: from a mitochondrial point of view. *J. Neurochem.* 143, 418–431. doi: 10.1111/jnc.14037.
- Guarente, L. (2006). Sirtuins as potential targets for metabolic syndrome. *Nature* 444, 868–874. doi: 10.1038/nature05486.
- Gut, P., and Verdin, E. (2013). The nexus of chromatin regulation and intermediary metabolism. *Nature* 502, 489–498. doi: 10.1038/nature12752.
- Hädel, S., Wirth, C., Rapp, M., Gallinat, J., and Schubert, F. (2013). Effects of age and sex on the concentrations of glutamate and glutamine in the human brain: Brain Glutamate and Glutamine With Age and Sex. *J. Magn. Reson. Imaging* 38, 1480–1487. doi: 10.1002/jmri.24123.
- Hagberg, A. A., Schult, D. A., and Swart, P. J. (2008). Exploring Network Structure, Dynamics, and Function using NetworkX. in *Proceedings of the 7th Python in Science Conference*, eds. G. Varoquaux, T. Vaught, and J. Millman (Pasadena, CA USA), 11–15.
- Halestrap, A. P., and Denton, R. M. (1974). Specific inhibition of pyruvate transport in rat liver mitochondria and human erythrocytes by α -cyano-4-hydroxycinnamate (Short Communication). *Biochem. J.* 138, 313–316. doi: 10.1042/bj1380313.
- Hersh, L. B., and Jencks, W. P. (1967). Isolation of an enzyme-coenzyme A intermediate from succinyl coenzyme A-acetoacetate coenzyme A transferase. *J. Biol. Chem.* 242, 339–340.
- Hertz, L., and Rothman, D. (2017). Glutamine-Glutamate Cycle Flux Is Similar in Cultured Astrocytes and Brain and Both Glutamate Production and Oxidation Are Mainly Catalyzed by Aspartate Aminotransferase. *Biology* 6, 17. doi: 10.3390/biology6010017.
- Horowitz, A. M., Fan, X., Bieri, G., Smith, L. K., Sanchez-Diaz, C. I., Schroer, A. B., et al. (2020). Blood factors transfer beneficial effects of exercise on neurogenesis and cognition to the aged brain. *Science* 369, 167–173. doi: 10.1126/science.aaw2622.
- Hosseini, L., Majdi, A., Sadigh-Eteghad, S., Farajdokht, F., Ziaee, M., Rahigh Aghsan, S., et al. (2022). Coenzyme Q10 ameliorates aging-induced memory deficits via modulation of apoptosis, oxidative stress, and mitophagy in aged rats. *Exp. Gerontol.* 168, 111950. doi: 10.1016/j.exger.2022.111950.
- Hou, Y., Dan, X., Babbar, M., Wei, Y., Hasselbalch, S. G., Croteau, D. L., et al. (2019). Ageing as a risk factor for neurodegenerative disease. *Nat. Rev. Neurol.* 15, 565–581. doi: 10.1038/s41582-019-0244-7.
- Howarth, C., Gleeson, P., and Attwell, D. (2012). Updated Energy Budgets for Neural Computation in the Neocortex and Cerebellum. *J. Cereb. Blood Flow Metab.* 32, 1222–1232. doi: 10.1038/jcbfm.2012.35.
- Huang, C.-Y., Oka, S.-I., Xu, X., Chen, C.-F., Tung, C.-Y., Chang, Y.-Y., et al. (2022). PERM1 regulates genes involved in fatty acid metabolism in the heart by interacting with PPAR α and PGC-1 α . *Sci. Rep.* 12, 14576. doi: 10.1038/s41598-022-18885-3.
- Huang, H., Zhou, F., Zhou, S., and Qiu, M. (2021). MYRF: A Mysterious Membrane-Bound Transcription Factor Involved in Myelin Development and Human Diseases. *Neurosci. Bull.* 37, 881–884. doi: 10.1007/s12264-021-00678-9.
- Hupfeld, K. E., Hyatt, H. W., Alvarez Jerez, P., Mikkelsen, M., Hass, C. J., Edden, R. A. E., et al.

- (2021). In Vivo Brain Glutathione is Higher in Older Age and Correlates with Mobility. *Cereb. Cortex* 31, 4576–4594. doi: 10.1093/cercor/bhab107.
- Huth, W., and Menke, R. (1982). Regulation of ketogenesis. Mitochondrial acetyl-CoA acetyltransferase from rat liver: initial-rate kinetics in the presence of the product CoASH reveal intermediary plateau regions. *Eur. J. Biochem.* 128, 413–419.
- Huynh, Q. K., Sakakibara, R., Watanabe, T., and Wada, H. (1980). Glutamic oxaloacetic transaminase isozymes from rat liver. Purification and physicochemical characterization. *J. Biochem. (Tokyo)* 88, 231–239.
- Iskusnykh, I. Y., Zakharova, A. A., and Pathak, D. (2022). Glutathione in Brain Disorders and Aging. *Mol. Basel Switz.* 27, 324. doi: 10.3390/molecules27010324.
- Ivanisevic, J., Stauch, K., Petrascheck, M., Benton, H., Epstein, A., Fang, M., et al. (2016). Metabolic drift in the aging brain. *Aging* 8, 1000–1020. doi: 10.18632/aging.100961.
- Izzo, A., Manco, R., Bonfiglio, F., Cali, G., De Cristofaro, T., Patergnani, S., et al. (2014). NRIP1/RIP140 siRNA-mediated attenuation counteracts mitochondrial dysfunction in Down syndrome. *Hum. Mol. Genet.* 23, 4406–4419. doi: 10.1093/hmg/ddu157.
- Jolivet, R., Allaman, I., Pellerin, L., Magistretti, P. J., and Weber, B. (2010). Comment on Recent Modeling Studies of Astrocyte–Neuron Metabolic Interactions. *J. Cereb. Blood Flow Metab.* 30, 1982–1986. doi: 10.1038/jcbfm.2010.132.
- Jolivet, R., Coggan, J. S., Allaman, I., and Magistretti, P. J. (2015). Multi-timescale Modeling of Activity-Dependent Metabolic Coupling in the Neuron-Glia-Vasculature Ensemble. *PLOS Comput. Biol.* 11, e1004036. doi: 10.1371/journal.pcbi.1004036.
- Jones, T. T., and Brewer, G. J. (2009). Critical age-related loss of cofactors of neuron cytochrome C oxidase reversed by estrogen. *Exp. Neurol.* 215, 212–219. doi: 10.1016/j.expneurol.2008.09.011.
- Jung, W. B., Im, G. H., Jiang, H., and Kim, S.-G. (2021). Early fMRI responses to somatosensory and optogenetic stimulation reflect neural information flow. *Proc. Natl. Acad. Sci.* 118, e2023265118. doi: 10.1073/pnas.2023265118.
- Kaiser, L. G., Schuff, N., Cashdollar, N., and Weiner, M. W. (2005). Age-related glutamate and glutamine concentration changes in normal human brain: 1H MR spectroscopy study at 4 T. *Neurobiol. Aging* 26, 665–672. doi: 10.1016/j.neurobiolaging.2004.07.001.
- Kang, I., Chu, C. T., and Kaufman, B. A. (2018). The mitochondrial transcription factor TFAM in neurodegeneration: emerging evidence and mechanisms. *FEBS Lett.* 592, 793–811. doi: 10.1002/1873-3468.12989.
- Katsyuba, E., Mottis, A., Zietak, M., De Franco, F., van der Velpen, V., Gariani, K., et al. (2018). De novo NAD⁺ synthesis enhances mitochondrial function and improves health. *Nature* 563, 354–359. doi: 10.1038/s41586-018-0645-6.
- Kauffman, F. C., Brown, J. G., Passonneau, J. V., and Lowry, O. H. (1969). Effects of changes in brain metabolism on levels of pentose phosphate pathway intermediates. *J. Biol. Chem.* 244, 3647–3653.
- Keenan, A. B., Torre, D., Lachmann, A., Leong, A. K., Wojciechowicz, M. L., Utti, V., et al. (2019). ChEA3: transcription factor enrichment analysis by orthogonal omics integration. *Nucleic Acids Res.* 47, W212–W224. doi: 10.1093/nar/gkz446.
- Kelly, M. P. (2018). Cyclic nucleotide signaling changes associated with normal aging and age-related diseases of the brain. *Cell. Signal.* 42, 281–291. doi: 10.1016/j.cellsig.2017.11.004.
- Kety, S. S. (1957). “The general metabolism of the brain in vivo,” in *Metabolism of the nervous system* (Elsevier), 221–237.
- Kim, S. Y., Yang, C.-S., Lee, H.-M., Kim, J. K., Kim, Y.-S., Kim, Y.-R., et al. (2018). ESRRA (estrogen-related receptor α) is a key coordinator of transcriptional and post-translational activation of autophagy to promote innate host defense. *Autophagy* 14, 152–168. doi: 10.1080/15548627.2017.1339001.
- King, Z. A., Lu, J., Dräger, A., Miller, P., Federowicz, S., Lerman, J. A., et al. (2016). BiGG Models:

- A platform for integrating, standardizing and sharing genome-scale models. *Nucleic Acids Res.* 44, D515–D522. doi: 10.1093/nar/gkv1049.
- Kiyatkin, E. A., and Lenoir, M. (2012). Rapid fluctuations in extracellular brain glucose levels induced by natural arousing stimuli and intravenous cocaine: fueling the brain during neural activation. *J. Neurophysiol.* 108, 1669–1684. doi: 10.1152/jn.00521.2012.
- Koga, M., Serritella, A. V., Messmer, M. M., Hayashi-Takagi, A., Hester, L. D., Snyder, S. H., et al. (2011). Glutathione is a physiologic reservoir of neuronal glutamate. *Biochem. Biophys. Res. Commun.* 409, 596–602. doi: 10.1016/j.bbrc.2011.04.087.
- Köhler, S., Schmidt, H., Fülle, P., Hirrlinger, J., and Winkler, U. (2020). A Dual Nanosensor Approach to Determine the Cytosolic Concentration of ATP in Astrocytes. *Front. Cell. Neurosci.* 14, 565921. doi: 10.3389/fncel.2020.565921.
- Krishnan, G. P., Filatov, G., Shilnikov, A., and Bazhenov, M. (2015). Electrogenic properties of the Na⁺/K⁺ + ATPase control transitions between normal and pathological brain states. *J. Neurophysiol.* 113, 3356–3374. doi: 10.1152/jn.00460.2014.
- Kulkarni, A. S., Gubbi, S., and Barzilai, N. (2020). Benefits of Metformin in Attenuating the Hallmarks of Aging. *Cell Metab.* 32, 15–30. doi: 10.1016/j.cmet.2020.04.001.
- Kumar, A., and Foster, T. C. (2007). “Neurophysiology of Old Neurons and Synapses,” in *Brain Aging: Models, Methods, and Mechanisms* Frontiers in Neuroscience., ed. D. R. Riddle (Boca Raton (FL): CRC Press/Taylor & Francis). Available at: <http://www.ncbi.nlm.nih.gov/books/NBK3882/> [Accessed June 28, 2023].
- Kuroda, T., Yasuda, S., Tachi, S., Matsuyama, S., Kusakawa, S., Tano, K., et al. (2019). SALL3 expression balance underlies lineage biases in human induced pluripotent stem cell differentiation. *Nat. Commun.* 10, 2175. doi: 10.1038/s41467-019-09511-4.
- Lajtha, A., and Reith, M. E. A. eds. (2007). *Handbook of Neurochemistry and Molecular Neurobiology*. Boston, MA: Springer US doi: 10.1007/978-0-387-30380-2.
- Lambeth, M. J., and Kushmerick, M. J. (2002). A computational model for glycogenolysis in skeletal muscle. *Ann. Biomed. Eng.* 30, 808–827.
- Ledford, H. (2010). Ageing: Much ado about ageing. *Nature* 464, 480–481. doi: 10.1038/464480a.
- Lee, C. S., Lee, C., Hu, T., Nguyen, J. M., Zhang, J., Martin, M. V., et al. (2011). Loss of nuclear factor E2-related factor 1 in the brain leads to dysregulation of proteasome gene expression and neurodegeneration. *Proc. Natl. Acad. Sci. U. S. A.* 108, 8408–8413. doi: 10.1073/pnas.1019209108.
- Lee, J. V., Carrer, A., Shah, S., Snyder, N. W., Wei, S., Venneti, S., et al. (2014). Akt-dependent metabolic reprogramming regulates tumor cell histone acetylation. *Cell Metab.* 20, 306–319. doi: 10.1016/j.cmet.2014.06.004.
- Lee, J. W., Ko, J., Ju, C., and Eltzschig, H. K. (2019). Hypoxia signaling in human diseases and therapeutic targets. *Exp. Mol. Med.* 51, 1–13. doi: 10.1038/s12276-019-0235-1.
- Lee, S., Devanney, N. A., Golden, L. R., Smith, C. T., Schwartz, J. L., Walsh, A. E., et al. (2023). APOE modulates microglial immunometabolism in response to age, amyloid pathology, and inflammatory challenge. *Cell Rep.* 42, 112196. doi: 10.1016/j.celrep.2023.112196.
- Lerchundi, R., Fernández-Moncada, I., Contreras-Baeza, Y., Sotelo-Hitschfeld, T., Mächler, P., Wyss, M. T., et al. (2015). NH₄⁺ triggers the release of astrocytic lactate via mitochondrial pyruvate shunting. *Proc. Natl. Acad. Sci.* 112, 11090–11095. doi: 10.1073/pnas.1508259112.
- Li, L.-Z., Zhao, Y.-W., Pan, H.-X., Xiang, Y.-Q., Wang, Y.-G., Xu, Q., et al. (2022). Association of rare PPARGC1A variants with Parkinson’s disease risk. *J. Hum. Genet.* 67, 687–690. doi: 10.1038/s10038-022-01074-5.
- Li, W., Yu, J., Liu, Y., Huang, X., Abumaria, N., Zhu, Y., et al. (2014). Elevation of brain magnesium prevents synaptic loss and reverses cognitive deficits in Alzheimer’s disease mouse model. *Mol. Brain* 7, 65. doi: 10.1186/s13041-014-0065-y.
- Listrom, D. C., Morizono, H., Rajagopal, S. B., McCANN, T. M., Tuchman, M., and Allewell, M. N. (1997). Expression, purification, and characterization of recombinant human glutamine

- synthetase. *Biochem. J.* 328, 159–163. doi: 10.1042/bj3280159.
- López-Otín, C., Blasco, M. A., Partridge, L., Serrano, M., and Kroemer, G. (2013). The Hallmarks of Aging. *Cell* 153, 1194–1217. doi: 10.1016/j.cell.2013.05.039.
- López-Otín, C., Blasco, M. A., Partridge, L., Serrano, M., and Kroemer, G. (2023). Hallmarks of aging: An expanding universe. *Cell* 186, 243–278. doi: 10.1016/j.cell.2022.11.001.
- Luder, A. S., Parks, J. K., Frerman, F., and Parker, W. D. (1990). Inactivation of beef brain alpha-ketoglutarate dehydrogenase complex by valproic acid and valproic acid metabolites. Possible mechanism of anticonvulsant and toxic actions. *J. Clin. Invest.* 86, 1574–1581. doi: 10.1172/JCI114877.
- Luo, Z., Tian, M., Yang, G., Tan, Q., Chen, Y., Li, G., et al. (2022). Hypoxia signaling in human health and diseases: implications and prospects for therapeutics. *Signal Transduct. Target. Ther.* 7, 218. doi: 10.1038/s41392-022-01080-1.
- Mächler, P., Wyss, M. T., Elsayed, M., Stobart, J., Gutierrez, R., von Faber-Castell, A., et al. (2016). In Vivo Evidence for a Lactate Gradient from Astrocytes to Neurons. *Cell Metab.* 23, 94–102. doi: 10.1016/j.cmet.2015.10.010.
- Mahan, D. E., Mushahwar, I. K., and Koeppe, R. E. (1975). Purification and properties of rat brain pyruvate carboxylase. *Biochem. J.* 145, 25–35. doi: 10.1042/bj1450025.
- Mahmoud, S., Gharagozloo, M., Simard, C., and Gris, D. (2019). Astrocytes Maintain Glutamate Homeostasis in the CNS by Controlling the Balance between Glutamate Uptake and Release. *Cells* 8, 184. doi: 10.3390/cells8020184.
- Majmundar, A. J., Wong, W. J., and Simon, M. C. (2010). Hypoxia-inducible factors and the response to hypoxic stress. *Mol. Cell* 40, 294–309. doi: 10.1016/j.molcel.2010.09.022.
- Maletic-Savatic, M., Vingara, L. K., Manganas, L. N., Li, Y., Zhang, S., Sierra, A., et al. (2008). Metabolomics of Neural Progenitor Cells: A Novel Approach to Biomarker Discovery. *Cold Spring Harb. Symp. Quant. Biol.* 73, 389–401. doi: 10.1101/sqb.2008.73.021.
- Mann, K., Deny, S., Ganguli, S., and Clandinin, T. R. (2021). Coupling of activity, metabolism and behaviour across the Drosophila brain. *Nature* 593, 244–248. doi: 10.1038/s41586-021-03497-0.
- Mantle, D., Heaton, R. A., and Hargreaves, I. P. (2021). Coenzyme Q10, Ageing and the Nervous System: An Overview. *Antioxidants* 11, 2. doi: 10.3390/antiox11010002.
- March-Diaz, R., Lara-Ureña, N., Romero-Molina, C., Heras-Garvin, A., Ortega-de San Luis, C., Alvarez-Vergara, M. I., et al. (2021). Hypoxia compromises the mitochondrial metabolism of Alzheimer’s disease microglia via HIF1. *Nat. Aging* 1, 385–399. doi: 10.1038/s43587-021-00054-2.
- Mattson, M. P., and Arumugam, T. V. (2018). Hallmarks of Brain Aging: Adaptive and Pathological Modification by Metabolic States. *Cell Metab.* 27, 1176–1199. doi: 10.1016/j.cmet.2018.05.011.
- McBean, G. (2017). Cysteine, Glutathione, and Thiol Redox Balance in Astrocytes. *Antioxidants* 6, 62. doi: 10.3390/antiox6030062.
- McCormack, J. G., and Denton, R. M. (1979). The effects of calcium ions and adenine nucleotides on the activity of pig heart 2-oxoglutarate dehydrogenase complex. *Biochem. J.* 180, 533–544. doi: 10.1042/bj1800533.
- McGettrick, A. F., and O’Neill, L. A. J. (2020). The Role of HIF in Immunity and Inflammation. *Cell Metab.* 32, 524–536. doi: 10.1016/j.cmet.2020.08.002.
- Meidenbauer, J. J., Ta, N., and Seyfried, T. N. (2014). Influence of a ketogenic diet, fish-oil, and calorie restriction on plasma metabolites and lipids in C57BL/6J mice. *Nutr. Metab.* 11, 23. doi: 10.1186/1743-7075-11-23.
- Menahan, L. A., Hron, W. T., Hinkelman, D. G., and Miziorko, H. M. (1981). Interrelationships between 3-Hydroxy-3-Methylglutaryl-CoA Synthase, Acetoacetyl-CoA and Ketogenesis. *Eur. J. Biochem.* 119, 287–294. doi: 10.1111/j.1432-1033.1981.tb05606.x.
- Meyer, D. J., Díaz-García, C. M., Nathwani, N., Rahman, M., and Yellen, G. (2022). The Na⁺/K⁺

- pump dominates control of glycolysis in hippocampal dentate granule cells. *eLife* 11, e81645. doi: 10.7554/eLife.81645.
- Milne, J. C., Lambert, P. D., Schenk, S., Carney, D. P., Smith, J. J., Gagne, D. J., et al. (2007). Small molecule activators of SIRT1 as therapeutics for the treatment of type 2 diabetes. *Nature* 450, 712–716. doi: 10.1038/nature06261.
- Mink, J. W., Blumenshine, R. J., and Adams, D. B. (1981). Ratio of central nervous system to body metabolism in vertebrates: its constancy and functional basis. *Am. J. Physiol.* 241, R203–212. doi: 10.1152/ajpregu.1981.241.3.R203.
- Mironov, S. L. (2007). ADP Regulates Movements of Mitochondria in Neurons. *Biophys. J.* 92, 2944–2952. doi: 10.1529/biophysj.106.092981.
- Mogilevskaya, E., Demin, O., and Goryanin, I. (2006). Kinetic model of mitochondrial Krebs cycle: unraveling the mechanism of salicylate hepatotoxic effects. *J. Biol. Phys.* 32, 245–271. doi: 10.1007/s10867-006-9015-y.
- Mongeon, R., Venkatachalam, V., and Yellen, G. (2016). Cytosolic NADH-NAD⁺ Redox Visualized in Brain Slices by Two-Photon Fluorescence Lifetime Biosensor Imaging. *Antioxid. Redox Signal.* 25, 553–563. doi: 10.1089/ars.2015.6593.
- Mormino, A., Coccozza, G., Fontemaggi, G., Valente, S., Esposito, V., Santoro, A., et al. (2021). Histone-deacetylase 8 drives the immune response and the growth of glioma. *Glia* 69, 2682–2698. doi: 10.1002/glia.24065.
- Mueggler, P. A., and Wolfe, R. G. (1978). Malate dehydrogenase. Kinetic studies of substrate activation of supernatant enzyme by L-malate. *Biochemistry* 17, 4615–4620. doi: 10.1021/bi00615a006.
- Mulukutla, B. C., Yongky, A., Daoutidis, P., and Hu, W.-S. (2014). Bistability in Glycolysis Pathway as a Physiological Switch in Energy Metabolism. *PLoS ONE* 9, e98756. doi: 10.1371/journal.pone.0098756.
- Mulukutla, B. C., Yongky, A., Grimm, S., Daoutidis, P., and Hu, W.-S. (2015). Multiplicity of Steady States in Glycolysis and Shift of Metabolic State in Cultured Mammalian Cells. *PLOS ONE* 10, e0121561. doi: 10.1371/journal.pone.0121561.
- Muraleedharan, R., Gawali, M. V., Tiwari, D., Sukumaran, A., Oatman, N., Anderson, J., et al. (2020). AMPK-Regulated Astrocytic Lactate Shuttle Plays a Non-Cell-Autonomous Role in Neuronal Survival. *Cell Rep.* 32, 108092. doi: 10.1016/j.celrep.2020.108092.
- Nazaret, C., Heiske, M., Thurley, K., and Mazat, J.-P. (2009). Mitochondrial energetic metabolism: A simplified model of TCA cycle with ATP production. *J. Theor. Biol.* 258, 455–464. doi: 10.1016/j.jtbi.2008.09.037.
- Nehlig, A. (2004). Brain uptake and metabolism of ketone bodies in animal models. *Prostaglandins Leukot. Essent. Fatty Acids* 70, 265–275. doi: 10.1016/j.plefa.2003.07.006.
- Neves, A., Costalat, R., and Pellerin, L. (2012). Determinants of brain cell metabolic phenotypes and energy substrate utilization unraveled with a modeling approach. *PLoS Comput. Biol.* 8, e1002686. doi: 10.1371/journal.pcbi.1002686.
- Neves, S. R. (2011). Obtaining and Estimating Kinetic Parameters from the Literature. *Sci. Signal.* 4. doi: 10.1126/scisignal.2001988.
- Ng, F., Wijaya, L., and Tang, B. L. (2015). SIRT1 in the brain-connections with aging-associated disorders and lifespan. *Front. Cell. Neurosci.* 9, 64. doi: 10.3389/fncel.2015.00064.
- Niccoli, T., and Partridge, L. (2012). Ageing as a Risk Factor for Disease. *Curr. Biol.* 22, R741–R752. doi: 10.1016/j.cub.2012.07.024.
- Nielsen, N. C., Zahler, W. L., and Fleischer, S. (1973). Mitochondrial D- -hydroxybutyrate dehydrogenase. IV. Kinetic analysis of reaction mechanism. *J. Biol. Chem.* 248, 2556–2562.
- Nishihara, E., Moriya, T., and Shinohara, K. (2007). Expression of steroid receptor coactivator-1 is elevated during neuronal differentiation of murine neural stem cells. *Brain Res.* 1135, 22–30. doi: 10.1016/j.brainres.2006.12.026.
- Niven, J. E. (2016). Neuronal energy consumption: biophysics, efficiency and evolution. *Curr. Opin.*

- Neurobiol.* 41, 129–135. doi: 10.1016/j.conb.2016.09.004.
- Oka, M., Suzuki, E., Asada, A., Saito, T., Iijima, K. M., and Ando, K. (2021). Increasing neuronal glucose uptake attenuates brain aging and promotes life span under dietary restriction in *Drosophila*. *iScience* 24, 101979. doi: 10.1016/j.isci.2020.101979.
- O’Neill, L. A. J., and Hardie, D. G. (2013). Metabolism of inflammation limited by AMPK and pseudo-starvation. *Nature* 493, 346–355. doi: 10.1038/nature11862.
- Orosz, F., Wágner, G., Ortega, F., Cascante, M., and Ovádi, J. (2003). Glucose conversion by multiple pathways in brain extract: theoretical and experimental analysis. *Biochem. Biophys. Res. Commun.* 309, 792–797. doi: 10.1016/j.bbrc.2003.08.072.
- Øyehaug, L., Østby, I., Lloyd, C. M., Omholt, S. W., and Einevoll, G. T. (2012). Dependence of spontaneous neuronal firing and depolarisation block on astroglial membrane transport mechanisms. *J. Comput. Neurosci.* 32, 147–165. doi: 10.1007/s10827-011-0345-9.
- Palla, A. R., Ravichandran, M., Wang, Y. X., Alexandrova, L., Yang, A. V., Kraft, P., et al. (2021). Inhibition of prostaglandin-degrading enzyme 15-PGDH rejuvenates aged muscle mass and strength. *Science* 371, eabc8059. doi: 10.1126/science.abc8059.
- Pamiljans, V., Krishnaswamy, P. R., Dumville, G., and Meister, A. (1962). Studies on the Mechanism of Glutamine Synthesis; Isolation and Properties of the Enzyme from Sheep Brain. *Biochemistry* 1, 153–158. doi: 10.1021/bi00907a023.
- Park, J. O., Rubin, S. A., Xu, Y.-F., Amador-Noguez, D., Fan, J., Shlomi, T., et al. (2016). Metabolite concentrations, fluxes and free energies imply efficient enzyme usage. *Nat. Chem. Biol.* 12, 482–489. doi: 10.1038/nchembio.2077.
- Pathak, D., Shields, L. Y., Mendelsohn, B. A., Haddad, D., Lin, W., Gerencser, A. A., et al. (2015). The Role of Mitochondrially Derived ATP in Synaptic Vesicle Recycling. *J. Biol. Chem.* 290, 22325–22336. doi: 10.1074/jbc.M115.656405.
- Pérez-Escuredo, J., Van Hée, V. F., Sboarina, M., Falces, J., Payen, V. L., Pellerin, L., et al. (2016). Monocarboxylate transporters in the brain and in cancer. *Biochim. Biophys. Acta BBA - Mol. Cell Res.* 1863, 2481–2497. doi: 10.1016/j.bbamcr.2016.03.013.
- Pochini, L., Scalise, M., Galluccio, M., and Indiveri, C. (2014). Membrane transporters for the special amino acid glutamine: structure/function relationships and relevance to human health. *Front. Chem.* 2. doi: 10.3389/fchem.2014.00061.
- Poliquin, P. O., Chen, J., Cloutier, M., Trudeau, L.-É., and Jolicoeur, M. (2013). Metabolomics and In-Silico Analysis Reveal Critical Energy Deregulations in Animal Models of Parkinson’s Disease. *PLoS ONE* 8, e69146. doi: 10.1371/journal.pone.0069146.
- Pospischil, M., Toledo-Rodriguez, M., Monier, C., Piwkowska, Z., Bal, T., Frégnac, Y., et al. (2008). Minimal Hodgkin–Huxley type models for different classes of cortical and thalamic neurons. *Biol. Cybern.* 99, 427–441. doi: 10.1007/s00422-008-0263-8.
- Power, J. M., Wu, W. W., Sametsky, E., Oh, M. M., and Disterhoft, J. F. (2002). Age-related enhancement of the slow outward calcium-activated potassium current in hippocampal CA1 pyramidal neurons in vitro. *J. Neurosci. Off. J. Soc. Neurosci.* 22, 7234–7243. doi: 10.1523/JNEUROSCI.22-16-07234.2002.
- Pritchard, J. B. (1995). Intracellular alpha-ketoglutarate controls the efficacy of renal organic anion transport. *J. Pharmacol. Exp. Ther.* 274, 1278–1284.
- Rackauckas, C., and Nie, Q. (2017). DifferentialEquations.jl – A Performant and Feature-Rich Ecosystem for Solving Differential Equations in Julia. *J. Open Res. Softw.* 5, 15. doi: 10.5334/jors.151.
- Recasens, M., Benezra, R., Basset, P., and Mandel, P. (1980). Cysteine sulfinatase aminotransferase and aspartate aminotransferase isoenzymes of rat brain. Purification, characterization, and further evidence for identity. *Biochemistry* 19, 4583–4589. doi: 10.1021/bi00561a007.
- Reimann, M. W., Nolte, M., Scolamiero, M., Turner, K., Perin, R., Chindemi, G., et al. (2017). Cliques of Neurons Bound into Cavities Provide a Missing Link between Structure and Function. *Front. Comput. Neurosci.* 11, 48. doi: 10.3389/fncom.2017.00048.

- Riddle, D. R. ed. (2007). *Brain Aging: Models, Methods, and Mechanisms*. Boca Raton (FL): CRC Press/Taylor & Francis Available at: <http://www.ncbi.nlm.nih.gov/books/NBK1834/> [Accessed August 29, 2023].
- Rizzo, V., Richman, J., and Puthanveetil, S. V. (2015). Dissecting mechanisms of brain aging by studying the intrinsic excitability of neurons. *Front. Aging Neurosci.* 6. doi: 10.3389/fnagi.2014.00337.
- Roberg, B., Torgner, I. A., and Kvamme, E. (1999). Inhibition of glutamine transport in rat brain mitochondria by some amino acids and tricarboxylic acid cycle intermediates. *Neurochem. Res.* 24, 809–814. doi: 10.1023/a:1020941510764.
- Robinson, M. B., and Jackson, J. G. (2016). Astroglial glutamate transporters coordinate excitatory signaling and brain energetics. *Neurochem. Int.* 98, 56–71. doi: 10.1016/j.neuint.2016.03.014.
- Rock, C. O., Calder, R. B., Karim, M. A., and Jackowski, S. (2000). Pantothenate Kinase Regulation of the Intracellular Concentration of Coenzyme A. *J. Biol. Chem.* 275, 1377–1383. doi: 10.1074/jbc.275.2.1377.
- Rodgers, J. T., Lerin, C., Haas, W., Gygi, S. P., Spiegelman, B. M., and Puigserver, P. (2005). Nutrient control of glucose homeostasis through a complex of PGC-1 α and SIRT1. *Nature* 434, 113–118. doi: 10.1038/nature03354.
- Roeder, L. M., Poduslo, S. E., and Tildon, J. T. (1982). Utilization of ketone bodies and glucose by established neural cell lines. *J. Neurosci. Res.* 8, 671–682. doi: 10.1002/jnr.490080412.
- Rolfe, D. F., and Brown, G. C. (1997). Cellular energy utilization and molecular origin of standard metabolic rate in mammals. *Physiol. Rev.* 77, 731–758. doi: 10.1152/physrev.1997.77.3.731.
- Ronowska, A., Szutowicz, A., Bielarczyk, H., Gul-Hinc, S., Klimaszewska-Łata, J., Dyś, A., et al. (2018). The Regulatory Effects of Acetyl-CoA Distribution in the Healthy and Diseased Brain. *Front. Cell. Neurosci.* 12. doi: 10.3389/fncel.2018.00169.
- Ross, J. M., Oberg, J., Brene, S., Coppotelli, G., Terzioglu, M., Pernold, K., et al. (2010). High brain lactate is a hallmark of aging and caused by a shift in the lactate dehydrogenase A/B ratio. *Proc. Natl. Acad. Sci.* 107, 20087–20092. doi: 10.1073/pnas.1008189107.
- Rybalkin, S. D., Hinds, T. R., and Beavo, J. A. (2013). “Enzyme Assays for cGMP Hydrolyzing Phosphodiesterases,” in *Guanylate Cyclase and Cyclic GMP Methods in Molecular Biology*, eds. T. Krieg and R. Lukowski (Totowa, NJ: Humana Press), 51–62. doi: 10.1007/978-1-62703-459-3_3.
- Satoh, A., Imai, S., and Guarente, L. (2017). The brain, sirtuins, and ageing. *Nat. Rev. Neurosci.* 18, 362–374. doi: 10.1038/nrn.2017.42.
- Savtchenko, L. P., Bard, L., Jensen, T. P., Reynolds, J. P., Kraev, I., Medvedev, N., et al. (2018). Disentangling astroglial physiology with a realistic cell model in silico. *Nat. Commun.* 9. doi: 10.1038/s41467-018-05896-w.
- Schaum, N., Lehallier, B., Hahn, O., Pálovics, R., Hosseinzadeh, S., Lee, S. E., et al. (2020). Ageing hallmarks exhibit organ-specific temporal signatures. *Nature* 583, 596–602. doi: 10.1038/s41586-020-2499-y.
- Schousboe, A., Waagepetersen, H. S., and Sonnewald, U. (2019). Astrocytic pyruvate carboxylation: Status after 35 years. *J. Neurosci. Res.* 97, 890–896. doi: 10.1002/jnr.24402.
- Sedlak, T. W., Paul, B. D., Parker, G. M., Hester, L. D., Snowman, A. M., Taniguchi, Y., et al. (2019). The glutathione cycle shapes synaptic glutamate activity. *Proc. Natl. Acad. Sci.* 116, 2701–2706. doi: 10.1073/pnas.1817885116.
- Seelig, M. S., and Preuss, H. G. (1994). Magnesium metabolism and perturbations in the elderly. *Geriatr. Nephrol. Urol.* 4, 101–111. doi: 10.1007/BF01436050.
- Sharma, H. K., and Rothstein, M. (1984). Altered brain phosphoglycerate kinase from aging rats. *Mech. Ageing Dev.* 25, 285–296. doi: 10.1016/0047-6374(84)90002-2.
- Shen, P., Xu, A., Hou, Y., Wang, H., Gao, C., He, F., et al. (2021). Conserved paradoxical relationships among the evolutionary, structural and expressional features of KRAB zinc-finger proteins reveal their special functional characteristics. *BMC Mol. Cell Biol.* 22, 7. doi:

- 10.1186/s12860-021-00346-w.
- Shestov, A. A., Valette, J., Uğurbil, K., and Henry, P.-G. (2007). On the reliability of ^{13}C metabolic modeling with two-compartment neuronal-glia models. *J. Neurosci. Res.* 85, 3294–3303. doi: 10.1002/jnr.21269.
- Shichkova, P., Coggan, J. S., Markram, H., and Keller, D. (2021). A Standardized Brain Molecular Atlas: A Resource for Systems Modeling and Simulation. *Front. Mol. Neurosci.* 14, 604559. doi: 10.3389/fnmol.2021.604559.
- Shin, H.-J. R., Kim, H., Oh, S., Lee, J.-G., Kee, M., Ko, H.-J., et al. (2016). AMPK-SKP2-CARM1 signalling cascade in transcriptional regulation of autophagy. *Nature* 534, 553–557. doi: 10.1038/nature18014.
- Simpson, I. A., Carruthers, A., and Vannucci, S. J. (2007). Supply and Demand in Cerebral Energy Metabolism: The Role of Nutrient Transporters. *J. Cereb. Blood Flow Metab.* 27, 1766–1791. doi: 10.1038/sj.jcbfm.9600521.
- Singh, A., D’Amico, D., Andreux, P. A., Fouassier, A. M., Blanco-Bose, W., Evans, M., et al. (2022). Urolithin A improves muscle strength, exercise performance, and biomarkers of mitochondrial health in a randomized trial in middle-aged adults. *Cell Rep. Med.* 3, 100633. doi: 10.1016/j.xcrm.2022.100633.
- Sizemore, A. E., Giusti, C., Kahn, A., Vettel, J. M., Betzel, R. F., and Bassett, D. S. (2018). Cliques and cavities in the human connectome. *J. Comput. Neurosci.* 44, 115–145. doi: 10.1007/s10827-017-0672-6.
- Smith, C. M., Bryla, J., and Williamson, J. R. (1974). Regulation of mitochondrial alpha-ketoglutarate metabolism by product inhibition at alpha-ketoglutarate dehydrogenase. *J. Biol. Chem.* 249, 1497–1505.
- Smith, R. N., Agharkar, A. S., and Gonzales, E. B. (2014). A review of creatine supplementation in age-related diseases: more than a supplement for athletes. *F1000Research* 3, 222. doi: 10.12688/f1000research.5218.1.
- Smithers, H. E., Terry, J. R., Brown, J. T., and Randall, A. D. (2017). Aging-Associated Changes to Intrinsic Neuronal Excitability in the Bed Nucleus of the Stria Terminalis Is Cell Type-Dependent. *Front. Aging Neurosci.* 9, 424. doi: 10.3389/fnagi.2017.00424.
- Sokoloff, L. (1996). “Cerebral Metabolism and Visualization of Cerebral Activity,” in *Comprehensive Human Physiology*, eds. R. Greger and U. Windhorst (Berlin, Heidelberg: Springer Berlin Heidelberg), 579–602. doi: 10.1007/978-3-642-60946-6_30.
- Stillman, C. M., Esteban-Cornejo, I., Brown, B., Bender, C. M., and Erickson, K. I. (2020). Effects of Exercise on Brain and Cognition Across Age Groups and Health States. *Trends Neurosci.* 43, 533–543. doi: 10.1016/j.tins.2020.04.010.
- Sugrue, M. M., and Tatton, W. G. (2001). Mitochondrial Membrane Potential in Aging Cells. *Neurosignals* 10, 176–188. doi: 10.1159/000046886.
- Sun, X., He, G., Qing, H., Zhou, W., Dobie, F., Cai, F., et al. (2006). Hypoxia facilitates Alzheimer’s disease pathogenesis by up-regulating BACE1 gene expression. *Proc. Natl. Acad. Sci. U. S. A.* 103, 18727–18732. doi: 10.1073/pnas.0606298103.
- Sun, Z., and Xu, Y. (2020). Nuclear Receptor Coactivators (NCOAs) and Corepressors (NCORs) in the Brain. *Endocrinology* 161, bqaa083. doi: 10.1210/endo/bqaa083.
- Suresh, S. N., Chavalmane, A. K., Pillai, M., Ammanathan, V., Vidyadhara, D. J., Yarreiphang, H., et al. (2018). Modulation of Autophagy by a Small Molecule Inverse Agonist of $\text{ERR}\alpha$ Is Neuroprotective. *Front. Mol. Neurosci.* 11, 109. doi: 10.3389/fnmol.2018.00109.
- Szklarczyk, D., Gable, A. L., Lyon, D., Junge, A., Wyder, S., Huerta-Cepas, J., et al. (2019). STRING v11: protein–protein association networks with increased coverage, supporting functional discovery in genome-wide experimental datasets. *Nucleic Acids Res.* 47, D607–D613. doi: 10.1093/nar/gky1131.
- Takahashi, H., Manaka, S., and Sano, K. (1981). Changes in extracellular potassium concentration in cortex and brain stem during the acute phase of experimental closed head injury. *J. Neurosurg.*

- 55, 708–717. doi: 10.3171/jns.1981.55.5.0708.
- Takeda, M., Briggs, L. E., Wakimoto, H., Marks, M. H., Warren, S. A., Lu, J. T., et al. (2009). Slow progressive conduction and contraction defects in loss of Nkx2-5 mice after cardiomyocyte terminal differentiation. *Lab. Investig. J. Tech. Methods Pathol.* 89, 983–993. doi: 10.1038/labinvest.2009.59.
- Tantama, M., Martínez-François, J. R., Mongeon, R., and Yellen, G. (2013). Imaging energy status in live cells with a fluorescent biosensor of the intracellular ATP-to-ADP ratio. *Nat. Commun.* 4, 2550. doi: 10.1038/ncomms3550.
- Taylor, C. T., and Scholz, C. C. (2022). The effect of HIF on metabolism and immunity. *Nat. Rev. Nephrol.* 18, 573–587. doi: 10.1038/s41581-022-00587-8.
- Theurey, P., Connolly, N. M. C., Fortunati, I., Basso, E., Lauwen, S., Ferrante, C., et al. (2019). Systems biology identifies preserved integrity but impaired metabolism of mitochondria due to a glycolytic defect in Alzheimer’s disease neurons. *Aging Cell* 18, e12924. doi: 10.1111/accel.12924.
- Thibonnier, M., Esau, C., Ghosh, S., Wargent, E., and Stocker, C. (2020). Metabolic and energetic benefits of microRNA-22 inhibition. *BMJ Open Diabetes Res. Care* 8, e001478. doi: 10.1136/bmjdr-2020-001478.
- Thiebold, A.-L., Lorenz, N. I., Foltyn, M., Engel, A. L., Divé, I., Urban, H., et al. (2017). Mammalian target of rapamycin complex 1 activation sensitizes human glioma cells to hypoxia-induced cell death. *Brain J. Neurol.* 140, 2623–2638. doi: 10.1093/brain/awx196.
- Tiveci, S., Akin, A., Çakır, T., Saybaşlı, H., and Ülgen, K. (2005). Modelling of calcium dynamics in brain energy metabolism and Alzheimer’s disease. *Comput. Biol. Chem.* 29, 151–162. doi: 10.1016/j.compbiolchem.2005.03.002.
- Tong, J., Fitzmaurice, P. S., Moszczynska, A., Mattina, K., Ang, L.-C., Boileau, I., et al. (2016). Do glutathione levels decline in aging human brain? *Free Radic. Biol. Med.* 93, 110–117. doi: 10.1016/j.freeradbiomed.2016.01.029.
- Tretter, L., Patocs, A., and Chinopoulos, C. (2016). Succinate, an intermediate in metabolism, signal transduction, ROS, hypoxia, and tumorigenesis. *Biochim. Biophys. Acta* 1857, 1086–1101. doi: 10.1016/j.bbabi.2016.03.012.
- Tripathi, M., Yen, P. M., and Singh, B. K. (2020). Estrogen-Related Receptor Alpha: An Under-Appreciated Potential Target for the Treatment of Metabolic Diseases. *Int. J. Mol. Sci.* 21, 1645. doi: 10.3390/ijms21051645.
- Tsuboi, K. K., Fukunaga, K., and Petricciani, J. C. (1969). Purification and specific kinetic properties of erythrocyte uridine diphosphate glucose pyrophosphorylase. *J. Biol. Chem.* 244, 1008–1015.
- Vali, S., Mythri, R. B., Jagatha, B., Padiadpu, J., Ramanujan, K. S., Andersen, J. K., et al. (2007). Integrating glutathione metabolism and mitochondrial dysfunction with implications for Parkinson’s disease: a dynamic model. *Neuroscience* 149, 917–930. doi: 10.1016/j.neuroscience.2007.08.028.
- Verkhatsky, A., and Nedergaard, M. (2018). Physiology of Astroglia. *Physiol. Rev.* 98, 239–389. doi: 10.1152/physrev.00042.2016.
- Vitale, P., Salgueiro-Pereira, A. R., Lupascu, C. A., Willem, M., Migliore, R., Migliore, M., et al. (2021). Analysis of Age-Dependent Alterations in Excitability Properties of CA1 Pyramidal Neurons in an APPS1 Model of Alzheimer’s Disease. *Front. Aging Neurosci.* 13, 668948. doi: 10.3389/fnagi.2021.668948.
- Volkova, M., Garg, R., Dick, S., and Boheler, K. R. (2005). Aging-associated changes in cardiac gene expression. *Cardiovasc. Res.* 66, 194–204. doi: 10.1016/j.cardiores.2004.11.016.
- Waitt, A. E., Reed, L., Ransom, B. R., and Brown, A. M. (2017). Emerging Roles for Glycogen in the CNS. *Front. Mol. Neurosci.* 10. doi: 10.3389/fnmol.2017.00073.
- Weber, B., and Barros, L. F. (2015). The Astrocyte: Powerhouse and Recycling Center. *Cold Spring Harb. Perspect. Biol.* 7, a020396. doi: 10.1101/cshperspect.a020396.
- White, H., and Jencks, W. P. (1976). Mechanism and specificity of succinyl-CoA:3-ketoacid coenzyme

- A transferase. *J. Biol. Chem.* 251, 1688–1699.
- Wilcock, A. R., Sharpe, D. M., and Goldberg, D. M. (1973). Kinetic similarity of enzymes in human blood serum and cerebrospinal fluid: Aspartate aminotransferase and lactate dehydrogenase. *J. Neurol. Sci.* 20, 97–101. doi: 10.1016/0022-510X(73)90121-4.
- Williamson, D., Lund, P., and Krebs, H. (1967). The redox state of free nicotinamide-adenine dinucleotide in the cytoplasm and mitochondria of rat liver. *Biochem. J.* 103, 514–527. doi: 10.1042/bj1030514.
- Winter, F., Bludszweit-Philipp, C., and Wolkenhauer, O. (2018). Mathematical analysis of the influence of brain metabolism on the BOLD signal in Alzheimer’s disease. *J. Cereb. Blood Flow Metab.* 38, 304–316. doi: 10.1177/0271678X17693024.
- Witthoft, A., Filosa, J. A., and Karniadakis, G. E. (2013). Potassium Buffering in the Neurovascular Unit: Models and Sensitivity Analysis. *Biophys. J.* 105, 2046–2054. doi: 10.1016/j.bpj.2013.09.012.
- Wittig, U., Rey, M., Weidemann, A., Kania, R., and Müller, W. (2018). SABIO-RK: an updated resource for manually curated biochemical reaction kinetics. *Nucleic Acids Res.* 46, D656–D660. doi: 10.1093/nar/gkx1065.
- Wu, F., Yang, F., Vinnakota, K. C., and Beard, D. A. (2007). Computer modeling of mitochondrial tricarboxylic acid cycle, oxidative phosphorylation, metabolite transport, and electrophysiology. *J. Biol. Chem.* 282, 24525–24537. doi: 10.1074/jbc.M701024200.
- Xu, K., Morgan, K. T., Todd Gehris, A., Elston, T. C., and Gomez, S. M. (2011). A Whole-Body Model for Glycogen Regulation Reveals a Critical Role for Substrate Cycling in Maintaining Blood Glucose Homeostasis. *PLoS Comput. Biol.* 7, e1002272. doi: 10.1371/journal.pcbi.1002272.
- Xue, X., Liu, B., Hu, J., Bian, X., and Lou, S. (2022). The potential mechanisms of lactate in mediating exercise-enhanced cognitive function: a dual role as an energy supply substrate and a signaling molecule. *Nutr. Metab.* 19, 52. doi: 10.1186/s12986-022-00687-z.
- Yamashita, D., Moriuchi, T., Osumi, T., and Hirose, F. (2016). Transcription Factor hDREF Is a Novel SUMO E3 Ligase of Mi2 α . *J. Biol. Chem.* 291, 11619–11634. doi: 10.1074/jbc.M115.713370.
- Yang, J.-S., Hsu, J.-W., Park, S.-Y., Li, J., Oldham, W. M., Beznoussenko, G. V., et al. (2018). GAPDH inhibits intracellular pathways during starvation for cellular energy homeostasis. *Nature* 561, 263–267. doi: 10.1038/s41586-018-0475-6.
- Yang, Q., Zhao, W., Xing, Y., Li, P., Zhou, X., Ning, H., et al. (2021). Dysfunction of an energy sensor NFE2L1 triggers uncontrollable AMPK signal and glucose metabolism reprogramming. *Molecular Biology* doi: 10.1101/2021.09.07.459348.
- Yang, S. Y., He, X. Y., and Schulz, H. (1987). Fatty acid oxidation in rat brain is limited by the low activity of 3-ketoacyl-coenzyme A thiolase. *J. Biol. Chem.* 262, 13027–13032.
- Yi, G., and Grill, W. M. (2019). Average firing rate rather than temporal pattern determines metabolic cost of activity in thalamocortical relay neurons. *Sci. Rep.* 9. doi: 10.1038/s41598-019-43460-8.
- Yoshino, J., Baur, J. A., and Imai, S.-I. (2018). NAD⁺ Intermediates: The Biology and Therapeutic Potential of NMN and NR. *Cell Metab.* 27, 513–528. doi: 10.1016/j.cmet.2017.11.002.
- Yuk, J.-M., Kim, T. S., Kim, S. Y., Lee, H.-M., Han, J., Dufour, C. R., et al. (2015). Orphan Nuclear Receptor ERR α Controls Macrophage Metabolic Signaling and A20 Expression to Negatively Regulate TLR-Induced Inflammation. *Immunity* 43, 80–91. doi: 10.1016/j.immuni.2015.07.003.
- Zhang, M. J., Pisco, A. O., Darmanis, S., and Zou, J. (2021a). Mouse aging cell atlas analysis reveals global and cell type-specific aging signatures. *eLife* 10, e62293. doi: 10.7554/eLife.62293.
- Zhang, P., Qu, H.-Y., Wu, Z., Na, H., Hourihan, J., Zhang, F., et al. (2021b). ERK signaling licenses SKN-1A/NRF1 for proteasome production and proteasomal stress resistance. *Cell Biology* doi: 10.1101/2021.01.04.425272.
- Zhang, X., Dash, R. K., Jacobs, E. R., Camara, A. K. S., Clough, A. V., and Audi, S. H. (2018).

- Integrated computational model of the bioenergetics of isolated lung mitochondria. *PLoS One* 13, e0197921. doi: 10.1371/journal.pone.0197921.
- Zhao, T., Kee, H. J., Bai, L., Kim, M.-K., Kee, S.-J., and Jeong, M. H. (2021). Selective HDAC8 Inhibition Attenuates Isoproterenol-Induced Cardiac Hypertrophy and Fibrosis via p38 MAPK Pathway. *Front. Pharmacol.* 12, 677757. doi: 10.3389/fphar.2021.677757.
- Zhou, M., Xia, X., Yan, H., Li, S., Bian, S., Sha, X., et al. (2019). The Model of Aging Acceleration Network Reveals the Correlation of Alzheimer's Disease and Aging at System Level. *BioMed Res. Int.* 2019, 4273108. doi: 10.1155/2019/4273108.
- Zhu, F., Wang, R., Pan, X., and Zhu, Z. (2019). Energy expenditure computation of a single bursting neuron. *Cogn. Neurodyn.* 13, 75–87. doi: 10.1007/s11571-018-9503-3.